

THESIS ON NATURAL AND EXACT SCIENCES B234

**Formation and Growth of $\text{Cu}_2\text{ZnSnS}_4$
Monograin Powder in Molten CdI_2**

GOD'SWILL CHIMEZIE NKWUSI



TALLINN UNIVERSITY OF TECHNOLOGY
School of Engineering
Department of Materials and Environmental Technologies

This dissertation was accepted for the defense of the degree of Doctor of Philosophy in Natural and Exact Sciences on 7 June, 2017

Supervisor: Mare Altosaar, PhD
Department of Materials and Environmental Technology, TUT

Opponents: Filipe Neves, PhD,
NLEG, National Laboratory of Energy and Geology, Portugal

Kaia Ernits, PhD
Head of R&D at crystalsol OÜ, Tallinn

Defence: 30 June 2017 at 14:00
Lecture hall: U06A-201
Tallinn University of Technology, Ehitajate tee 5, Tallinn

Declaration:

I hereby declare that this doctoral thesis, my original investigation and achievement, submitted to Tallinn University of Technology in partial fulfilment of my doctoral degree program, has not been submitted for any academic degree.

God'swill Nkwusi



European Union
European Regional
Development Fund



Investing
in your future

Copyright: God'swill Nkwusi, 2017

ISSN 1406-4723

ISBN 978-9949-83-124-1 (publication)

ISBN 978-9949-83-125-8 (PDF)

LOODUS- JA TÄPPISTEADUSED B235

**$\text{Cu}_2\text{ZnSnS}_4$ moodustumine ja monoterapulbri
kasv CdI_2 sulafaasi keskkonnas**

GOD'SWILL CHIMEZIE NKWUSI

TABLE OF CONTENTS

LIST OF PUBLICATIONS	7
AUTHOR'S OWN CONTRIBUTION	8
LIST OF ABBREVIATIONS AND SYMBOLS	9
INTRODUCTION	10
1. LITERATURE REVIEW	12
1.1 Solar cells	12
1.2 Absorber materials in thin film solar cells	13
1.3 The monograin growth technology and the use of flux in the synthesis of single crystalline powder materials.....	14
1.4 Monograin layer solar cells.....	15
1.5 Phase diagrams	17
1.5.1 Phase diagrams of binary precursor compounds.....	17
(Cu-S, Sn-S, and Zn-S).....	17
1.5.2 Quasi-binary phase diagrams.....	19
1.5.3 Quasi ternary and quaternary mixtures.....	21
1.6 Theoretical background of molten salt synthesis and the CZTS formation process in molten fluxes.....	24
1.7 Some limitations identified in the monograin growth process.....	25
1.8 Summary of literature review and aim of the current study.....	26
2. EXPERIMENTAL	28
2.1 Methodology, materials and sample preparation.....	28
2.2 Determination of thermal processes and their enthalpies.....	29
2.3 Preparation of samples for growth process studies	30
2.4 Instrumentation	31
3. RESULTS AND DISCUSSIONS	32
3.1 Synthesis and characterization of CZTS monograin powder in molten CdI ₂ ...	32
3.2 Impact of synthesis-growth conditions on the material properties.....	34
3.2.1 Impact of flux concentration and synthesis time on the grain size and yield of powders	34
3.2.2 Impact of flux amount and synthesis-growth time on grain morphology	35
3.2.3 Phase analysis by Raman.....	36
3.2.4 Compositional analyses by EDX	37
3.2.4.1 Cd concentration in CZTS powder crystals by EDX.....	37
3.2.4.2 Composition of synthesized powders by EDX.....	39
3.2.5 Activation energy of Cd incorporation to the CZTS crystals in the synthesis process.....	40
3.3 Studies of interactions of precursors with CdI ₂	41
3.3.1 Synthesis temperature of mixtures.....	41
3.3.2 CdI ₂	42
3.3.3 CdI ₂ +Cu ₂ S	43
3.3.4 CdI ₂ +SnS	45
3.3.5 CdI ₂ +ZnS	47
3.3.6 Mixture for synthesis of Cu ₂ SnS ₃ (CdI ₂ +SnS+Cu ₂ S+S).....	51
3.3.7 Mixture for synthesis of quaternary CZTS compound (CdI ₂ +SnS+Cu ₂ S+S+ZnS).....	53

CONCLUSIONS	56
ACKNOWLEDGEMENTS.....	58
KOKKUVÕTE	59
ABSTRACT.....	61
REFERENCES	63
Appendix A.....	71
Appendix B.....	99
Appendix C.....	111

LIST OF PUBLICATIONS

The thesis is based on the following papers, referred to in the text by Roman numerals

- I. **Nkwusi, G.**, Leinemann, I., Raudoja, J., Mikli, V., Kärber, E., Altosaar, M. Impact of growth-synthesis conditions on $\text{Cu}_2\text{Zn}_{1-x}\text{Cd}_x\text{SnS}_4$ monograin material properties. *Superlattices and Microstructures*, **98** (2016) 400-405; (1.1)
- II. **Nkwusi, G.**, Leinemann, I., Altosaar, M. The Processes and Enthalpies in Synthesis of $\text{Cu}_2\text{ZnSnS}_4$ in Molten CdI_2 . *International Advanced Research Journal of Science, Engineering and Technology*, **3** (2016) 113-119; (1.2)
- III. **Nkwusi, G.**, Leinemann, I., Raudoja, J., Mikli, V., Kauk-Kuusik, M. Altosaar, M., Mellikov E. (2014). Synthesis of $\text{Cu}_2(\text{ZnCd})\text{SnS}_4$ Absorber Material for Monograin Membrane Applications.– [CD-ROM] *MRS Proceedings 2014: 2013 MRS Fall Meeting. SCHOLARONE Manuscripts, (Symposium W – Next-Generation Inorganic Thin-Film Photovoltaics)*, 1638. (3.1)

AUTHOR'S OWN CONTRIBUTION

The contributions by the author in the papers I, II and III included in the thesis are as follows:

- I Raman and XRD sample preparation, quenching, sample washing and reporting of the results, major part of Raman measurement, plotting and analysis of the results, preliminary SEM-EDX measurements on a simple laboratory set-up, data analyses, and reporting/ interpretation of the results and major part of writing;
- II DTA, Raman and XRD data analyses, and reporting/ interpretation of the results, major part of thermodynamic calculations (ΔG) of the work with HSC program and major part of writing;
- III Sample preparation, quenching, sample washing for Raman, and XRD, reporting of the results of preliminary simple laboratory SEM-EDX measurements, data analyses, and reporting/ interpretation of the results, major part of Raman measurements, plotting and analysis of the results, analysis of XRD results and reporting, major part of writing.

LIST OF ABBREVIATIONS AND SYMBOLS

ΔH_f	-	enthalpy of formation
ΔG	-	change in Gibbs free energy
ΔH	-	change in enthalpy
ΔH_{fus}	-	enthalpy of melting, heat of fusion
a-Si	-	amorphous silicon
at.	-	Atomic
cc	-	centered cubic
c-Si	-	crystalline silicon
CCdTS	-	copper cadmium tin sulfide, Cu_2CdSnS_4
CIGSe	-	copper indium-gallium diselenide, $Cu(InGa)Se_2$
CISe	-	copper indium diselenide, $CuInSe_2$
CTS	-	copper tin sulfide, Cu_2SnS_3
CZTS	-	copper zinc tin sulfide, Cu_2ZnSnS_4
CZTSe	-	copper zinc tin selenide, $Cu_2ZnSnSe_4$
CZTSSe	-	copper zinc tin sulpho-selenide, $Cu_2ZnSn(SSe)_4$
DTA	-	differential thermal analysis
EDX	-	energy dispersive X-ray spectroscopy
g	-	gaseous phase
$h\nu$	-	energy of photon
<i>i</i>	-	intrinsic
ICDD	-	International Centre for Diffraction Data
J	-	Joule
JCDPS	-	Joint Committee on Powder Diffraction Standards
KS	-	kesterite
L	-	liquid phase
MGL	-	monograin layer
MS	-	mass spectroscopy
NREL	-	National Renewable Energy Laboratory
<i>p-n</i>	-	hole-electron
PCE	-	power conversion efficiency
PV	-	photovoltaic
SEM	-	scanning electron microscopy
T_b	-	boiling temperature
TCO	-	transparent conductive oxide
TG	-	thermogravimetric
T_m	-	melting temperature
UV	-	ultraviolet
W_p	-	Watt peak
wt.	-	weight

INTRODUCTION

Recently, research in the field of low-cost solar cells has become popular in many countries. High-efficiency copper zinc tin sulphide (CZTS) based solar cell have received huge attention due to the need to develop a more environmentally friendly solar absorber material with relatively abundant and non-toxic elemental components¹. Currently, one of the greatest limitations for large scale production of CZTS-based solar cells is the inability to reach efficiencies higher than the current record at 12.6%² made by the IBM company using the hydrazine-solution method. In 1988, *Ito et al.* reported first evidence of the PV effect of CZTS, using the thin film technology in which the active absorber material is a thin-film with a typical thickness of about 1 micrometer³. In 2007, an efficiency of 6.7% was reported. Till now, with more concerted efforts, the CZTS based solar cell has attained double efficiency, which is still far from the theoretical limit of 30%⁴. But unlike CZTS, other chalcogenides, such as Cu(InGa)Se₂ (CIGSe) and CdTe, have shown significant improvement in the device efficiencies (CIGSe 23.3% and CdTe 22.1% respectively⁵ within the last 30 years and have currently reached mass production⁶. This has posed serious questions on how to improve the efficiency of CZTS-type solar cells to reach a mass production level.

From a scientific and technical point of view, the development of new technologies with higher conversion efficiencies and low production costs are a key requirement for enabling the deployment of solar energy at a large scale. The technology of monograin layer (MGL) solar cell is an alternative to the thin film technology. It allows the separation of materials formation from module fabrication. Large-area modules of monograin membranes are fabricated at room temperature in a continuous roll-to-roll process. Homogeneous composition of monograin powders gives an additional advantage, leading to up-scaling of homogeneous modules^{7,8}. The best CZTS monograin layer solar cell has shown a conversion efficiency of 7.04% (active area 9.38%⁹). The monograin powder growth technology explores the use of suitable fluxes to aid the growth of single crystalline CZTS powders known as monograin powders¹⁰. In the monograin layer solar cell technology, a narrow size fraction of the powder grains, usually 30 to 100 μm , is embedded into a thin layer of the epoxy resin, forming a monolayer that serves as the light absorbing layer. As the synthesis of the monograin absorber material is carried out in molten flux, different fluxes (KI, NaI, CdI₂, and SnCl₂) have been used for the synthesis- growth¹⁰⁻¹². The shape, size and properties of powder particles are influenced by different factors: time, temperature, nature and amount of used flux salt. Also, some other low melting intermediate components formed during the heating up period of synthesis and before the used flux salt melts can influence the shape and size of formed powder crystals through sintering of initial precursor particles. However, the impact of growth-synthesis conditions of CZTS in molten CdI₂ on the CZTS monograin material properties (morphology, yield, Cd incorporation from CdI₂) have not been studied yet. Knowledge about the formation process, understanding of the

chemical reaction pathway and the fundamental thermodynamic properties of the material may give additional information about the reasons for the poor crystal quality sometimes encountered and other limitations of the material. In addition, the constituent elements of the used salts (for example, K, Na and I) growing into the crystals dope the semiconductor compound at the level of their solubility at the growth temperature. CdI₂ contains only iodine as foreign dopant, Cd incorporates into crystal lattice as a substitutional component of compounds belonging to the group I₂-II-IV-VI₄. In this case, it is possible to study the impact of cationic substitution in the CZTS monograin powder.

In this thesis, we present the results of studies on chemical reactions and the enthalpies leading to the formation of CZTS in molten CdI₂^{II}. Using different analytical methods – DTA, EDX, XRD, Raman, sieving and SEM – we have analyzed the reactions occurring in the separate mixtures of CdI₂ with individual binary precursor compounds (ZnS, SnS, and Cu₂S), and in the mixtures for synthesis of ternary Cu₂SnS₃ and quaternary Cu₂ZnSnS₄ compounds^{II}. Focus was also on the impact of preparation conditions (temperature, time, amount of CdI₂ in synthesis) on the growth process and on the quality of Cu₂ZnSnS₄ monograin powder crystals^I.

The thesis is divided into three parts. The first part provides the literature overview; the second part describes the materials and methods used in this work. The third part describes and reports the experimental results obtained. It is subdivided into three main subparts: the first section presents the results of the formation and growth of CZTS in the molten CdI₂ as flux^{III}. The second subsection presents the impact of preparation condition on the material properties^I. The last part reports the thermo-analytical studies of mixtures of CdI₂ with different precursors and results in the enthalpies of the reactions occurring in different systems, starting from the individual binary precursors in the flux, followed by mixtures for the formation of ternary and quaternary compounds^{III}. The results obtained and the conclusions of the work are summarized in the final part of the experimental section.

1. LITERATURE REVIEW

1.1 Solar cells

The history of solar technology is dated back to the 7th century Before Christ, where magnifying glass was used to concentrate the sun's rays to make fire and to burn ants^{13,14}. The starting point of the research and development of solar cells was set by the discovery of the photovoltaic (PV) effect by the French experimental physicist Al  xandre Edmond Becquerel in 1839¹⁵. In 1883, an American inventor Charles Fritts described the first solar cells made from selenium wafers^{6,17}. By 1905, Albert Einstein published his paper explaining the photoelectric effect on a quantum basis¹⁸. In the year 1954, Chapin *et al.*¹⁹ at Bell Labs invented and developed silicon single-crystalline solar cell with 6% efficiency and improved the efficiency up to 15%. Today, silicon-based cells, also known as monocrystalline silicon, (classified as first generation solar cells) still dominate the solar cell industry. Photovoltaics is the most efficient method to produce electricity from the sun. The world's record with an efficiency of 25.6% was set in 2014 for Si (crystalline) laboratory solar cell⁶ and 22.5% for commercially produced solar cells in 2010⁶. Other types of cells have been developed to add diversity in potential applications and also offer alternative options for low-cost PV cells. These alternative cells are based on different technologies, including the polycrystalline, the thin film and other emerging solar cell technologies, such as the monograin, quantum dot, and nanocrystals. For the thin film technology, the layers of semiconductor absorber materials are much thinner, only a few nanometers to tens of micrometers when compared to crystalline silicon, which is between 100- 500  m^{20,21}. They are made by depositing one or more thin layers (thin films) of photovoltaic material on a substrate. They are cheaper and inexpensive to make, but efficiency is lower when compared to the monocrystalline silicon-based technology. They also consume a larger area per watt produced. The efficiency loss can be compensated by the low cost of production. Currently researched thin film solar cells include: amorphous silicon (a-Si) and other thin-film silicon (TF-Si), Cadmium Telluride (CdTe), Copper Indium Gallium Selenide (CIS or CIGSe), Dye-sensitized solar cell (DSC), and Copper Zinc Tin Sulphide (CZTS) solar cell. The other types of cells are organic dyes and organic polymers that are deposited on supporting substrates. However, recent results reported cover advancements in the efficiencies and performance of copper zinc tin sulfide (CZTS), copper zinc tin selenide (CZTSe) and solid solutions of them (CZTSSe) for both thin film and monograin technology. But so far, no commercial production has been reached for these materials²²⁻²⁶.

1.2 Absorber materials in thin film solar cells

In the manufacture of solar absorber materials, despite the continued rapid cost reduction, concerns about material price and availability as well as toxicity have been raised. The high demand for indium used in copper indium gallium selenide (CIGSe) and the presence of cadmium as a major element in the case of CdTe have proved essential in the development of the current commercially available low-cost solar absorbers. $\text{Cu}_2\text{ZnSn}(\text{SSe})_4$ (CZTSSe) enables us to alleviate the material bottlenecks present in CIGSe and CdTe. CZTS offers favorable optical and electronic properties similar to CIGSe (copper indium gallium selenide). But unlike CIGSe and CdTe, CZTS is composed only of abundant and non-toxic elements. The desire for clean solar technology has been a major motivation for alternative thin film solar cell materials. The first CZTS was shown to exhibit photovoltaic (PV) effect in 1988³ and in 1997, a solar cell efficiency of 2.3% was recorded for CZTS with more progress every year^{27–32}. Conventionally, a solar cell absorber should be a direct bandgap semiconductor material with a bandgap of 1–1.5 eV^{33,34} and with a high optical absorption coefficient, i.e., greater than 10^4 cm^{-1} , long diffusion length, low recombination velocity, it should be able to form a good electronic *p-n* junction³⁵. The chalcopyrites are similar to the kesterite in some regards and thus a comparison of both materials can provide vital information on how to improve the efficiency of CZTS. For instance, I₂-II-IV-VI₄ quaternary compound $\text{Cu}_2\text{ZnSnS}_4$ (and related compounds) can be presented as CuInSe_2 (compounds of group I–III–VI ternaries), where indium, which is very expensive, has been replaced by Zn and Sn, which are cheap and readily available^{36,37}. In the Laboratory of Semiconductor Materials of Tallinn University of Technology, we use CZTS solar cell absorber material in the monograin layer (MGL) form where every grain functions (works) as a single solar cell. The problems of the grain boundaries appearing in the thin-film solar cell technologies do not exist in the MGL solar cell³⁸. The aim of the studies of the group of Tallinn University of Technology researchers started in 2008 is to create and commercialize modules of powder-based $\text{Cu}_2\text{ZnSn}(\text{S}_x\text{Se}_{1-x})_4$ (CZTSSe) MGL solar cells. The studies have continued in collaboration with the Tallinn University of Technology spin-off company *Crystalsol OÜ*. A pilot production line was set up in the research and development facility of *Crystalsol GmbH* in Austria³⁸.

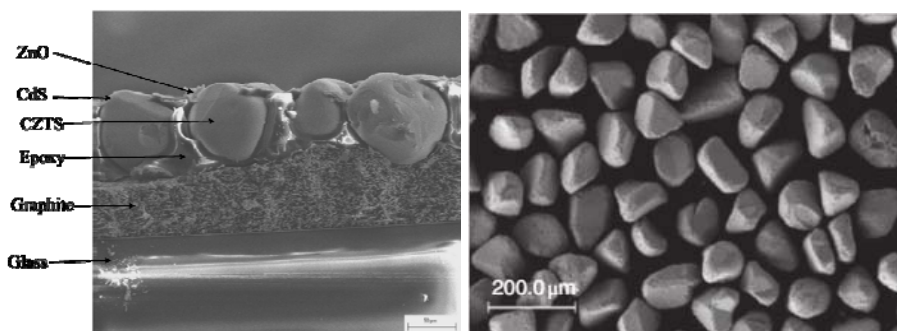


Figure 1. Cross-section of monograin layer solar cell structure (left) and SEM micrograph of an overview of $\text{Cu}_2\text{ZnSn}(\text{Se},\text{S})_4$ monograin powder synthesized in KI flux (size fraction 90-100 μm)³⁹.

1.3 The monograin growth technology and the use of flux in the synthesis of single crystalline powder materials

In the monograin technology, a solvent material is used to synthesize an absorber material usually referred to as flux material. The amount of the used flux material makes the main difference between monograin growth and sintering of the formed crystals in the thin film technology. In the thin film technology, a limited amount of the liquid phase (which allows the formation of contracting force between the crystals) (CuSe , $\text{Na}_2\text{S}(\text{Se})$) formed in the thin film production process helps to grow the initial larger absorber crystallites and sinter them into compact and continuous thin films^{38,40}. Meanwhile, in the monograin growth technology, it proceeds in the molten fluxes, which are present in an amount that fills all empty space between crystals and allows increasing the repulsive forces between crystals. In this case, initially formed crystals start to grow separate from each other and, as a result, single-crystalline powder forms. Since it is generally difficult to grow high-quality single crystals of the CZTS-type compounds from their melt due to the high melting temperature of the precursor materials, and because most of the compounds grow through a peritectic reaction or have a solid state phase transition during the cooling process⁴¹, the monograin technology helps to achieve this goal. The powder growth technology explores the use of suitable salts as fluxes to aid the growth of single crystalline CZTS powders known as monograin powders^{42,43} and by melting, the used salt creates a molten phase between the solid precursor particles. The molten phase between crystals helps to promote fast diffusion of constituent elements through the liquid phase and as compared to the thin film sintering process, a more homogeneous material can be produced. The driving force in the isothermal growth process of monograin materials is the difference in the surface energies of crystals of different sizes. The growth of single-crystalline powder grains takes place at temperatures higher than the melting point of the used flux material, but it could be much lower than the

melting point of the forming semiconductor compound. The role of the molten salts is to enhance the rate of solid state reactions due to much higher diffusion rates between reaction components in the molten media³⁸; to lower the reaction temperature; to increase the degree of homogeneity (the distribution of constituent elements in the solid product); to control the particle size and shape; and to control their agglomeration state. This melt acts as a contracting or as a repulsion agent depending on the amount of it. If a suitable solvent material is present in an amount sufficient for the repulsion of initial crystallites, it allows growing separate powder grains. This leads to the formation and growth of single-crystalline powder materials with uniform composition and narrow-disperse granularity known as monograin powders. Some important requirements for a flux material include:

- Low melting point - lower than the melting point of $\text{Cu}_2\text{ZnSnS}_4$;
- It should be stable, readily available, inexpensive and soluble in water – easily removable⁴⁴;
- It should have a low vapor pressure at the heating temperature and it should not cause undesirable reactions with either the reactants or the product;
- It should allow the possibility to control the composition of $\text{Cu}_2\text{ZnSnS}_4$ (not contain constituent elements of the compound);
- It consists of components that could improve the properties of $\text{Cu}_2\text{ZnSnS}_4$ (as dopants)^{38,39}.

To improve the quality of the grains used in solar cells, different salts (KI, ZnI_2 , CdI_2 and NaI) have been studied as fluxes⁴³. Each of these flux materials has one advantage to be considered over the others. For instance, KI is not highly hygroscopic, with high melting temperature (686 °C)^{45,46} NaI is more hygroscopic than KI⁴⁴, but with a lower melting temperature (651 °C)⁴⁷. CdI_2 has a low melting temperature (387 °C)^{48,49} and is much less hygroscopic compared⁵⁰ to NaI and KI but concerns may be raised with respect to the amount of Cd present after synthesis.

1.4 Monograin layer solar cells

The history of monograin membrane technology is dated back as far as the 1960s when Ties Siebold te Velde from the Philips Company filed the first patent in 1965 on monograin layers, mainly of II-VI group compounds, using already a *p-n* junction. During the next year, they filed the first patent on monograin membrane devices⁵¹. The first patent of researchers of TTÜ for using monograin powders as solar cell absorbers “Monocrystalline powder and monograin membrane production” was filed in 1998 (WO9967449, priority date June 25, 1998) by M. Altosaar, D. Meissner, and E. Mellikov⁸. In their work, monocrystalline absorber crystals were synthesized and the formed powder grains were grown in the molten phase of a suitable flux salt. The resultant monograin powder was used in PV solar cells as absorber material in the monograin layer (MGL) form. The MGL

solar cell combines the features of a monocrystalline solar cell and a thin film solar cell.

In the MGL design, each *p-type* single crystal of an absorber covered with a thin layer of *n-type* material (usually CdS, deposited by chemical solution deposition before making membrane) works as an individual solar cell. To make a monograin membrane, grains of known size are embedded into a thin layer of epoxy resin (or some other polymer) to avoid the coverage of the upper surfaces of crystals with a polymer to form a monolayer. Narrow size fractions of the powder grains separated by sieving from powder grains (usually with diameter between 30 to 100 μm) are used for a membrane. The polymer film thickness is adjusted to half of the grain size. This implies that for a perfect monograin layer, the shape of the grains is very important. Spherical grains give a higher possibility to form a perfect monolayer and prevent stacking of grains when compared to the grains with tetrahedral pyramidal structure, which could give higher packing density⁸. After polymerization of epoxy, the CdS layer is deposited onto the front side of the monograin layer, followed by a ZnO window layer by RF-sputtering and then glued onto the glass. After glueing the structures on glass, the back contact area of crystals is opened by etching epoxy with H_2SO_4 , followed by an additional abrasive treatment. The back contact is made using graphite paste. The final solar cell structure is graphite/CZTS/CdS/ZnO (see Figure 2). Currently, CZTS monograin layer solar cells have shown power conversion efficiency of about 9.38% (calculated from the active area of the solar cell)^{9,39}.

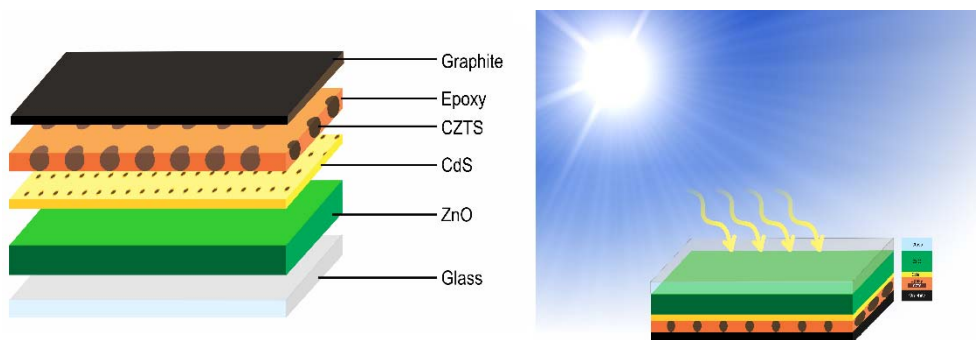


Figure 2. Scheme of monograin layer solar cell structure: graphite/CZTS/CdS/ZnO on glass (or a polymer encapsulation can be used).

1.5 Phase diagrams

The T-x phase diagrams provide information about the phases in the equilibrium state at certain temperatures depending on the composition of its component materials. In our system, CZTS is synthesized using three binary precursors (Cu_xS , SnS , and ZnS) and elemental sulphur in a molten flux to achieve the desired deviation from stoichiometry under experimentally clarified Cu-poor and Zn-rich growth conditions. Previous studies including those by the research group of Tallinn University of Technology have already demonstrated the complexity of the phase diagram of CZTS⁵² but a good understanding of the currently available information will help to guide our work and provide a better understanding of the results obtained. According to previous work by Nagoya *et al.*, the first-principles studies of the phase stability and defect formation in $\text{Cu}_2\text{ZnSnS}_4$ showed that CZTS is thermodynamically stable for a small confined domain of chemical potentials. It means that a slight deviation in the optimal growth conditions will result in the formation of secondary phases⁵³. This section gives a general overview of the phase diagrams of the used binary precursors, formed ternary CTS and quaternary CZTS compounds.

1.5.1 Phase diagrams of binary precursor compounds (Cu-S, Sn-S, and Zn-S)

In the synthesis of CZTS in CdI_2 starting from the binary precursors Cu_2S , SnS , ZnS and S , we studied the thermal behavior of each individual compound by using phase diagrams as comparable material. Cu_2S , ZnS and SnS_2 melt congruently at 1130 °C, 1700 °C and 860 °C, respectively, with very narrow homogeneity regions⁵⁴. Figure 3 presents the phase diagram of Cu-S and Sn-S. The phase diagram of Cu-S shows that at low temperature, copper sulphide may occur in different phases, such as the monoclinic low α - chalcocite (αCh), hexagonal high temperature-chalcocite (βCh), and covellite (Cv) (CuS). The covellite goes through peritectic transformation to digenite with deliberation of S and is stable up to 507 ± 2 °C⁵⁵. The hexagonal high temperature-chalcocite (βCh) is stable from 103.5 ± 0.5 °C at the Cu-rich limit of stoichiometric Cu_2S , and also from 93 ± 2 °C to 435 °C at 33.44 at.% S to 33.34 at.% S. There is cubic γ -modification at temperatures above 435 °C. ZnS is a well-known wide-gap semiconductor (3.6 eV) of *n*- type conductivity⁵⁶. It exists both in the zinc-blende structure and in the wurtzite structure with the phase transition zinc blende \leftrightarrow wurtzite occurring at 1020 °C⁵⁷. For a SnS system, it is known that the S-Sn system contains four solid solution phases: (a) the four elemental solid phases (α -S, β -S, α -Sn and β -Sn) where α -, β - are low-temperature and high-temperature phases of the elements, respectively; (b) the liquid and the intermediate compounds of Sn-S that contain: (1) the low-temperature α -phase, (2) B16 spatial group Pbnm (α - SnS), (3) high-temperature β -phase with type II lattice B33 and (4) the spatial group Cmcm (β -SnS); (c) a gas phase of SnS, Sn_2S_3 , and SnS_2 ⁵⁸ and (d) allomorphs⁵⁹. The

elasticity of SnS vapor showed that the melting point of SnS in a neutral atmosphere is 880 °C, and the boiling point at normal air pressure is 1230 °C. The maximum melting point of 881 °C was found for SnS at sulfur pressure $3.34 \times 10^3 \text{ Pa}$ ⁵⁸.

All the binaries melt at a very high temperature^{59,60}, as compared to the melting temperature of the flux material (CdI_2). The compounds existing in Cu-S, Zn-S and Sn-S binary systems and their thermal stability regions, crystal structures, XRD cards, and Raman data are presented in Table 1.

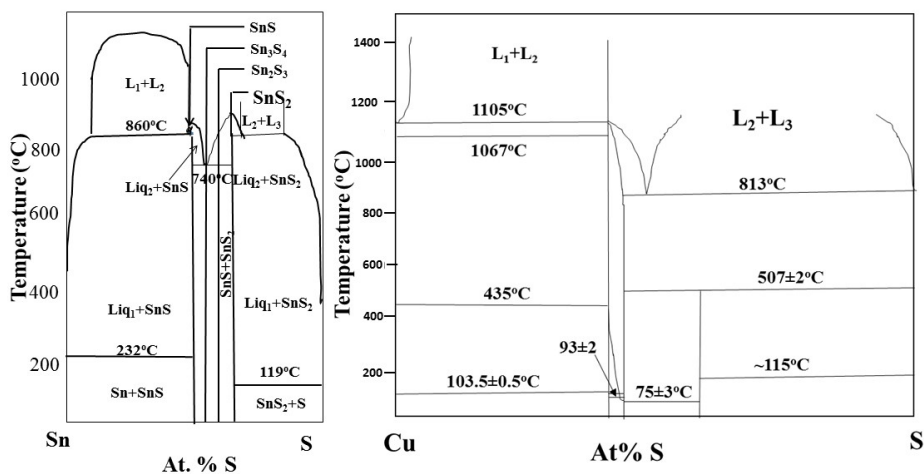


Figure 3. Phase diagram of (a) Sn-S system, (b) phase diagram of Cu-S system adopted from^{55,58,59}.

Table 1. Compounds in Cu-S, Zn-S and Sn-S binary systems

Compound Formula	Mineral name	Stability area (°C)	Crystal structure/ space group	XRD ICDD file no	Raman peaks (cm ⁻¹)
CuS	Covellite	T < 507	hexagonal	06-0464 75-2233	474 ⁶³⁻⁶⁵
Cu ₂ S	Low-temp. Chalcocite	0 < T < 104	orthorhombic	23-0961 73-1138	257,478,4 65
	High-temp. Chalcocite	90 < T < 435	hexagonal	84-0206	264, 475 ⁶⁶⁻⁶⁸
Cu _x S	Digenite (Cu1.86-1.80S)	72 < T < 1130	rhombohedral	47-1748 84-1770	259,264,4 66,475 ^{68,6} 9
	Djurleite (Cu1.95-1.91S)	T < 93	orthorhombic	42-0564 83-1463	
	Anilite (Cu1.75-1.65S)	T < 75	orthorhombic	72-0617	
ZnS	Wurtzite	T < 1020	hexagonal	79-2204	275,352 ⁶⁷
	Sphalerite	T > 1020	cubic	05-0566 71-5975	
SnS	Herzenbergite	T < 602	orthorhombic		96,163, 186,220,2 88 ^{60, 69, 70}
		T > 602	<i>Pnma</i>		
Sn ₂ S ₃	Ottemanite		<i>Pnma</i>	75-21830	52, 60, 307 ^{61,72}
SnS ₂	Berndtite		Hexagonal an extended R3 ⁻ polytype <i>P3m1</i>	23-0677 83-1705	312 ^{61,70,71}

1.5.2 Quasi-binary phase diagrams

The studies of the interaction between Cu₂S, SnS and ZnS in CdS showed that the solubility of Cu₂S in CdS at eutectic point (1011 °C) is 55 mol% CdS and decreases to 40 mol% CdS at 915 °C and 10 mol% at 555 °C⁵⁴. In the case of a SnS-CdS system, the SnS₂-CdS system is also an eutectic type with eutectic point coordinates at 22 mol% CdS at 770 °C. Two different studies by Piskach *et al.* showed the formation of different compounds (CdSn₂S₅, CdSn₃S₃ and Cd₂SnS₄)⁶². The ZnS-CdS phase diagram was studied by Ballantyne and Ray *et al.*⁷³. They

found the formation of solid solutions over the complete range of compositions in sphalerite (sph), wurtzite (wu) and greenockite (grn) structure (the melting point of CdS is 1750 °C). And there exist equilibria between the zinc blende and wurtzite $Cd_xZn_{1-x}S$ solid solutions formed⁷⁴⁻⁷⁶. In the Cu_2S –Zn(Cd)S system, the maximum solubility of ZnS in Cu_2S was 42 mol% of ZnS at the peritectic temperature at 1185 °C with limited solubility in the solid state⁵⁴, but it decreases as the temperature falls to less than 1 mol% ZnS at 397°C^{77,78}. In the phase diagram of Cu_2S – SnS_2 system (Figure 4), the liquidus line starts at the melting point of Cu_2S at approximately 810 °C and decreases down to the first eutectic point at $T_{eut1}=800$ °C and ends at the melting point of SnS_2 at 865 °C. At the first eutectic point, Cu_4SnS_4 , Cu_2S , liquid and vapor phase in equilibrium. The eutectic composition denotes the lowest possible solidification and melting temperatures in the sub-system Cu_4SnS_4 – Cu_2S ⁷⁷.

According to Fiechter *et al.* and Olekseyuk *et al.*, four stable ternary phases of CTS; $Cu_4Sn_3S_8$, Cu_4SnS_4 , Cu_2SnS_3 and $Cu_2Sn_3S_7$ exist, three of these ternaries Cu_4SnS_4 , Cu_2SnS_3 and $Cu_2Sn_3S_7$ form in the Cu_2S – SnS_2 section and their melting point was determined as 833, 860 and 803 °C, respectively^{54,77}. $Cu_2Sn_3S_7$ is stable only at 685 °C, other ternaries are stable at room temperature. They were characterized by four eutectic points and a series of solid–solid phase transitions for $x > 50$ mol% SnS_2 with a wide homogeneity range of $Cu_2Sn_{3+x}S_{7+2x}$ at elevated temperatures and a polymorphic transformation of the ternary compound Cu_2SnS_3 found at 780 °C^{77,79}. Cu_2SnS_3 can be formed from two eutectic sections $L \rightleftharpoons Cu_2SnS_3 + \alpha$ and $L \rightleftharpoons Cu_2SnS_3 + \gamma$ at 820 and 788 °C, respectively. In addition, the quasi-ternary system Cu_4SnS_4 and $Cu_2Sn_4S_9$ were formed by $\alpha + Cu_2SnS_3$ at 810 °C and $Cu_2SnS_3 + \gamma$ at 670 °C, respectively, where α and γ are Cu_2S and SnS_2 , respectively (Figure 4). The solubility of (Cu_2S – SnS_2) is minor and does not exceed 5 mol% of either one. Cu_2S undergoes polymorphic transformations at 383 and 108 °C as Cu_2S : $\alpha \rightleftharpoons \alpha' + Cu_4SnS_4$ and $\alpha' \rightleftharpoons \alpha'' + Cu_4SnS_4$, where α , α' and α'' and low, medium and high-temperature phases of Cu_2S . In the ZnS – SnS_2 system, the studies by Nekrasov *et al.* and G.H. Moh *et al.* reported in^{80,81} showed that ZnS – SnS_2 is a quasi-binary section of a ternary system with no ternary phases formed in the system. The eutectic point coordinates were found to be 2.5 mol% ZnS at 800 °C and the solubility does not exceed 1 mol% of ZnS in SnS_2 and 5 mol% of SnS_2 in ZnS. In the formation of CZTS, ZnS – SnS_2 was observed as the limiting side of the reaction⁵⁴.

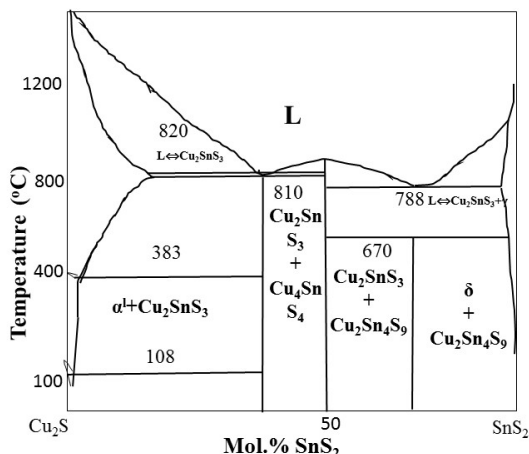


Figure 4. Summary of the phase diagram of the Cu_2S – SnS_2 system; α and γ are Cu_2S and SnS_2 , respectively⁸².

1.5.3 Quasi ternary and quaternary mixtures

The study of the phase diagram of Cu_4SnS_4 – CdS by Olekseyuk and Piskach revealed the formation of the quaternary compound $\text{Cu}_2\text{CdSnS}_4$ that melts congruently at 905 °C⁶². A eutectic section is formed between Cu_2SnS_3 and $\text{Cu}_2\text{CdSnS}_4$ at 853 °C and 15 mol% CdS . The various transitions and phases formed were reported in⁶². At various compositions of mixtures of Cu_2S – SnS – CdS , different quaternary phases ($\text{Cu}_2\text{CdSn}_3\text{S}_8$, $\text{Cu}_2\text{CdSnS}_4$, $\text{Cu}_2\text{CdSn}_4\text{S}_9$) were formed with their character and temperatures reported in⁶². The quasi-ternary Cu_2S – CdS – SnS_2 system is separated into two quasi-ternary subsystems Cu_2S – Cu_2SnS_3 – CdS and CdS – Cu_2SnS_3 – SnS by the quasi-binary Cu_2SnS_3 – CdS .

In the Cu_2SnS_3 – ZnS system (Figure 5), a quaternary compound, $\text{Cu}_2\text{ZnSnS}_4$, forms in it at 980 °C by the peritectic reaction $\text{L} + \beta \rightleftharpoons \text{Cu}_2\text{ZnSnS}_4$ (where β is the solid solution range of the low-temperature modification of ZnS). According to⁵⁴, the study of an isothermal section of Cu_2S – ZnS – SnS_2 at 397 °C showed the formation $\text{Cu}_2\text{ZnSn}_3\text{S}_8$ quaternary compound. $\text{Cu}_2\text{ZnSn}_3\text{S}_8$ is formed by the reaction $\text{SnS}_2 + \text{Cu}_2\text{ZnSnS}_4 \rightleftharpoons \text{Cu}_2\text{ZnSn}_3\text{S}_8$ at 697 °C. At 670 °C, a ternary compound $\text{Cu}_2\text{Sn}_4\text{S}_9$ forms in the quasi-binary section of Cu_2S – SnS_2 by the peritectoid reaction $\text{Cu}_2\text{SnS}_3 + \text{SnS}_2 \rightleftharpoons \text{Cu}_2\text{Sn}_4\text{S}_9$. The formation of $\text{Cu}_2\text{Sn}_4\text{S}_9$ causes the existence of a plane at 660 °C in the quasi-ternary phase diagram of Cu_2S – SnS_2 – ZnS system, which corresponds to the reaction $\text{Cu}_2\text{SnS}_3 + \text{SnS}_2 + \text{Cu}_2\text{ZnSnS}_4 \rightleftharpoons \text{Cu}_2\text{ZnSn}_3\text{S}_8 + \text{Cu}_2\text{Sn}_4\text{S}_9$.

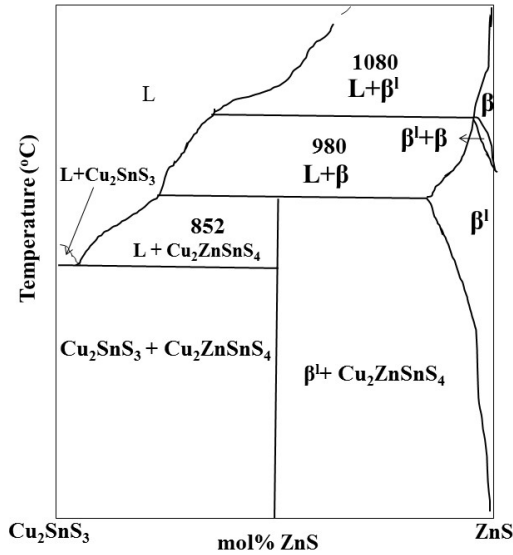


Figure 5. Phase diagram of various quasi ternary mixtures of CTS+ZnS where β and β^l are high-temperature and low-temperature ZnS, respectively.

In Figure 6, considering the Cu₂S–A section (A=50 mol% ZnS and 50 mol% SnS₂)⁵⁴, the liquidus consists of three lines that limits the field of primary crystallization of the α -solid solution. The lines are 880 and 790 °C, which correspond to ternary peritectic reactions $L+\beta^l\leftrightarrow\alpha+\delta$ and $L+\beta^l\leftrightarrow\delta+\gamma$, respectively and at 697 °C where Cu₆Sn₃S₈ is formed (given that α , β , β^l , γ and δ are Cu₂S, LT-ZnS, HT-ZnS, SnS₂ and Cu₂ZnSnS₄, respectively) and at 697 °C where Cu₆Sn₃S₈ is formed. The single phase region δ is limited by the three phase region $L+\beta^l+\delta$, and the line between them is two-phase $\beta^l+\delta$ homogeneity region of the δ -solid solution, which has a tendency to increase slightly with temperature (see Figure 6). The SnS₂–B section (B=50 mol% ZnS, 50 mol% Cu₂S) also contains three horizontal lines that correspond to ternary peritectic reactions similar to Cu₂S–A section (A=50 mol% ZnS, 50 mol% SnS₂) at 697, 790 and 880 °C. The quaternary compound Cu₂ZnSnS₄ has a homogeneity region of 3 mol% of either initial component at 733 °C. Further away from this point and 733 °C, the field apart breaks into the two two-phase fields; $\gamma+\text{Cu}_2\text{ZnSn}_3\text{S}_8$ and $\text{Cu}_2\text{ZnSn}_3\text{S}_8+\delta$, which is caused by the formation of Cu₂ZnSn₃S₈. In the Cu₄SnS₄–Cu₂ZnSnS₄ section, the crystallization of the alloys terminates in the ternary peritectic reaction $L+\text{Cu}_2\text{SnS}_3\leftrightarrow\text{Cu}_4\text{SnS}_4+\delta$ at 807 °C and the solubility based on Cu₂ZnSnS₄ is less than 5 mole% of Cu₄SnS₄. Considering the Cu₂Sn₄S₉–ZnS section, the liquidus of the Cu₂Sn₄S₉–ZnS section consists of lines that correspond to the fields of primary crystallization of the γ -, δ -, β^l - and β -solid solutions and the secondary crystallization that ends at 763 °C in a ternary eutectic reaction. In the sub-solidus region, the phase equilibria are caused by the formation of Cu₂Sn₄S₉ on the side

and of $\text{Cu}_2\text{ZnSn}_3\text{S}_8$ within the concentration triangle. Investigation of the Cu_2S - ZnS - SnS_2 pseudo-ternary system showed that the single-phase Cu_2ZnSn_4 is present only within a rather narrow range of compositions^{54,83}. Theoretically, even a 2-3% compositional variation could lead to phase separation. The CZTS compound exists under the line between Cu_2Sn_3 and ZnS ⁸⁴. Table 2 shows Raman and XRD data for our materials.

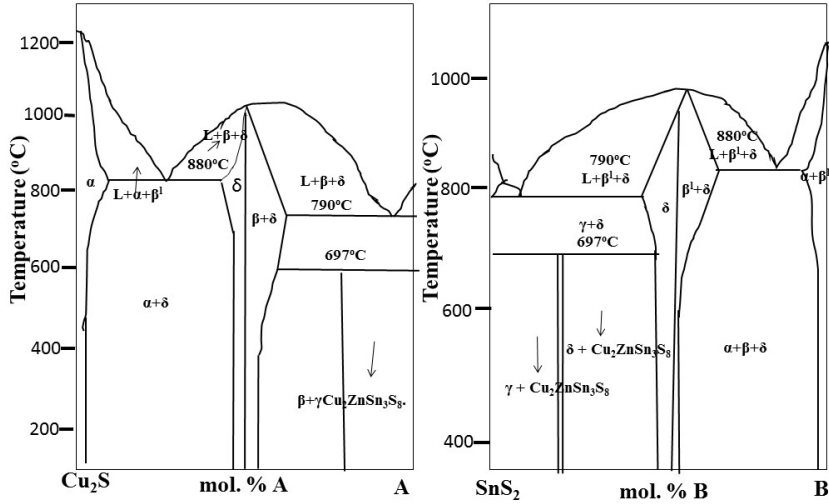


Figure 6. The phase diagram of Cu_2S -A (A-50 mol% ZnS , 50 mol% SnS_2) and SnS_2 -B (B-50 mol% ZnS , 50 mol% Cu_2S) where α , β , β' , γ and δ are Cu_2S , LT- ZnS , HT- ZnS SnS_2 and Cu_2ZnSn_4 , respectively.

Table 2. Compounds existing in Cu-S, Zn-S and Sn-S binary systems

Compound formula	Mineral name	(°C)	Crystal structure/ space group	XRD	Raman peaks (cm^{-1})
Cu_2SnS_3	Mohite	-	Monoclinic	04-010-5719	290, 352, 314, 374 ^{71,85}
		T > 400	Cubic	89-2877	267, 303, 356 ^{66,67}
		T < 400	Tetragonal	89-4714 ⁸⁶	297, 337, 352 ^{66,67}
CZTS	Kesterite	>500 ⁸⁷	Tetragonal	26-0575	68, 82, 97, 140, 164, 255, 263, 271, 287, 302, 316, 338, 347, 353, 367, 374 ^{88,89}

1.6 Theoretical background of molten salt synthesis and the CZTS formation process in molten fluxes

Kesterite structured $\text{Cu}_2\text{ZnSnS}_4$ (CZTS) (and other compounds of this group) as absorber for a solar cell is a promising semiconductor for low-cost and sustainable energy production^{23,90}. As reported earlier, different molten salts (fluxes) have been used in ceramics as additives to enhance the rates of solid state reactions for a long time⁹¹. In this case, the amount of salt is small, typically a few percent of the total weight. The small amount of flux helps to sinter together and grow solid crystals (particles) in the thin film technology also³⁸. In contrast, in the molten salt synthesis, a large amount of salt is used as the solvent to control powder characteristics (size, shape, etc.). In this sense, the molten salt synthesis is different from the flux method, which uses the salt as an additive to enhance the reaction rate. Salt with a low melting point is added to the reactants and heated above the melting point of the salt. The molten salt acts as the solvent. In many cases, the formation reaction occurs in the presence of solid reactant particles. In this sense, molten salt is somewhat different from ordinary solvents, which dissolve all reactant particles and the product particles precipitate from a homogeneous liquid phase⁹¹.

The role of flux material makes the main difference between the monograin growth (solid precursor particles are surrounded with a large amount of molten flux that allows growth of individual crystals and no sintering together) and the thin film synthesis methods (limited amount of flux helps to sinter individual crystals together, forming a solid film). In the isothermal crystalline growth process of monograin materials, the driving force is the differences in the surface energies of crystals of different sizes. The growth of single-crystalline powder grains takes place at temperatures higher than the melting point of the used flux material, i.e., much lower than the melting point of the semiconductor compound. An optimal amount of the used flux material is observed if the volume of the liquid phase is about 0.7 of the volume of the solid phase⁹². As the monograin powder growth is carried out at high temperatures in a molten salt, the semiconductor compound crystals are doped with the constituent elements of the used salts (KI, NaI) at the level of their solubility at the synthesis temperature. On the other hand, the used precursor compounds and the formed CZTS dissolve in the molten flux to some extent. The solubility of precursor compounds in KI was determined by I. Klavina *et al.*¹⁰ as follows: 3.6 mol% CuSe, 0.27 mol% SnSe and 0.086 mol% ZnSe at $T=740$ °C. The solubility of $\text{Cu}_2\text{ZnSnSe}_4$ in KI was determined as 0.61 mol%. In addition, the doping of the synthesized monograin powder with Na and K, also with Cl, has a rather strong influence on the monograin absorber material properties^{93,94}. On the contrary, use of CdI_2 as a flux in monograin powder growth allows us to produce a material without K (Na) doping and allows further possibilities to study the influence of intentional Na and/or K doping of CZTS. K. Timmo *et al.* showed that the solubility of the synthesized material in the flux affects the shape of growing grains⁹⁵.

In the monograin technology (MGT), the growth process is carried out in a closed ampoule and proceeds via isothermal conditions with the flux salt being saturated by precursors and the formed compound. The dissolution and crystal growth processes go on simultaneously; the smaller crystals dissolve in the flux and deposit onto surfaces of larger crystals through mass transport (diffusion) in the molten phase that surrounds every crystal. The dissolution is more intensive in places where the surface energy is higher (grain borders, tips) and deposition on plain surfaces (facets). Increasing the solubility of the formed compound in the flux (by increasing the temperature or by using a flux material that permits higher solubility), the dissolution process can prevail and the border of crystals takes more rounded shape. At equilibrium, the dissolution-deposition rates are equal to each other and crystals tend to attain equilibrium shape. The equilibrium can be related to the volume of the growth solution and the time of growth^{96,97}. In the review paper of M. A. Lovette *et al.*⁹⁷, the formation of a solid polyhedron with volume V from a fluid phase was described by Gibbs-Thomson for the change of free Gibbs energy ΔG . Although Gibbs was the first to develop the criteria for equilibrium crystal shapes, he recognized that crystal shapes are usually determined by kinetics rather than by thermodynamics alone. In the synthesis-growth process, solid, powdery precursors are used⁹⁵. They have different solubility in molten salts, which is comparatively low. When the mixtures are heated up and the molten phase starts to form but the dissolution of solids in the liquid flux has not reached the equilibrium state, the primary solid particles can sinter together. When the amount of liquid phase increases, it could penetrate into capillaries, repelling the weakly joined particles from each other.

1.7 Some limitations identified in the monograin growth process

Current information about the chemical reaction pathway leading to the formation of CZTS in molten salts is limited. According to Jackson *et al.*, CZTS is thermodynamically stable with respect to its component elements⁵². Studies have already demonstrated the complexity of its phase diagram and the possibility to form multiple secondary phases which may be due to incomplete reaction or partial decomposition of the material at certain reaction conditions, such as temperature, pressure and synthesis time. It was previously reported that in CZTS thin film growth by the vacuum evaporation method, CZTS began to decompose intensively at a temperature above 500 °C under sulfur pressure of 10^{-2} Pa, also with some SnS evaporation at temperatures as low as 350 °C⁹⁸ according to equations (1) and (2). This report showed that the partial pressure of sulphur is critical in the region 10^{-4} mbar (10^{-2} Pa) and sufficient SnS vapor can prevent irreversible evaporation⁸⁷.



Another significant finding by Scragg *et al.* was the gain in the configurational entropy caused by high-temperature annealing (≥ 500 °C), which leads to significant cation disorder⁹⁹. Furthermore, there is no adequate information about the route to the formation of CZTS in molten flux. Fundamental thermodynamic properties of the material are not well understood. The presence of secondary phases on the surface of grown absorber material crystals is still a major setback because it can lower the final output parameters of a solar cell and be detrimental to solar cell efficiency. For instance, zinc sulfide (ZnS) is a stable binary phase with a high negative enthalpy of formation of 205 kJmol^{-1} and has a much larger bandgap than CZTS. ZnS separate phase leads to the formation of internal barriers in thin films, which are expected to degrade the solar cell performance¹⁰⁰. In their study¹⁰¹, Qin Li *et al.* reduced experimentally the band gap of ZnS from 3.1 to 2.3 eV by the formation of $\text{Zn}_{1-x}\text{Cd}_x\text{S}$ ¹⁰¹. For CIGS solar cells, the band gap of 1.1~1.13 eV is considered to be optimum. In CZTS, the band gap is 1.3-1.5 eV¹⁰²⁻¹⁰⁴. Jie Fu *et al.*¹⁰⁴ suggested that the ideal way to reach the optimum band gap level would be to reduce the S content by introducing some selenium in the synthesis process or by the metal cation substitution process. In their work, they incorporated successfully about 5% of Cd into the host lattice of CZTSSe to form a homogeneous $\text{Cu}_2\text{Zn}_{1-x}\text{Cd}_x\text{Sn}(\text{SSe})_4$, which improved the crystal growth process, lowered the band gap (1.12 eV) and improved the solar cell efficiency from 5.41 to 8.11 %¹⁰⁴. This result was also confirmed by Sun *et al.*¹⁰² where the solar cell efficiency was increased from 5.3 to 9.8 %. The exchange of Zn with Cd helps to reduce the formation of Cu_{Zn} and Zn_{Cu} antisite defects which form due to the similar ion radii of Cu and Zn¹⁰⁴. And finally, the substitution of Zn with Cd also helps to reduce the narrow single-phase region of CZTS¹⁰⁵. As part of the efforts to improve CZTS solar cell efficiency, new strategies are needed to produce a more homogeneous material and minimize secondary phases. An understanding on how to resolve the aforementioned limitations could help to explain the formation process and to understand the properties of the as-grown monograin powder. This adds weight to the study of the reactions path and mechanism for the formation of CZTS.

1.8 Summary of literature review and aim of the current study

From the review of literature, the following main observations can be presented:

1. The direct band gap of 1.45-1.5 eV, large absorption coefficient 10^4 cm^{-1} , and abundant and nontoxic constituent elements make CZTS attractive as an absorber material for solar cell application. CZTS thin film technology has been overtaken and developed from the technology of CIGSe, but the non-vacuum methods developed lately are even more efficient, reaching the CZTSSe solar cell efficiency with tuned band gap material up to 12.6 %.
2. Monograin technology allows us to produce absorber materials in single crystalline powder form and to use monograin membrane layers made

from these powders in solar cell structures where each grain can work as a single crystalline solar cell. So far, 9.5 % of certified efficiency has been reached for $\text{Cu}_2\text{ZnSn}(\text{SeS})_4$ monograin layer solar cells.

3. Previous reports have shown that quaternary selenide CZTSe in monograin powder form can be synthesized in different flux materials, such as KI ($T_m=686\text{ }^\circ\text{C}^{106}$), NaI ($T_m=661\text{ }^\circ\text{C}^{107}$), and CdI_2 ($T_m=387\text{ }^\circ\text{C}^{108}$). CdI_2 can be used as a low-temperature flux, allowing the formation of CZTSe at much lower temperatures than in KI and NaI.
4. According to I. Leinemann *et al.*, the formation process of $\text{Cu}_2\text{ZnSnSe}_4$ takes place in NaI and KI fluxes and the chemical interactions between the binary precursor compounds CuSe, SnSe, ZnSe in molten NaI and KI in vacuum ampoules but not for CdI_2 . It was shown that monograin powders of $\text{Cu}_2\text{ZnSnSe}_4$ with tailored chemical composition could be synthesized and the powder crystals can be grown by isothermal heating of initial binary compound precursors in molten KI. In conclusion, they found that NaI as a flux material is preferable due to the possibility to reduce the synthesis temperature, but the issue of hygroscopicity of NaI is a drawback. KI is a good choice but it has a high melting temperature^{11,12}.
5. Recent studies have shown that the metal cationic substitution of Cd with Zn could help improve the efficiencies of CZTSSe solar cells^{102,109,110}. In studies where Zn is partly replaced with Cd, the bandgap shifting to the lower energy side occurs^{104,111,112}, enabling better fitting of the solar cell absorber material with the solar spectrum.

However, the formation pathway of $\text{Cu}_2\text{ZnSnS}_4$ in molten CdI_2 is still unexplored and the chemical interactions of precursors with molten CdI_2 are unclear. Neither has the impact of growth-synthesis conditions of CZTS in CdI_2 on the CZTS monograin material properties been studied.

Therefore, the aim of the present thesis is:

- to study the formation of CZTS crystals in molten CdI_2 in closed vacuum ampoules starting from binary compound precursors (ZnS, SnS, Cu_2S , S) and to describe the chemical pathway;
- to find out and describe the physical and chemical processes occurring in the thermal heating of CdI_2 with individual precursor compounds, also in the mixture of CdI_2 with precursors for synthesis of ternary CTS and quaternary CZTS compounds in closed vacuum ampoules;
- to study the influence of growth process conditions on the CZTS monograin material properties by using prolonged heating durations and increased flux concentrations at different temperatures on the shape of the crystals, on the Cd content in product crystals and on the yield of useful size fractions of the grown monograin powders.

2.0 EXPERIMENTAL

This section presents the experimental procedures for this work in brief. Comprehensive details are reported in the publications given in Appendix A.

2.1 Methodology, materials and sample preparation

In this thesis, the chemical interactions between the used precursor compounds and CdI_2 as a flux material in the synthesis of CZTS were studied [II, III]. The investigations of mixtures of CdI_2 with individual binary compounds (Cu_2S , ZnS , and SnS) and S were followed by studies on more complicated mixtures for synthesis of Cu_2SnS_3 (CTS) and $\text{Cu}_2\text{ZnSnS}_4$ (CZTS). We started with the determination of temperatures and enthalpies of possible reactions or phase changes by the differential thermal analysis (DTA) in CdI_2 /precursor mixtures of 0.25g, where the ratio of CdI_2 /precursor was kept at the ratio 1:1. DTA studies were performed in vacuum-sealed quartz ampoules adopted for the used DTA set-up. For DTA calibrations, the same flux salt CdI_2 was used as reference material because the traditionally used reference materials were not stable in contact with quartz ampoules or gave a very weak signal. After that, to determine the processes accompanied with thermal effects, we prepared individual samples for every thermal effect detected by DTA and heated them for prolonged time (4 hours) at temperatures a little above the recorded effect and quenched. Then the phase composition of these larger samples was analyzed by Raman spectroscopy, by X-ray diffraction (XRD) and by energy dispersive X-ray spectroscopy (EDX) and the changes in the phase compositions were found by comparison. The scheme of the sequence of experimental work is given in Figure 7.

The probability of possible chemical reactions was evaluated by the calculations of Gibbs free energy change using "Database of HSC Chemistry Ver. 6.0". All used binary precursor materials (Cu_2S , SnS and ZnS) for CZTS were self-synthesized, starting from high purity (99.999%) elements (MERCK) in evacuated quartz ampoules. Before using the binary compounds for the experiments, their composition was controlled by XRD, Raman and EDX analysis methods. CdI_2 (>99%) was purchased from Sigma-Aldrich company. Composition of precursor material mixtures was taken into consideration to have the quaternary compound with the final composition $\text{Cu}_{1.85}\text{ZnSnS}_{3.85}$ that is characterized by molar ratios: $\text{Cu}/(\text{Zn}+\text{Sn})=0.92$, $\text{Zn}/\text{Sn}=1$ and $\text{S}/\text{metals}=1$ to result in Cu-poor composition. Flux material and precursors (in mass ratio 1:1) were mixed by grinding in an agate mortar, sample mixtures were degassed and encapsulated into quartz ampoules. Separate mixtures of every individual precursor with flux: ($\text{Cu}_2\text{S}+\text{CdI}_2$), (CdI_2+S), ($\text{ZnS}+\text{CdI}_2$), ($\text{SnS}+\text{CdI}_2$), mixtures for ternary Cu_2SnS_3 (CTS) compound ($\text{Cu}_2\text{S}+\text{SnS}+\text{S}+\text{CdI}_2$) and for quaternary $\text{Cu}_2\text{ZnSnS}_4$ compound ($\text{Cu}_2\text{S}+\text{SnS}+\text{ZnS}+\text{S}+\text{CdI}_2$) were studied by the DTA method. A DTA setup

(Thermogravimetric Analyzer Labsys 1600, Setaram Instrumentation) was used to determine temperatures of phase changes and/or chemical interactions between the initial binaries and the flux material. An empty degassed and sealed quartz ampoule of equal mass was used as a reference for the DTA measurement.

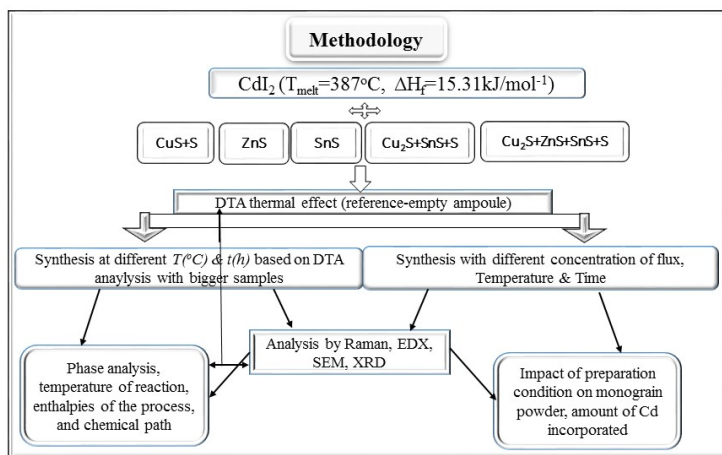


Figure 7. Scheme of the sequence of experimental work.

2.2 Determination of thermal processes and their enthalpies

We recorded the thermal effects in the studied samples by DTA and the changes in the phase composition of different mixtures by Raman and XRD analyses ^[11]. Pure flux material (CdI₂) was selected as the reference material for the DTA enthalpy calibrations for two reasons: firstly, the processes taking place in the synthesis occur in the same temperature region as the melting of flux material and secondly, our experimentally determined melting point of flux coincides with the value found from literature ($T_m=387\text{ }^\circ\text{C}$)¹⁰⁸. Our readings from DTA curves in $\mu\text{V s}$ were converted to J/mol using the value of enthalpy of fusion of CdI₂ (15.31 kJ/mol ¹¹³), considering that our experimental heat value for melting of CdI₂ is $666 \pm 2\ \mu\text{V s}$, which corresponds to $\approx 5.23\text{ J}$ (constant for our calculations). The enthalpies of the individual processes occurring concurrently with the melting process of CdI₂ were determined by subtracting enthalpy of pure CdI₂ from the cumulative enthalpy values of processes in the mixtures. The DTA heating and cooling were carried out in two runs. The obtained energy values were used for the evaluation of the enthalpies of the occurring processes with an error margin estimated at 5 %, given

as the largest deviation of the individual process value of the average value. The applied heating and cooling rates from room temperature to 800 °C were 5 °C and 10 °C per minute, respectively. After recording the thermal effects by DTA, the changes in the phase composition of different precursor mixtures with CdI₂ were determined by Raman and XRD analyses. For the phase analyses, separate mixture samples with larger amounts, but in the same molar proportions as for DTA, were prepared for each thermal effect observed in the DTA curves. The samples were heated in closed quartz ampoules for 4 hours at temperatures slightly higher than the observed thermal effects in DTA curves. After heating, larger samples were quenched from the heating temperature to room temperature in cold water. The heated and quenched powder samples were analyzed by SEM, EDX, Raman and XRD methods, both before and after separation of CdI₂ (by washing with deionized water).

2.3 Preparation of samples for growth process studies

To study the impact of preparation on the growth process, the concentration of flux salt in the synthesis mixtures was varied so that the ratio of the liquid flux (V_{CdI_2}) volumes to solid precursors for CZTS (V_{CZTS}), ($V_{\text{CdI}_2}/V_{\text{CZTS}}$) = 5, 3, 1, 0.5 (if the ratio $V_{\text{CdI}_2}/V_{\text{CZTS}}$ =1, it is marked as C_1). The volumes were determined by considering the density of the flux material and the density of the precursor, the solubility of CZTS in flux was not taken into account^l. Table 3 presents the properties of precursor material and the flux material, as well as CZTS.

Table 3. Precursors used for the synthesis of CZTS and their densities

Compound (phase)	Density (g/cm ³)
Cu ₂ S (solid)	5.6 ¹¹⁴
ZnS (solid)	4.09 ¹¹⁵
SnS (solid)	5.22 ¹¹⁶
CdI ₂ (liquid)	5.64 ¹¹⁶
CZTS (solid)	4.56 ¹¹⁷

We carried out the time-dependent experiments at 650 °C for 24, 160 and 300 hours. Samples were quenched rapidly to the room temperature in cold water. The formed powder particles were separated from the flux material by washing several times with deionized water. Sample was dried and separated into various size fractions ranging from ≤38 micrometer to ≥125 micrometer by sieving using the Retsch AS200 sieving machine. The concentration of Cd incorporated into CZTS was studied as depending on the synthesis temperature and time and determined by EDX from polished powder crystals. Samples were heated for 15 hours at 280 °C, 370 °C, 500 °C, 600 °C, 700 °C and 780 °C and at 600 °C for 6, 22, 32, and 60 hours. 280 and 370 °C were considered based on the effect observed by DTA. The

element ratios in the mix of binary precursors for CZTS synthesis were chosen as $[\text{Cu}]/([\text{Zn}]+[\text{Sn}])=0.92$ and $[\text{Zn}]/[\text{Sn}]=1.03$, considering that single phase CZTS monograin powders can be grown in molten KI with precursor metal ratios $[\text{Cu}]/([\text{Zn}]+[\text{Sn}])=0.92 \leq 0.95$ and $[\text{Zn}]/[\text{Sn}]=1.0 \leq 1.03$ ^{54,118,119,83}. The Cd incorporated into the crystals was determined by EDX from polished crystals.

2.4 Instrumentation

The morphology and chemical composition of the synthesized powders were analyzed using energy dispersive X-ray spectroscopy (SEM- AsB and by 20 keV EDX) on Zeiss HR-SEM ULTRA 55. The EDS analysis was made at least from 10 crystals of each analyzed sample. The phases formed in the annealed samples were determined by the Raman spectra recorded using a Horiba LabRam HR high-resolution spectrometer equipped with a multichannel CCD detection system in a backscattering configuration. Incident laser light of 532 nm was focused on different $1 \mu\text{m}^2$ spots of the studied sample and an average of five readings were taken for every sample to obtain an objective phase composition of the sample. The XRD measurements were performed using a Bruker D5005 diffractometer. For the analysis, the ICDD-4 + 2009 database was used. The DTA analysis was carried out using a Thermogravimetric Analyzer Labsys 1600, Setaram Instrumentation.

3 RESULTS AND DISCUSSIONS

3.1 Synthesis and characterization of CZTS monograin powder in molten CdI₂

In our earlier studies¹²⁰, we applied the combination of different analytical methods - the experimental DTA results with the phase analysis by Raman and XRD. As a result, we found that the formation of CZTS in the mixture of CdI₂ flux with binary precursors in amounts needed for the formation of near-stoichiometric composition of Cu₂ZnSnS₄ (Cu₂S+SnS+ZnS+S+CdI₂) started already at temperatures lower than 400 °C. At 280 °C, much below the melting point of CdI₂, the formation of CZTS quaternary compound was not detected. As the temperature increased up to 370 °C, just below the melting temperature of pure CdI₂, the formation of CZTS began. At this temperature, the Raman spectra confirmed the presence of different secondary phases co-existing with CZTS as it was shown in^{120,III}. In order to study the formed phases present in the quaternary system, mixtures of CdI₂+SnS+Cu₂S+S+ZnS were a) heated to 500 °C and quenched and b) heated to 800 °C and cooled down to 350 °C before quenching to room temperature, respectively. The phase analysis showed that in sample mixtures (Cu₂S+SnS+ZnS+S+CdI₂) heated and quenched at 500 °C, besides Cu₂SnS₃, ZnI₂ was also found. Samples quenched at 800 °C showed that the ternary Cu₂SnS₃ compound had reacted with ZnS to form Cu₂SnS₃, Cu₂Zn_{1-x}Cd_xSnS₄, Cu₂ZnSnS₄ and Zn_{1-x}Cd_xS, which confirms that the other (exo-endo) reactions also occur alongside in the molten phase of CdI₂. Analyzing the DTA results, we recognized that the formation of CZTS proceeded in two stages. In the first step, Cu₂SnS₃ formed from Cu₂S, SnS, and S. After that, Cu₂SnS₃ reacted with ZnS to form CZCdTS. In Figure 8, Raman spectrum of the washed CZTS sample heated up to 800 °C and cooled down to 350 °C is presented. CZCdTS is the prevailing phase with its characteristic Raman peaks at 92, 166, 249, 285, 333, 372 cm⁻¹^{121,122}. All Raman peaks were shifted slightly to lower wave numbers of pure CZTS. Raman peak at 110 cm⁻¹ could belong to CdI₂¹²³ used as flux material and Raman peak of SnI₄ as a secondary phase can be detected at 145 cm⁻¹, as it was described also in the previous report¹²⁰ CuI, Cu_{1.6}S, SnI₄ phases were also detected by XRD in the unwashed samples but not in washed samples. CuI is soluble in KI or NaI solutions, as also described in our previous report, allowing separation of single phase CZCdTS^{120,II}. The synthesis temperature of 800 °C was chosen for experimental purpose to see if the lower melting temperature of CdI₂ could avoid sintering that occurs when KI (T_{mKI}=685 °C) as flux was used. Also, syntheses at higher temperatures are possible (T_{Synt}=700≥x≤780 °C) in a small range of temperatures above the melting temperature of KI as flux. Using CdI₂ (T_{mCdI2} = 387 °C) synthesis is possible in a

large temperature region ($T_{\text{synt}}=370 \geq x \leq 800$ °C) that could increase or decrease the sintering effect which may not be favorable for monograin growth¹²⁴⁻¹²⁶.

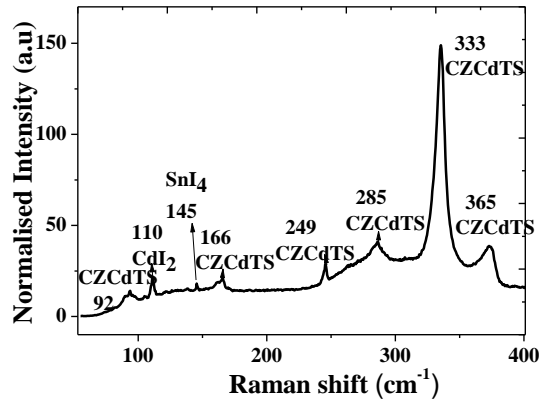


Figure 8. Raman spectrum of CZTS sample heated up to 800 °C and cooled down to 350 °C. CdI₂ is mainly washed out. The shift in Raman peak to a lower wave number value confirmed the formation of CZCdTS.

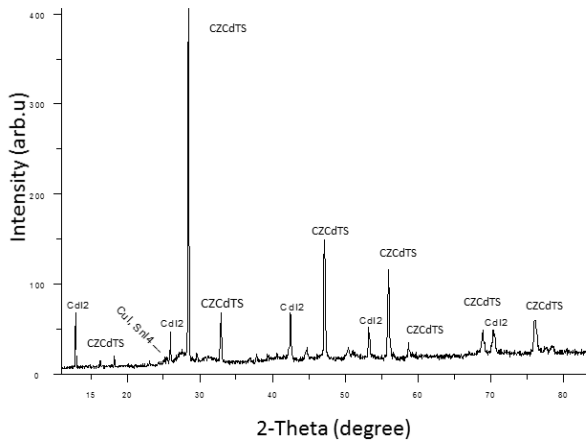


Figure 9. XRD pattern of the mixture of Cu₂S+SnS+ZnS+S+CdI₂ heated up to 800 °C, cooled to 350 °C and quenched to room temperature.

3.2 Impact of synthesis-growth conditions on the material properties

Focus in this part is on the impact of synthesis-growth conditions on the material properties. We considered the effects of temperature, synthesis time and amount of flux on the grain size and yield, composition of the synthesized CZTS and concentration of Cd in the as-grown CZTS monograin powder.

3.2.1 Impact of flux concentration and synthesis time on the grain size and yield of powders

By sieving the powders into different size fractions, the amount of fractions with grain size $\geq 45 \mu\text{m}$ (usable in monograin solar cells)⁴³ was determined. In Figure 10, the total quantity of synthesized powder material with size $\geq 45 \mu\text{m}$ without considering the different fractions and the yield of the total amount of CZTS monograins powder decreases as the volume ratio of the liquid flux (V_{CdI_2}) to solid precursors for CZTS (V_{CZTS}), i.e., ($V_{\text{CdI}_2}/V_{\text{CZTS}}$) increases from 0.5 to 5 at 650 °C and for 24, 160 and 300 hours, respectively. It is understandable if we consider that by increasing the amount of liquid phase, the diffusion between different crystals takes more time and the amount dissolved in the molten phase of flux increases. However, the lowest used amount of CdI₂ (0.5 C_l) (see Figure 10, left) results in grains with sizes over 45 μm in larger amounts than could be expected from the small linear decline when $C_l \geq 1$ (see Figure 10a, right). This phenomenon could be understandable under the consideration that the single grain growth limit is roughly determined as $V_{\text{Liquid}}/V_{\text{Solid}} \geq 0.5$ ¹²⁷. Therefore, the amount of larger grains (formed due to a higher degree of sintering) is increased for $C = 0.5$ in comparison with used larger flux amounts ($C > 0.5$) where single grain growth prevails^[1].

In addition, at $C < 0.5$, the amount of flux is insufficient to aid the growth process and sintering to prevail. As the density of CZTS is not determined for higher temperatures, the amounts for initial liquid to solid volume ratio < 0.5 could result in both the single grain growth and some sintering process occurring at the same time and at $C_l < 0.5$, even greater sintering may occur, which may affect the quality of the CZTS monograin powder¹²⁸. In addition, the yield of the total amount of CZTS monograins decreases as the flux amount increases and vice versa - it increases as the growth time increases (see Figure 10b). It is also seen that the total yield of powder is larger than the total amount of initial precursor compounds ($\text{Cu}_2\text{S} + \text{SnS} + \text{ZnS} + \text{S}$) for the synthesis, particularly for heating times 160 and 300 hours. The increase in the total amount of yield over the summarized amount of precursor compounds can take place due to the replacement of Zn by Cd (with higher molar mass than Zn) in the crystal lattice of formed CZCdTS compound when CdI₂ is the only source of Cd. During the growth process, the concentration gradient drives the mass transfer of the crystal constituents from the fluid phase to the crystal phase. The mass flux at the

growth interface depends on the direction-dependent concentration gradient¹²⁸ and the larger the flux amount, the slower and less chance of higher agglomeration and vice versa, which leads to smaller grains that can be easily washed off during the separation of monograin powder from the flux. In summary, Figure 10a shows that the grain size and the total yield of synthesized powder increases by the synthesis time but decreases with the increasing flux amount.

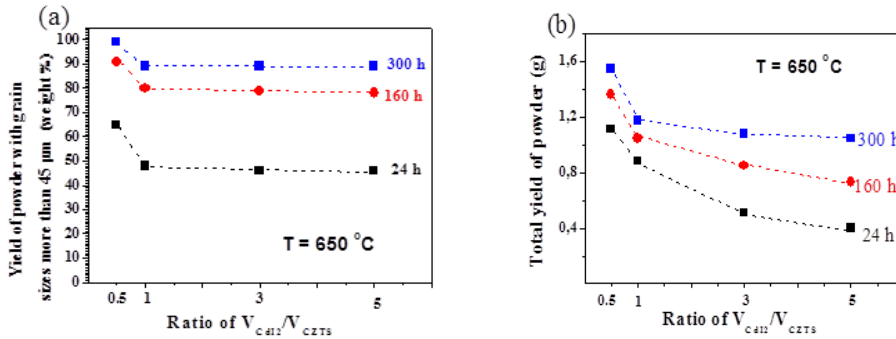


Figure 10. CZCdTS powder fractions with grain size larger than $45 \mu m$ (a) grain size distribution (b) total yield of synthesized powder. The synthesis temperature is $650 \text{ }^\circ C$ with different heating time 24, 160 and 300 hours, the left side of Figure 10a emphasizes the effect of sintering due to small flux amount ($0.5C_1$)¹.

3.2.2 Impact of flux amount and synthesis-growth time on grain morphology

SEM images of individual CZCdTS crystals synthesized at $650 \text{ }^\circ C$ are presented in Figure 11. It can be seen that the grains produced by using smaller flux amounts are less faceted and have a more rounded shape. With the time increasing as well as with the increasing flux amount, faceted crystals became more obvious. The most round shaped grains were formed in the samples with the lowest amount of CdI_2 heated for 160 hours. Longer time (300 hours) promotes the faceting. However, in the crystals heated for 300 hours, secondary agglomeration can also be observed – the crystals are formed from different blocks. The primary sintering effect at the lowest used flux amount ($0.5C_1$) seems to be helpful for getting rounder and compact grains after long crystallization time (160 and 300 hours). Comparison of all the syntheses at $650 \text{ }^\circ C$ shows that the grains are less faceted and larger and the yield is higher as the flux concentration decreases. This can be attributed to the effect of sintering.

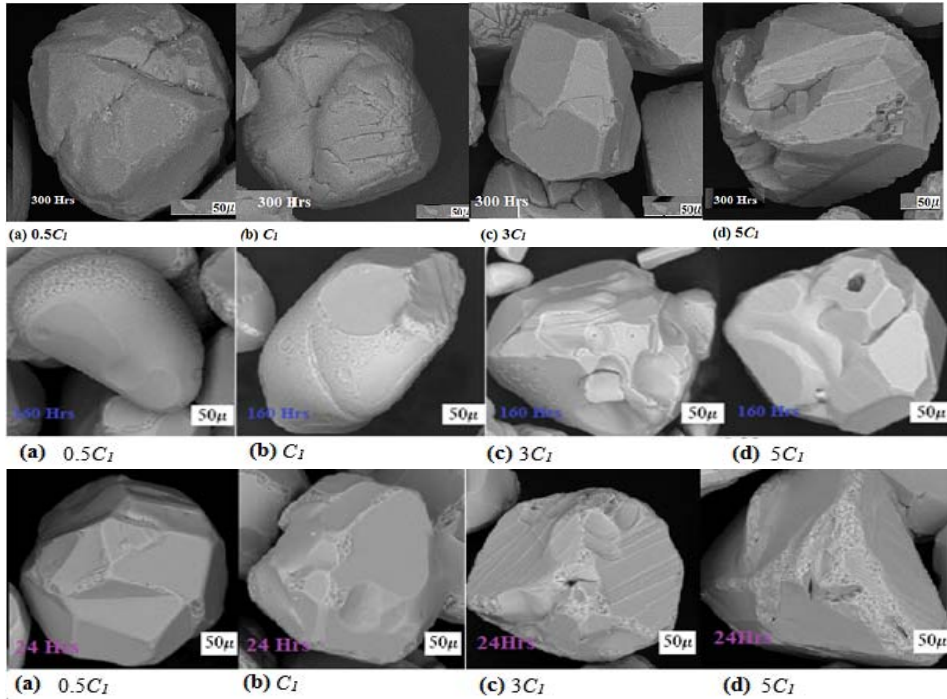


Figure 11. SEM images of individual CZCdTS powder grains synthesized at $T= 650\text{ }^{\circ}\text{C}$ for 300 (upper row), 160 (middle row) and 24 (lower row) hours with increasing (from left to right) amount of CdI_2 . C_1 corresponds to $V_{\text{CdI}_2}/V_{\text{CZTS}}=1\text{ }^{\dagger}$.

3.2.3 Phase analysis by Raman

Raman spectra of powder crystals synthesized under different conditions (temperature, time, and flux amount) are presented in Figure 12. Raman spectrum of the sample held for 300 hours at $650\text{ }^{\circ}\text{C}$ and synthesized with the lowest flux amount ($0.5C_1$) shows that the most intensive Raman peak is at 337 cm^{-1} , which is close to the most intensive Raman peak position of pure CZTS (at 338 cm^{-1}) while the most intensive Raman peak of the sample with the highest amount of CdI_2 ($5C_1$) is at 332 cm^{-1} , at the same place as the most intensive Raman peak of pure $\text{Cu}_2\text{CdSnS}_4$ (332 cm^{-1})¹²⁹ (see Figure 12a). In¹¹⁹ it was found that with an increasing Cd content in the $\text{Cu}_{1.85}(\text{Cd}_x\text{Zn}_{1-x})_{1.1}\text{SnS}_{4.1}$ monograin powders grown in KI, the peak position of A1 Raman mode decreased linearly from 338 to 332 cm^{-1} in the interval of x values from 0 to 0.4. Then, with higher Cd contents, the A1 peak position did not shift any more. In our study, Raman peak of CZTS, synthesized for 15 hours at different temperatures ($500, 600, 700$ and $780\text{ }^{\circ}\text{C}$) is shifted to 332 cm^{-1} , as the temperature increased to $780\text{ }^{\circ}\text{C}$ (see Figure 12b). The shift of Raman peak confirms that solid solution of $\text{Cu}_2\text{Zn}_{1-x}\text{Cd}_x\text{SnS}_4$ is formed in our powder samples.

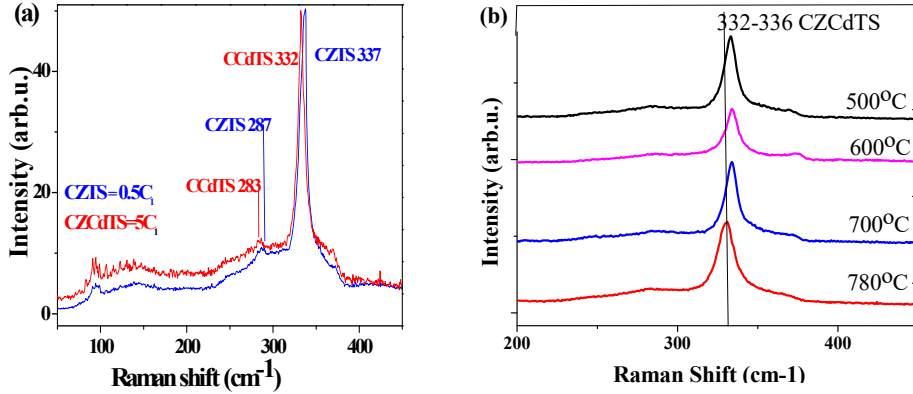


Figure 12. Normalized Raman spectra of powder crystals (a) synthesized with different ratios of CdI_2/CZTS (red=5 and blue $\text{CdI}_2/\text{CZTS}=0.5$) (b) synthesized at different temperatures for 15 hours and $\text{CdI}_2/\text{CZTS} = 1$. The Raman peak shifts from 336 cm^{-1} at 500°C to 332 cm^{-1} at 780°C .

3.2.4 Compositional analyses by EDX

We determined the cadmium concentration in the as-grown CZTS powders synthesized at different temperatures for constant time and for different time at constant temperature. Our focus was also on the influence of different amounts of CdI_2 present in the synthesis of CZTS monograin powders on the final composition of powders.

3.2.4.1 Cd concentration in CZTS powder crystals by EDX

We determined the Cd concentration in CZTS crystals grown for 15 hours in CdI_2 of constant volume ratio $V_{\text{CdI}_2}/V_{\text{CZTS}}=1$ at different synthesis temperatures. It is seen that Cd concentration in the as-grown CZTS monograin powder heated at different temperatures for constant time increases with temperature (Figure 13a). In addition, with the increasing amount of used CdI_2 , the Cd concentration in the formed compound also increases as the flux amount increases (see Figure 13b). However, from Figure 13c it is obvious that annealing for 6 hours leads to a large dispersion in the measurement data. This is attributable to the non-equilibrium status of the system. Furthermore, the Cd concentration in CZTS grown at constant temperature (600°C) for different annealing times showed no increase, it stayed constant after heating for 22 hours. Due to the inconsistency in the obtained data we can conclude that 6 hours is not enough to reach the

equilibrium. This result is also confirmed by the Raman peak position in Figure 13d. It can be seen that the Raman peak shifts from 336 cm^{-1} (6 hours) to 333 cm^{-1} for 22 hours and remains constant (up to 60 hours). This confirms that the Cd incorporation into CZTS is not a time dependent process. The maximum amount of Cd incorporated into $\text{Cu}_2\text{Z}_{1-x}\text{Cd}_x\text{SnS}_2$ is at $x=0.3$ at $780 \text{ }^\circ\text{C}$ and increases to $x=0.4$ as the flux amount increases to $5C_1$.

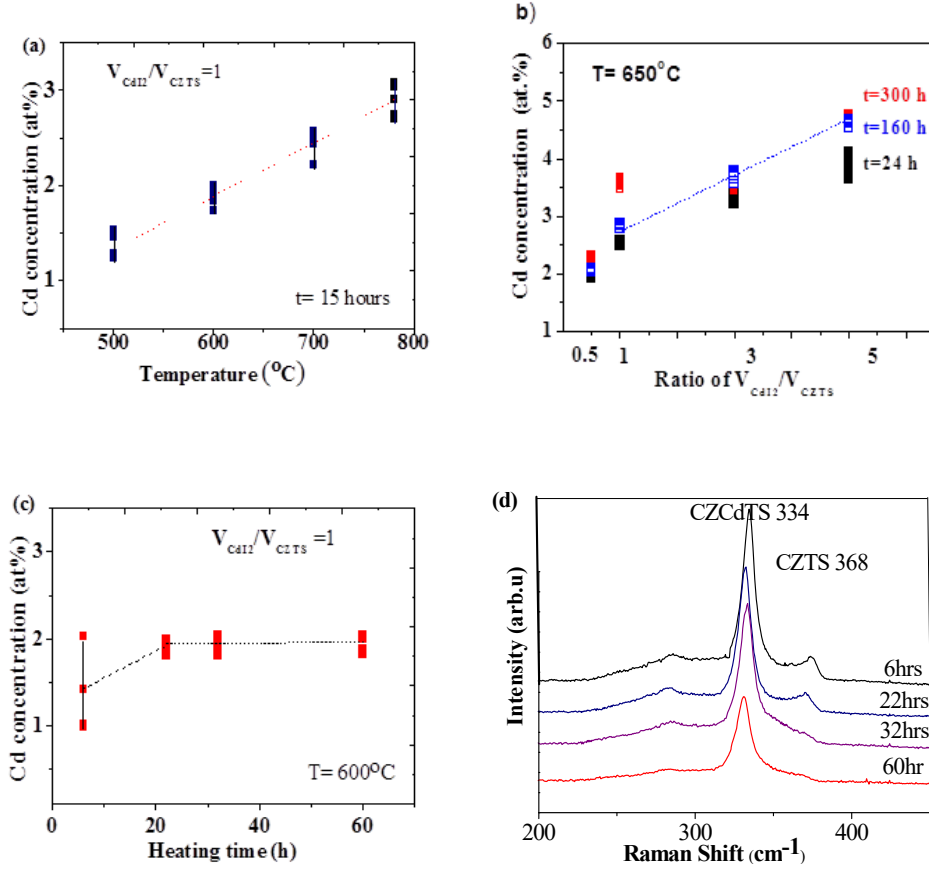


Figure 13. Cd content incorporated into CZTS (a) from constant amount of CdI_2 flux ($V_{\text{CdI}_2}/V_{\text{CZTS}} = 1$) as a function of heating temperature, (b) as a function of CdI_2/CZTS for different time ($24, 160$ and 300 hours) at $T = 650 \text{ }^\circ\text{C}$, (c) Cd content in powders heated in the constant amount of CdI_2 at $600 \text{ }^\circ\text{C}$ for different time, (d) Raman spectra of CZTS heated in the constant amount of CdI_2 at $600 \text{ }^\circ\text{C}$ for different time. Raman peak shifts from 334 cm^{-1} at 6 hours to 332 cm^{-1} at 22 hours and remains constant until 60 hours .

3.2.4.2 Composition of synthesized powders by EDX

The common formula of the product powders is almost the same for all samples with a deviation in the range of limits for EDX and can be expressed as $\text{Cu}_{1.9\pm 0.01}\text{Zn}_{1-x}\text{Cd}_x\text{SnS}_{3.97\pm 0.04}$ with variable Cd content (x values). The values of x depending on the heating conditions are given in Table 4. As it can be seen, the Cd concentration in $\text{Cu}_2\text{Zn}_{1-x}\text{Cd}_x\text{SnS}_4$ increases with the increasing amount of CdI_2 in the synthesis. The incorporation of Cd into $\text{Cu}_2(\text{ZnCd})\text{SnS}_4$ through the intermediate formation of $\text{Zn}_{1-x}\text{Cd}_x\text{S}$ is occurring by the replacement of Zn^{2+} by Cd^{2+} . All the used analytical methods confirm that during the synthesis of CZTS in CdI_2 , as the flux Cd incorporates from CdI_2 into the crystal lattice of CZTS, the result is the formation of solid solutions with a common formula of $\text{Cu}_{1.9\pm 0.01}\text{Zn}_{1-x}\text{Cd}_x\text{SnS}_{3.97\pm 0.04}$. This is in contrast to the results of Pilvet *et al.*¹¹⁹, where it was shown that by using CdS and ZnS as precursors, the whole row of solid solutions of $\text{Cu}_{1.85}(\text{Cd}_x\text{Zn}_{1-x})_{1.1}\text{SnS}_{4.1}$ ($0 \leq x \leq 1$) can be synthesized. In our system, the Cd content is limited by the amount of CdI_2 in the synthesis-growth process.

Table 4. Composition of CZCdTS for different flux concentrations and heating time as determined by EDX ($T=650\text{ }^\circ\text{C}$), deviation error of ± 0.02

	Heating time (h)		
	24	160	300
$V_{\text{CdI}_2}/V_{\text{CZTS}}$	Value of x in $\text{Cu}_{1.9\pm 0.01}(\text{Zn}_{1-x}\text{Cd}_x)\text{SnS}_{3.97\pm 0.04}$		
0.5	0.15	0.18	0.16
1	0.15	0.26	0.22
3	0.25	0.28	0.28
5	0.3	0.35	0.35

Figure 14 shows the changes in Zn concentration in powders grown at different temperatures. It can be seen that [Zn] in the CZTS powders is reduced as compared with the Zn content in precursors and it decreases with increasing temperature and also with the increasing Cd content. Such behavior can be attributed to the replacement of Zn by Cd. In addition, the sum of Zn and Cd contents also increases with increasing temperature. The ratio of $[\text{Zn}]/[\text{Sn}]$ decreases while the ratio $[\text{Cu}]/[\text{Sn}]$ increases due to the decrease in [Zn] in the final powder. It was suggested that the decrease in the Cu content in the precursors should lead to an increase in the substitution of Zn atoms by Cd atoms¹¹⁹; therefore, a decrease in [Zn] can be attributed to the substitution of Cd at Zn site from CdI_2 . The single phase solid solution of $\text{Cu}_2\text{Zn}_{1-x}\text{Cd}_x\text{SnS}_4$ forms intensively, starting from $500\text{ }^\circ\text{C}$ ¹²⁰. As the direct exchange reaction between solid ZnS and CdI_2 resulting in the formation of CdS and ZnI_2 is

thermodynamically not favored (based on available thermodynamic data), the formation of solid solution $\text{Cu}_2\text{Zn}_{1-x}\text{Cd}_x\text{SnS}_4$ (Cd incorporation at the Zn site) can take place due to the processes in liquid CdI_2 that may result in the formation of continuous row of solid solution between ZnS and CdS ^{101,130}. In the next step, $\text{Zn}_{1-x}\text{Cd}_x\text{S}$ reacting with Cu_2SnS_3 results in the formation of $\text{Cu}_2\text{Zn}_{1-x}\text{Cd}_x\text{SnS}_4$ ^{III}, although we believe that the dissolution of ZnS in CdI_2 occurs in the liquid phase.

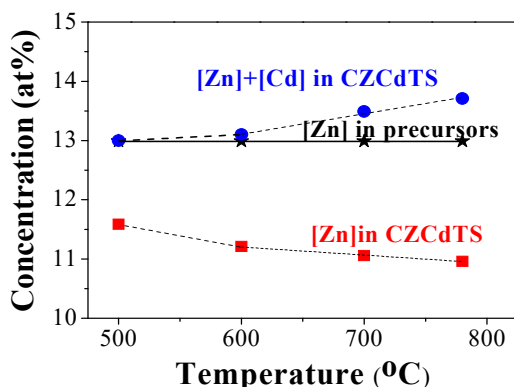


Figure 14. Variation of Zn concentration in the $\text{Cu}_2\text{Zn}_{1-x}\text{Cd}_x\text{SnS}_4$ powders synthesized in CdI_2 at different temperatures¹.

3.2.5 Activation energy of Cd incorporation to the CZTS crystals in the synthesis process

In Figure 15, the Arrhenius plot of Cd concentration in the formed $\text{Cu}_2\text{Zn}_{1-x}\text{Cd}_x\text{SnS}_4$ is shown. The Cd concentration in the formed CZCdTS increased with temperature and it could be expressed as $[\text{Cd}] \sim e^{-\Delta E/kT}$. The overall activation energy of the Cd incorporation process estimated from the Arrhenius plot is $17.5 \pm 2 \text{ kJ mol}^{-1}$. The formation of $\text{Zn}_{1-x}\text{Cd}_x\text{S}$ seems to be a major step for the Cd incorporation from CdI_2 into the crystal lattice of the CZTS monograins¹³¹. The formation of solid solution of $\text{Cu}_2\text{Zn}_{1-x}\text{Cd}_x\text{SnS}_4$ was reported earlier in¹²⁰ and in¹. By our first considerations, based on ΔG calculations of different reactions, the only possible route for Cd incorporation is through the CZTS formation reaction in participation of more electronegative CdI_2^+ ion. The latter was found in the gaseous phase of CdI_2 by the mass spectrometric investigations with modified Knudsen cell–mass spectrometer by W. Kunczewicz-Kupczyk *et al.*¹³². In their work, they confirmed the presence of CdI_2^+ , Cd^+ and I^- formed as fragment ions in the gaseous phase of CdI_2 (g), consisting mainly of monomers CdI_2 (g) and dimers Cd_2I_4 (g) at 261 to 340 °C. But the formation of ZnI_2 and CdS by the participation of gas phase ions seems to be improbable. In the next part of the thesis, we present results of different chemical interactions occurring between CdI_2 and precursor compounds.

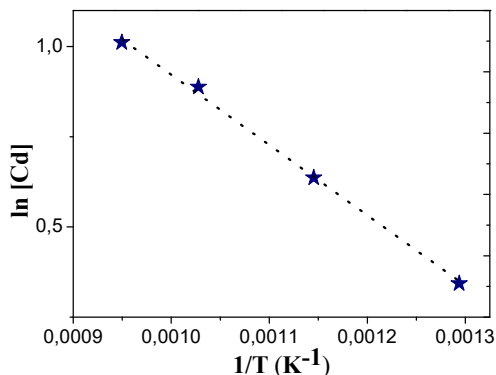


Figure 15. Arrhenius plot of $[Cd]$ in $Cu_2Zn_{1-x}Cd_xSnS_4$ powders grown in the constant amount of CdI_2 flux (ratio of precursors to $CdI_2=1:1$) for constant time (32 hours) at different temperatures.

3.3 Studies of interactions of precursors with CdI_2

To understand the entire formation process of the CZTS in molten CdI_2 , our studies of the interactions of CdI_2 with every individual precursor separately started by considering the enthalpies in the entire synthesis process. Our aim was to understand the individual chemical reactions that could occur between CdI_2 and the precursors in different combinations. All the possible chemical reactions and their thermodynamic probabilities (by ΔG calculations) will be reported.

3.3.1 Synthesis temperature of mixtures

The melting temperatures of CdI_2 and the studied mixtures (Cu_2S+CdI_2), ($ZnS+CdI_2$), ($SnS+CdI_2$), ($Cu_2S+SnS+S+CdI_2$) and ($Cu_2S+SnS+ZnS+S+CdI_2$) from the DTA curves are presented in Figure 16. It can be seen that the melting of the flux in the mixtures of the precursors with flux takes place at lower temperatures than the melting temperature of pure CdI_2 ($387\text{ }^\circ\text{C}$)¹⁰⁸. The lowering of melting temperatures shows some solubility of the precursors in molten CdI_2 and/or the formation of new phases. It is well known that the amount of dissolved solute is dependent on the amount of solvent and temperature. For the melting temperatures in Figure 16, the ratio of the precursor to flux material mixtures needed to synthesize a single phase $Cu_2Zn_{1-x}Cd_xSnS_4$ was considered and presented for all the mixtures.

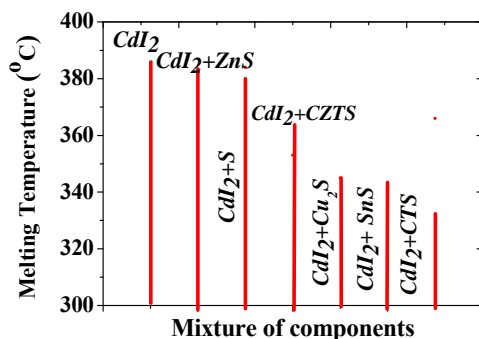


Figure 16. Melting temperatures of studied mixtures as determined from the DTA curves.

3.3.2 CdI_2

At temperatures above the melting point, CdI_2 could exist in gaseous form both in its monomeric ($CdI_2(g)$) and dimeric ($Cd_2I_4(g)$) form^{133,134}. According to Corbett *et al.*^{135,136}, molten CdI_2 has brown color, which is due to the free iodine that is in equilibrium with the melt. Iodine is an oxidizing agent, which may limit the reactions between CdI_2 and the precursors. The DTA curves of pure CdI_2 (see Figure 17) gave an endothermic effect at 385 °C in heating and an exothermic effect at 366 °C in the cooling cycle, which can be attributed to the melting and freezing of CdI_2 with an enthalpy signal of $666 \pm 2 \mu V s$. This signal is equal to 5.23 J, as calculated from the obtained peak area for corresponding 0.125 g (0.00034 moles) of CdI_2 (the molar mass of $CdI_2=366.22 \text{ g mol}^{-1}$ and the molar fusion enthalpy value for pure CdI_2 is $15.31 \text{ kJ mol}^{-1}$ ¹¹³). Any deviation from this value in the mixtures studied may be attributed to the various interactions and processes occurring in the sample mixtures.

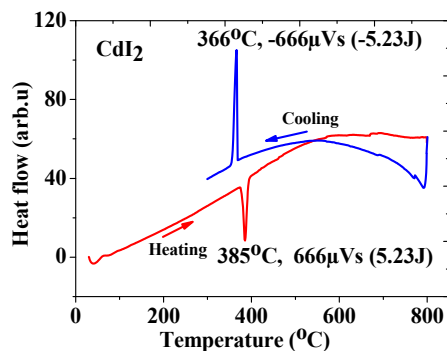


Figure 17. DTA curves of CdI_2 .

3.3.3 CdI₂+Cu₂S

The DTA curve of the mixture of CdI₂+Cu₂S (Figure 18) shows an endothermic melting effect at 353 °C and an exothermic effect of freezing of CdI₂ at 338 °C. We can observe a decrease in the energy value of the melting process from 5.23 J (666 μV s) for pure CdI₂ to 2.1 J (264 μV s) in CdI₂+Cu₂S mixture. This decrease can be ascribed to the simultaneous exothermic reactions occurring alongside the melting of CdI₂. By XRD and Raman; we found different compounds - Cu_{1.96}S, CuI, Cu₂Cd₃I₄S₂, CdS and Cu₄Cd₃ in CdI₂+Cu₂S sample heated for 4 hours at temperatures slightly above the melting point of the mixture (353 °C) (see Table 5). This confirms the chemical interaction between the flux material and Cu₂S. By XRD and Raman analyses; we found that some of these processes occurring during the melting and freezing of the mixture CdI₂+Cu₂S are reversible: Cu₂S, as observed by XRD, transformed to Cu_{1.96}S and re-transformed to Cu₂S by cooling down, which is in accordance with the Cu-S phase diagram⁵⁵. In the heating process, in addition to the main fusion peak at 353 °C, another endothermic DTA peak is observed at 400 °C. The phase analysis of the larger sample heated and quenched at 420 °C shows that this peak corresponds to the decomposition of Cu₂Cd₃I₄S₂ to CdS, CdI₂ and Cu₄Cd₃ and I₂ (see equation 5) with a summary thermal effect of 77 mV s (0.6 J). The phases detected by Raman are given in Figure 19 (XRD patterns can be found in Appendix B)

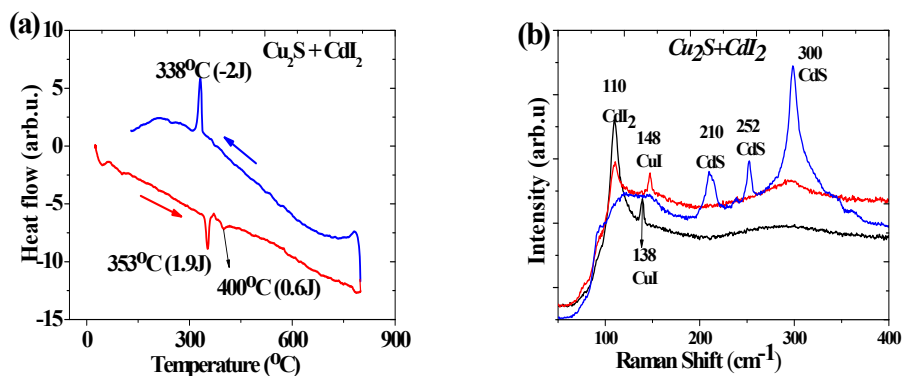


Figure 18. DTA curves (a) and Raman spectra (b) of Cu₂S+CdI₂: red - heated and quenched at 353 °C, blue - heated and quenched at 400 °C, black- heated to 800 °C and cooled down to 330 °C before quenching to room temperature.

Table 5. Annealing conditions, determined phases, reactions and their calculated ΔG values for the $\text{CuS}+\text{CdI}_2$ mixture

Annealing conditions (°C)	Phases by XRD	Phases by Raman/peak position (cm^{-1})	Equation	Reactions	ΔG (kJ mol^{-1})/Temperature (°C)
Heated to 353, annealed for 4 hours	CuS, $\text{Cu}_{1.96}\text{S}$, CuI, $\text{Cu}_2\text{Cd}_3\text{I}_4\text{S}_2$ CdS, Cu_4Cd_3	CdS/294 ²⁴ CdI ₂ /110 ¹³⁷ CuI/148 ^{10,138}	1	$\text{Cu}_2\text{S} + \text{CdI}_2 = 2\text{CuI} + \text{CdS}$ ^{139,140}	-49.1 / T=300
			2	$\text{CdS} + \text{Cu}_2\text{S} + 2\text{CdI}_2 = \text{Cu}_2\text{Cd}_3\text{I}_4\text{S}_2$	Proposed
Heated to 400, annealed for 4 hours			3	$\text{Cu}_2\text{S} + \text{CdI}_2(\text{g}) = 2\text{CuI} + \text{CdS}$ ^{139,140}	-43.6 / T=300
Heated to 800 and cooled down to 330	CdS, Cu_4Cd_3 , CuS, $\text{Cu}_2\text{Cd}_3\text{I}_4\text{S}_2$, CuI	CdS/294 ²⁴ CuS/474 ⁶³⁻⁶⁵	4	$\text{CuS} + \text{CdI}^+(\text{g}) = \text{CuI} + \text{CdS}$ ^{139,141}	-151.9 / T=300
			5	$2\text{Cu}_2\text{Cd}_3\text{I}_4\text{S}_2 = \text{Cu}_4\text{Cd}_3 + 2\text{CdS} + \text{CdI}_2 + \text{I}_2$	Proposed

3.3.4 CdI₂+SnS

The melting effect of this mixture was observed at 345 °C (see Figure 20), i.e., at much lower temperature than for pure CdI₂. This fact suggests a higher solubility/interaction of SnS in CdI₂. In the XRD and Raman studies, the larger samples (a) were heated to 800 °C and cooled down to 350 °C and then quenched to room temperature and (b) cooled down to 250 °C from 800 °C before quenching rapidly. It was revealed that SnI₄, Sn₂SI₂, and CdS had been formed (shown in Table 6). The final freezing of SnS+CdI₂ mixture can be detected in the cooling curve at 300 °C. The enthalpy observed in the cooling process is -6.23 J. It can be attributed to the exothermic freezing of CdI₂ with cumulatively formed tin iodides and CdS, as observed by phase analysis. The phases detected by Raman are given in Figure 21. XRD patterns are presented in Appendix B.

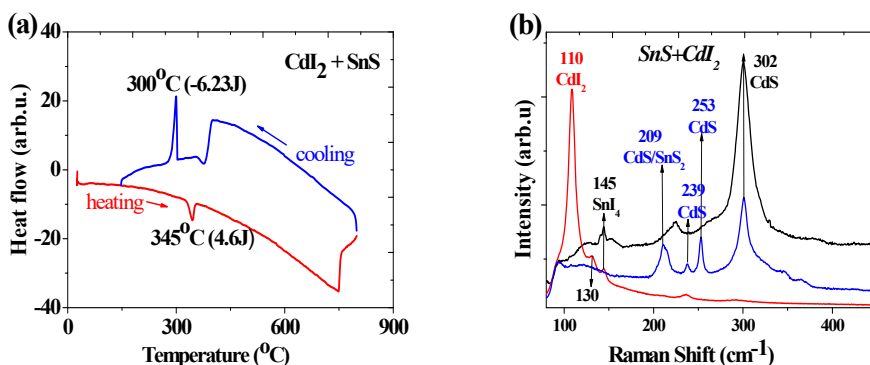


Figure 19. (a) DTA curves of CdI₂+SnS mixture (b) Raman spectra of SnS+CdI₂ heated and quenched at different temperatures :blue- heated and quenched at 353°C, red - heated to 800 °C and cooled down to 300 °C before quenching to room temperature, black - heated to 800 °C and cooled down to 250°C before quenching to room temperature.

Table 6. Annealing conditions, determined phases, reactions and their calculated ΔG values for SnS+CdI₂ mixture

Annealing conditions (°C)	Phases by XRD	Phases by Raman/peak position (cm ⁻¹)	Equation	Reactions	ΔG (kJ mol ⁻¹)/Temperature (°C)
Heated to 350 and quenched	CdI ₂ , CdS, SnI ₂ , Sn ₂ SI ₂	SnS CdS/301 ²⁴	6	SnS + CdI ₂ (g) = SnI ₂ + CdS ^{142,143}	-79.470/T ≥ 0
			7	2SnS + I ₂ = Sn ₂ SI ₂ + S	proposed on phases observed
			8	2SnS + CdI ₂ = Sn ₂ SI ₂ + CdS	proposed on phases observed
Heated to 800 and cooled down to 300 and 250	SnI ₄ , SnS, SnSI ₂ , CdS, SnI ₂	CdS SnI ₄ /145	9	CdI ₂ (g) + S = I ₂ + CdS	-43.220 T=0 °C
			10	SnS ₂ (g) ↔ SnS + S ^{72,143}	9.741/T=400
			11	SnI ₄ + 2CdS = SnS + 2CdI ₂ + S	-196.792/T=100
			12	I ₂ + CdS = CdI ₂ (g) + S	-11.667/T=100
			13	SnS ₂ + 2CdI ⁺ (g) = 2CdS + SnI ₂ /(SnSI ₂) ¹⁴⁴	-50.033/T=800
			14	2CdI ⁺ (g) + 2S = I ₂ + 2CdS	-378.909/T=80
					-131.958/T=800

3.3.5. CdI₂+ZnS

The DTA heating and cooling curves of this mixture of CdI₂ +ZnS are presented in Figure 20a. It shows an endothermic peak at 382 °C in the heating cycle, slightly lower than the melting temperature of pure CdI₂ ($T_{\text{melt}}=385$ °C, see Figure 17) with the thermal effect of 2.7 J, which is lower than in the melting of pure CdI₂. It means that some exothermic process compensates the endothermic melting effect. However, no new phases other than CdI₂ and ZnS were found by XRD and Raman in the sample heated and quenched at 385 °C, which may be due to the low sensitivity of XRD; but the lowering of the enthalpy suggests that some interaction is occurring in the liquid phase. In the cooling curve, two exothermic peaks at 354 °C and 338 °C are seen. The peak at 354 °C, slightly lower than the freezing temperature of pure CdI₂ ($T_f=366$ °C), confirms the solidification of CdI₂ with an enthalpy value of 3.1 J. The peak at 338 °C corresponds to an energy signal of about 1.8 J (234 μV s), which is much lower than that of the freezing of pure CdI₂. Analysis by XRD showed that a solid solution of Zn_{1-x}Cd_xS was formed in the mixture of ZnS+CdI₂ (see Figure 21). The XRD pattern for the samples cooled down to 330 °C, confirms the formation of Zn_{1-x}Cd_xS solid solution¹⁰¹. As the formation of Zn_{1-x}Cd_xS is only found in the cooling phase, we can conclude that Zn_{1-x}Cd_xS was formed in the molten phase by replacement of Zn by Cd. Solid solutions were formed by precipitation in cooling due to lowered solubility at 338 °C. The overall enthalpy of the process was found as 1.8 J.

In equation (17), a thermo-dynamical possibility of a reaction exists between ZnS and CdI⁺ for temperatures between 0 and 1000 °C. In equation (15), the calculations of Gibbs energy change gave positive values for the reaction between solid CdI₂ and ZnS. Therefore, the CdS formation from solids is thermodynamically impossible, coupled with the fact that CdS was not found in the solid product. The probability of the reactions (15) and (20) should be therefore excluded. However, we found Zn_{1-x}Cd_xS and Cu₂Zn_{1-x}Cd_xSnS₄, respectively, (see Tables 7 and 9) in the studied samples. The phases detected by Raman are given in Figure 20b.

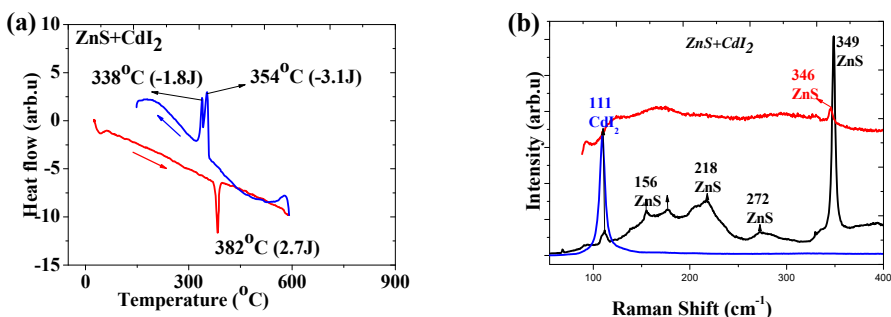


Figure 20. (a) DTA curves of the CdI₂+ZnS mixture, (b) Raman spectra of the ZnS+CdI₂: blue - heated and quenched at 385 °C, red - heated to 800 °C and cooled down to 330 °C before quenching to room temperature, black - heated to 800 °C and cooled down to 350 °C before quenching to room temperature.

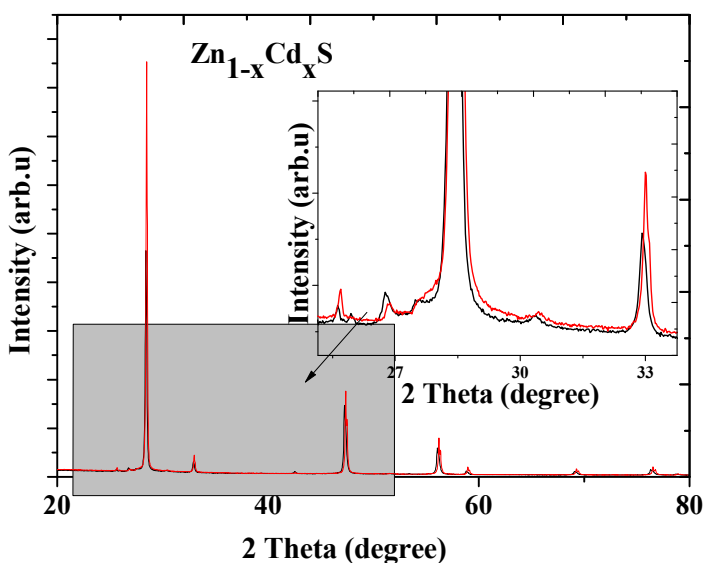


Figure 21. XRD pattern of Zn_{1-x}Cd_xS, (red-samples heated to 800 °C and cooled down to 354 °C before quenched to room temperature, black- samples heated to 800 °C and cooled down to 330 °C before quenching to room temperature).

Li Q. *et al.*¹⁰¹ described similar formation of Zn_{1-x}Cd_xS solid solutions from solid powder of Zn- and Cd- thiourea (Tu) complexes under high-temperature heat-treatment (500 °C for 30 min in N₂). Decomposition of Zn-Cd-Tu complexes provided active Cd²⁺, Zn²⁺ and S²⁻ that reacted and formed Zn_{1-x}Cd_xS solid solutions. In our study, some amount of ZnS dissolves in liquid CdI₂ and in

cooling when solubility is decreasing, the solid solution crystallizes out on cooling to 338 °C. More information could be found by studying the properties of liquid (and/or gaseous) phase of CdI₂. Considering that the process under discussion takes place simultaneously with melting of CdI₂, the possible reactions involving CdI₂ (g) seem to be less probable and we should consider the processes in liquid phase. It is well known that many salts in their molten phase are in the form of ionic liquids, but not CdI₂. It was found that the melt of MX₂ (M=Zn, Cd, Hg and X=Cl, Br, I) has an extremely low ionic conductivity¹⁴⁵. MX₂ salts retain their solid phase structure even in liquid phase, in which the small metal²⁺ ions occupy tetrahedrally coordinated sites in a closely packed anion structure, with a strong intermediate range ordering^{146,147}. Also, measurements of the scattering of thermal neutrons from natural samples of molten ZnCl₂, ZnBr₂ and ZnI₂ confirmed a structural model of [ZnI₄]²⁻, in which the small Zn²⁺ ions occupy tetrahedrally coordinated sites in a closely packed anion structure, with a strong intermediate range ordering¹⁴². Therefore, we suppose that a small amount of ZnS dissolves in liquid CdI₂ and the bonds of solid ZnS should be broken in the dissolution process. The dissolved Zn²⁺ can displace Cd²⁺ ions in the closely packed anion structure [CdI₄]²⁻ in molten CdI₂. In the solidification, S²⁻ ions react with delimitated Cd²⁺ ions, forming CdS and ZnI₂ (see reaction 17), precipitating from the melt as solid solution of Zn_{1-x}Cd_xS at 354 °C. We see also solidification at 338 °C, at much lower temperature than in the pure CdI₂. Probably ZnI₂-CdI₂ liquid solution freezes at 338 °C. According to Chikanov *et al.*¹³⁰, in ZnI₂-CdI₂ mixtures there forms a continuous row of solid solutions¹⁴⁴. After opening the ampoule, ZnI₂ could not be detected by phase analyses due to its high hygroscopicity. The phases detected by Raman are shown in Figure 20b. (XRD patterns can be found in Appendix B).

Table 7. Annealing conditions, determined phases, reactions and calculated ΔG values for ZnS+CdI₂ mixture

Annealing conditions (°C)	Phases by XRD	Phases by Raman/peak position (cm ⁻¹)	Equation	Reactions	ΔG (kJ mol ⁻¹)/ Temperature (°C)
Annealed at 385 and quenched to RT	ZnS, CdI ₂	ZnS/ 218, 272 CdI ₂ / 110	15	ZnS _(s) + CdI ₂ (s, l) = ZnI ₂ + CdS ¹⁴⁴	44.1/T=0 51.8/ T=800
Heated to 800, cooled down and quenched at 330 to RT	Zn _{0.94} Cd _{0.06} S (Zn _{0.8} Cd _{0.2})S CdI ₂ , ZnS	CdI ₂ , ZnS	16	ZnS + CdI ₂ (g) = ZnI ₂ + CdS ¹⁴⁸	-8.28/ T=300 Positive T>300
			17	ZnS + I ⁺ + CdI ⁺ (g) = CdS + ZnI ₂ (g) ¹⁴⁸	-59.455/ T=300 -86.182/ T=800
Heated to 800, cooled down to and quenched at 350 to RT	CdI ₂ , ZnS	CdI ₂ , ZnS	18	ZnS + I ⁺ + CdI ⁺ (g) = ZnS + CdI ₂ ¹⁴⁸	-186.686/ T=300 -112.968/ T=800
			19	ZnS + I ⁺ + CdI ⁺ (g) = Zn _{1-x} C _x dS + 1-xCdI ₂	Proposed
			20	ZnS + CdI ₂ (l) = Zn _{1-x} Cd _x S (l) + ZnI ₂ (l)	Proposed

3.3.6 Mixture for synthesis of Cu_2SnS_3 ($\text{CdI}_2+\text{SnS}+\text{Cu}_2\text{S}+\text{S}$)

In the mixture of $\text{Cu}_2\text{S}+\text{SnS}+\text{S}+\text{CdI}_2$, we observed two endothermic peaks in the heating process with enthalpy signals of 0.7J ($88\mu\text{Vs}$) and 2.0J ($265\mu\text{Vs}$) at 339 and 360 °C, respectively. The former is attributed to the melting of CdI_2 while the latter is attributed to the transformation of Cu_2S to $\text{Cu}_{1.96}\text{S}$ similar to $\text{Cu}_2\text{S}+\text{CdI}_2$ (Part 3.3.3). The low enthalpy signal in Figure 22a can be attributed to the net effect of the endothermic melting of CdI_2 and the exothermic formation of SnS_2 and Cu_2SnS_3 alongside the other concurrent processes. This confirms a high solubility/interaction between the flux material and the precursor compounds. The enthalpy calculation for the cumulative formation process in the heating can be given as ($666\mu\text{V s} - 88\mu\text{V s} = 578\mu\text{V s}$) - this corresponds to $13 \pm 2\text{ kJ mol}^{-1}$. In the cooling process, the enthalpy signal was observed as a single freezing exothermic process attributed to the freezing of CdI_2 with an enthalpy signal of 2.7 J ($343\mu\text{V s}$). The XRD analysis of the sample mixture of $\text{CdI}_2+\text{SnS}+\text{Cu}_2\text{S}+\text{S}$ heated to 800 °C and then cooled down to 340 °C before quenching rapidly to room temperature showed the presence of Cu_2SnS_3 and another ternary CTS. In the second heating/cooling process, we observed single endothermic/exothermic peaks for the melting and freezing of the mixture with close enthalpy signal values, as observed in the first heating/cooling process. The reaction between $\text{Cu}_2\text{S}+\text{SnS}+\text{S}$ in the flux leads to the formation of ternary compounds Cu_2SnS_3 ⁵⁴ and Cu_4SnS_6 ¹⁴⁹ (see Table 8), as detected by XRD and the formation of the ternaries takes place during the melting of the flux (CdI_2). Figure 22 shows the Raman spectra of the studied mixtures.

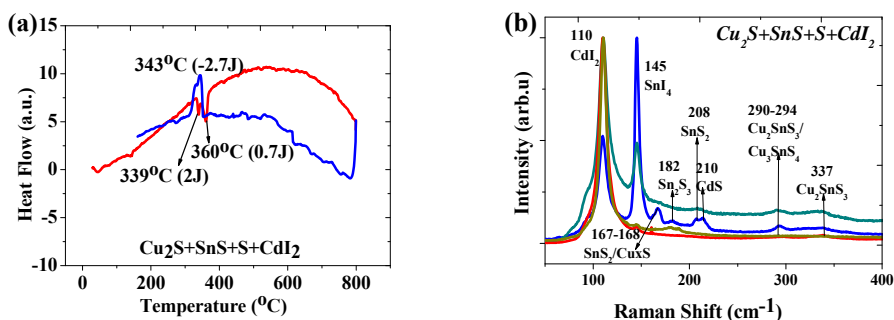


Figure 22. (a) DTA curves of $\text{CdI}_2+\text{SnS}+\text{Cu}_2\text{S}+\text{S}$ mixture (b) Raman spectra of $\text{Cu}_2\text{S}+\text{SnS}+\text{S}+\text{CdI}_2$ heated and quenched at different temperatures: blue - heated to 339 °C quenched to room temperature, red - heated to 360 °C and quenched to room temperature, pink- heated to 800 °C and cooled down to 340 °C before quenching to room temperature, black - heated to 800 °C and cooled down to 470 °C before quenching to room temperature.

Table 8. Annealing conditions, determined phases, reactions and calculated ΔG values for $CdI_2+SnS+Cu_2S+S$ mixture

Annealing conditions (°C)	Phases by XRD	Phases by Raman/peak position (cm^{-1})	Equation	Reactions	ΔG ($kJ\ mol^{-1}$)/Temperature (°C)
Heated to 339	CdI_2 , $Cu_{1.96}S$,	Raman spectra are very difficult to analyze due to the overlapping of peaks of multi-component systems	23	$2CuS = Cu_2S + S(l)^{144,150}$	-4.48/T=500 -39.88/ T=1000
Heated to 360	CuI , SnS , Sn_2SI_2 , Cu_2SnS_3	Raman spectra are very difficult to analyze due to the overlapping of peaks of multi-component systems	24	$2SnS + 2S = 2SnS_2$	-28.6/T=400
	25		$2CuS + SnS$ (melt) = $Cu_2SnS_3^{34,77}$	Proposed	
Heated to 800 and cooled down to 340	CdI_2 , Cu_2S , SnS_2 , CuI , Cu_2SnS_3 , Cu_4SnS_6 ,	Raman spectra are very difficult to analyze due to the overlapping of peaks of multi-component systems	26	$2CuS + SnS$ (melt) = Cu_2SnS_3 $Cu_2S + SnS = Cu_2SnS_3^{34,77}$	Proposed
	27		$2Cu_2S + SnS_2 + 2S = Cu_4SnS_6^{34}$	Proposed	

3.3.7 Mixture for synthesis of quaternary CZTS compound (CdI₂+SnS+Cu₂S+S+ZnS)

DTA curves show that the mixture of CdI₂ with the binary precursors in the required stoichiometric composition for the formation of Cu₂ZnSnS₄ melts and solidifies at 366 °C and at 353 °C, respectively, with thermal effects of 2.4 J (308 μV s) in the endothermic and exothermic processes (see Figure 23a). Considering the reduced enthalpy signals, the melting/solidification processes are accompanied by other multiple processes proceeding simultaneously, as described in the previous sections. By the DTA analysis, we found that the formation of CZTS in molten CdI₂ proceeds via an exothermic process with an enthalpy signal of (666 μV s - 308 μV s = 358 μV s), which corresponds to an enthalpy value of 8 ± 2 kJ mol⁻¹. Most of the secondary phases formed during the intermediate processes were consumed during the formation process giving rise to Cu₂Zn_{1-x}Cd_xSnS₄ as the prevailing phase. All phases detected by Raman and XRD and the proposed reaction path are summarized in Table 9. The formed solid solution of Cu₂Zn_{1-x}Cd_xSnS₄ was confirmed by the EDX analysis and by the shift of Raman peak from 338 cm⁻¹ to 333 cm⁻¹ ¹²⁹. We suggest that the formation of Cu₂Zn_{1-x}Cd_xSnS₄ solid solution proceeded via an intermediate reaction between Zn_{1-x}Cd_xS and Cu₂SnS₃ by equation (28) or directly by reaction (29) in the molten phase of CdI₂. Phases detected by Raman are given in Figure 23b, all details of the XRD patterns for the phases detected are presented in Appendix B.

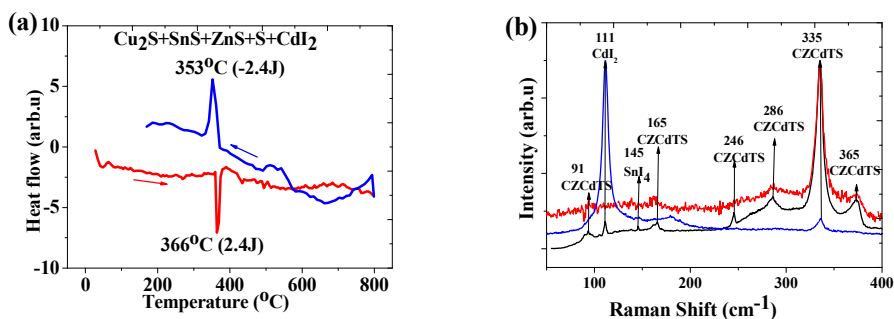


Figure 23. (a) DTA curves of precursor mixture CdI₂+SnS+Cu₂S+S+ZnS, (b) Raman spectra of Cu₂S+SnS+ZnS+S+CdI₂: blue - heated to 800°C and quenched to room temperature, red - heated to 800 °C and cooled to 600°C before quenching to room temperature, black - heated to 800 °C and cooled down to 350 °C and quenched rapidly to room temperature.

Table 9. Annealing conditions, determined phases, reactions and calculated ΔG values for $CdI_2+SnS+Cu_2S+ZnS+S$ mixture

Annealing conditions (°C)	Phases by XRD	Phases by Raman/Raman peak position (cm ⁻¹)	Equation	Reactions	ΔG (kJ mol ⁻¹) Temperature (°C)
Heated to 800	$Cu_2Zn_{1-x}Cd_xSnS_4$	$CdI_2/110^{10}$ $CuI/148^{10,138}$ $Cu_2Zn_xCd_{1-x}SnS_4/333, 374^{67}$	28	$Cu_2SnS_3 + Zn_{1-x}Cd_xS = Cu_2Zn_{1-x}Cd_xSnS_4$	Proposed
Heated to 800 and cooled to 600	$CdI_2,$ $Cu_2-xS,$ $Cu_2SnS_3,$ $Cu_2Zn_{1-x}Cd_xSnS_4,$ $SnI_4,$	$CdI_2/110^{10}$ $CuI/148^{10,138}$ CZTS $Cu_2Zn_xCd_{1-x}SnS_4/333, 374^{67}$	29	$Cu_2S + SnS + Zn_{1-x}Cd_xS + S = Cu_2Zn_{1-x}Cd_xSnS_4$	
Heated to 800 and cooled to 350	$CdI_2,$ $CuI,$ $SnI_4,$ $Cu_2Zn_{1-x}Cd_xSnS_4$	$CdI_2/110^{10}$ $CuI/148^{10,138}$ $Cu_2Zn_xCd_{1-x}SnS_4/333, 374^{67}$			

The ΔG calculations presented in Figure 24 show that the most probable route to the $\text{Cu}_2\text{Zn}_{1-x}\text{Cd}_x\text{SnS}_4$ formation is possible by the intermediate formation of $\text{CdI}^+(\text{g})$. The interaction between solid binaries (ZnS , SnS , and CuS) and CdI_2 at a temperature lower than 400°C is not favorable because ΔG is positive for $\text{Zn}_{1-x}\text{Cd}_x\text{S}$ formation; therefore, this rules out the possibility to form a quaternary $\text{Cu}_2\text{Zn}_{1-x}\text{Cd}_x\text{SnS}_4$. As mentioned earlier, there exists a thermo-dynamical possibility for a reaction between ZnS and CdI^+ to form $(\text{Zn}_{1-x}\text{Cd}_x\text{S})$ for temperatures between 0 and 1000°C , which is the only favorable path for the formation $\text{Cu}_2\text{Zn}_{1-x}\text{Cd}_x\text{SnS}_4$ by means of gas phase reaction. However, we have recognized that the formation of liquid phase of CdI_2 triggers all the observed exothermic processes that are accompanied by a sudden decrease in the fusion enthalpy and the melting temperature of CdI_2 , suggesting that the formation of $\text{Cu}_2\text{Zn}_{1-x}\text{Cd}_x\text{SnS}_4$ proceeds in molten phase. However, we could not find data for thermodynamical calculations of processes in liquid CdI_2 . Therefore, we may seek further understanding of the processes occurring in molten CdI_2 .

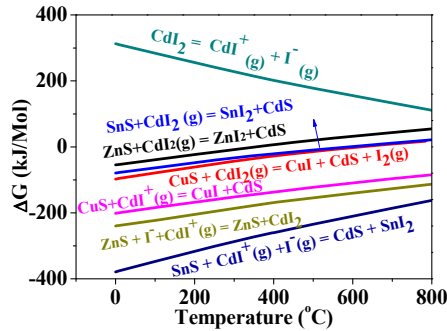


Figure 24. Calculated ΔG values for different reactions showing the possible reaction probability for the synthesis of $\text{Cu}_2\text{ZnCdSnS}_4$ in molten CdI_2 .

In this work, we found that the Cd concentration in the formed CZCdTS increases with increasing amounts of CdI_2 in the synthesis. Cd incorporation is dependent on the temperature and on the amount of CdI_2 , but not influenced by the heating time. The direct exchange reaction between solid ZnS and CdI_2 , resulting in the formation of CdS and ZnI_2 is thermodynamically impossible because $\Delta G > 0$. By the DTA analysis, we obtained a much lower endothermal effect of melting of the precursor mixture of $\text{ZnS} + \text{CdI}_2$ in comparison with pure CdI_2 . The reason can be in the occurrence of some simultaneous compensating exothermal process. We detected also some lowering of the melting temperature that may occur due to the dissolution of ZnS in molten CdI_2 . Therefore, we believe that the formation of CdS and $\text{Zn}_{1-x}\text{Cd}_x\text{S}$ is enabled by the dissolution of some ZnS in molten CdI_2 . It is well known that the amount of dissolved solute is dependent on the amount of solvent and temperature, as in the case of Cd content in $\text{Zn}_{1-x}\text{Cd}_x\text{S}$ and also Cd content in the formed CZCdTS monograins, which was found to be dependent on the temperature and on the amount of used CdI_2 as solvent in the present work.

CONCLUSIONS

Based on the results of my PhD research, the following conclusions were reached:

- 1) We found that solid solutions $\text{Cu}_2\text{Zn}_{1-x}\text{Cd}_x\text{SnS}_4$ with limited Cd content form in the synthesis of CZTS in molten CdI_2 from binary precursor compounds through an intermediate formation of $\text{Zn}_{1-x}\text{Cd}_x\text{S}$.
 - Based on our experimental findings, $\text{Cu}_2\text{Zn}_{1-x}\text{Cd}_x\text{SnS}_4$ formation can be described as a two-stage process: firstly, $\text{Zn}_{1-x}\text{Cd}_x\text{S}$ and Cu_2SnS_3 form in molten CdI_2 ; secondly, $\text{Zn}_{1-x}\text{Cd}_x\text{S}$ and Cu_2SnS_3 react to form $\text{Cu}_2\text{Zn}_{1-x}\text{Cd}_x\text{SnS}_4$.
 - The solubility of ZnS in the liquid phase of CdI_2 is suggested to be a limiting factor in the $\text{Zn}_{1-x}\text{Cd}_x\text{S}$ formation, which determines the amount of Cd incorporated into CZTS crystals.
 - The formation of liquid phase CdI_2 was accompanied by a sudden decrease in the enthalpy of fusion for CdI_2 in the mixtures with precursors. We therefore suggest that the formation process starts slightly below the melting temperature of pure CdI_2 and proceeds through the liquid phase at the melting of the flux.
- 2) From the study of the physical and chemical process occurring in the thermal heating of mixtures of CdI_2 with individual precursor compounds, we conclude the following:
 - The melting temperatures of CdI_2 in each studied mixture were found to be lower than the melting temperature of pure CdI_2 , which is attributed to the interaction between the precursor compound and the flux.
 - The overall enthalpy values of the processes in each studied mixture are formed via an exothermic process alongside the endothermic melting of the CdI_2 , which gives rise to a lower melting temperature and enthalpy of fusion of the CdI_2 flux.
 - The formation of Cu_2SnS_3 from $\text{Cu}_2\text{S}+\text{SnS}+\text{S}$ in CdI_2 gave an enthalpy value of $13 \pm 2 \text{ kJ mol}^{-1}$ while the formation reaction of $\text{Cu}_2\text{Zn}_x\text{Cd}_{1-x}\text{SnS}_4$ in the liquid phase of CdI_2 takes place with the experimentally determined enthalpy of $8 \pm 2 \text{ kJ mol}^{-1}$.
 - The low enthalpy of $\text{Cu}_2\text{Zn}_x\text{Cd}_{1-x}\text{SnS}_4$ formation compared to high enthalpy of the ternary Cu_2SnS_3 formation could confirm that the solid $\text{Cu}_2\text{Zn}_x\text{Cd}_{1-x}\text{SnS}_4$ solution is formed from the reaction between Cu_2SnS_3 and $\text{Zn}_{1-x}\text{Cd}_x\text{S}$.
 - The activation energy of the Cd incorporation process into the CZCdTS crystals was estimated as $17.5 \pm 2 \text{ kJ/mol}$.
- 3) From the study of the influence of growth process conditions on the CZTS monograin material properties, we found that the properties of the synthesized monograin powder can be modified by changing the synthesis conditions:

- Materials synthesized with smaller flux concentrations and at higher temperatures show less facet and have a more rounded shape. With increasing time as well as with increasing flux concentrations, faceted crystals became more obvious. The most round shaped grains were formed in the samples with the lowest used amount of CdI_2 .
- The yield of usable powder grains with a size of 50-100 μm was higher as the flux concentration decreased. This may be due to the increased sintering effect.
- The amount of Cd incorporated into forming $\text{Cu}_2\text{Zn}_{1-x}\text{Cd}_x\text{SnS}_4$ from CdI_2 increases as the synthesis temperature rises and the amount of used CdI_2 grows.

ACKNOWLEDGEMENTS

First of all, I would like to appreciate God who has made my Journey through this Ph.D. program a great success. To my amiable and lovely wife, Mrs. Yemisi Nkwusi, I want to thank you for your love, care and understanding, you have been a great motivation for me, God will continue to strengthen you. I would also like so say a big thank-you to my Parents and siblings for their prayers and support and to all my friends, I appreciate your support and words of encouragement.

To my Supervisor, senior researcher Mare Altsaar and my colleague Inga Leinemann, you have been so amazing, word cannot express how much I appreciate your effort. Your patience and understanding have been my greatest encouragement and motivation to succeed during my program.

To all the Member staff at the previous Department of Chemical and Materials Technology, my colleagues, S. Kumar, M. Pilvet and senior colleagues, Senior researchers V. Mikli, J. Raudoja, K. Timmo, M. Grossberg, T. Varema, the director of the previous institute M. Kauk-Kuusik, Professor A. Öpik, Professor D. Meissner, Professor E. Mellikov, I want to appreciate the space you gave me to advance my career even as a foreigner, Dr R. Kuusik, thank you for your kind support in making DTA analyses in the your laboratory, Dr. T. Kaljuvee for DTA measurements, Dr. R. Traksmaa for XRD measurements. To Professor R. Gronsky of the Department of Material Science and Engineering at University of California, Berkeley, I appreciate your support while I was at UC Berkeley.

This work was supported by institutional research funding IUT 19-28 of the Estonian Ministry of Education and Research and by the European Union through the European Regional Development Fund, Project TK141. Funding for facilities used in this research was provided by the core infrastructure support IUT-T4 of the Estonian Ministry of Education and Research; and Doctoral Studies and Internationalization Program DoRa of the European Social Funds, the Estonian Ministry of Education and Research Contracts No. SF0140099s08, TK117, AR10128 and by grants (No 8964, ETF 9425, ETF 9346).

KOKKUVÕTE

Antud doktoritöö keskendub keemiliste protsesside uurimisele, mis toimuvad $\text{Cu}_2\text{ZnSnS}_4$ (CZTS) süntees-kasvatusel sulas CdI_2 -s eesmärgiga selgitada välja võimalused ühefaasilise monoterapulbri sünteesiks, mis sobib kasutamiseks absorberkihina monoterakiht-päikesepatareides. Otsene keelutsoon 1,43-1,5 eV, suur valguse neeldumisvõime (absorptsioonikoefitsient üle 10^4 cm^{-1}) ja odavate koostiselementide laialdane esinemine maakoos teevad CZTS atraktiivseks päikesepatarei absorbermaterjaliks. $\text{Cu}_2\text{ZnSn}(\text{SeS})_4$ baasil kilelise päikesepatarei rekordefektiivsus on 12.6 %.

Üheks odavaks absorbermaterjaliks sünteesi- ja saamismeetodiks on monoterapulbrite sünteeskasvatus, milles iga sünteesuv kristall võib moodustuda ja kasvada kui monokristall. Praegu on $\text{Cu}_2\text{ZnSn}(\text{Se,S})_4$ monoterakiht-päikesepatarei (crystalsol OÜ) sertifitseeritud kasutegur 9.5 %, mis on monoterakiht päikesepatarei struktuuri tõttu väiksem kui aktiivmaterjali kasutegur selles (ligikaudu 13%). Töö eesmärgiks oli kirjeldada keemilisi vastasmõjusid CZTS pooljuhtühendi sünteesiprotsessis osalevate lähteühendite ja sulafaasilist keskkonda võimaldava CdI_2 vahel ja leida võimalused CZTS ühefaasilise monoterapulbrilise absorbermaterjali sünteesiks ja tootmiseks. Uuringud olid vajalikud, kuna ühefaasilise absorbermaterjali saamine sulades soolades on keerukas mitmete kõrvalühendite tekkevõimaluse tõttu ja kuna CZTS sünteeskasvatuse keemilist kulgu CdI_2 -s polnud seni veel uuritud.

Doktoritöö keskendub CZTS keemilise moodustumise kirjeldamisele kasutades lähteühenditena Cu_2S , ZnS , SnS ja elementaarset väävlit. Käesolevas doktoritöös kasutati erinevaid analüüsimeetodeid: differentsiaal-termilist analüüsi (DTA) termiliste efektide toimumise avastamiseks uuritavates proovides ja nendes toimuvate protsesside soojusefektide määramiseks, skaneerivat elektronmikroskoopiat (SEM) moodustunud kristallide morfoloogia uurimiseks, energia-dispersiivset spektroskoopiat (EDX) elementkoostise ja Raman spektroskoopiat ning röntgendifraktsiooni (XRD) faasikoostiste määramisel. Keemiliste protsesside toimumise tõenäosust hinnati-kontrolliti Gibbsi vaba energia muutuste arvutuste abil kasutades andmebaasi „*Database of HSC Chemistry Ver. 6.0*”. DTA uuringud viidi läbi vastavale analüüsiseadmele kohandatud suletud kvartsampullides. DTA kalibratsiooniks kasutati võrdlusainena sama CdI_2 , mis sünteeskasvatuselgi, kuna tavaliselt kasutatavad võrdlusained ei sobinud kalibreerimiseks kvartsampullides. Pärast DTA abil detekteeritud termiliste efektidega kaasnevate protsesside toimumistemperatuuride leidmist ja protsessientalpiate määramist valmistati identsed proovid suuremates kogustes iga avastatud protsessi jaoks ja kuumutati proove 4 tundi kinnistes vaakumampullides DTA abil leitud temperatuuridest veidi kõrgematel temperatuuridel, et leida toimunud faasimuutused. Sellisel teel leiti ühendid, mis tekkisid või lagunesid vastavatel temperatuuridel. Kasutades ülalkirjeldatud eksperimentaalset lähenemist ja analüütiliste võimaluste

kompleksi määrati antud töös eksperimentaalselt Cu_2SnS_3 ja $\text{Cu}_2\text{Zn}(\text{Cd})\text{SnS}_4$ tekkeentalpiad.

Töö tulemusena leiti, et CZTS monoterapulbrite sünteeskasvatusel sula CdI_2 keskkonnas toimub Cd inkorporeerumine $\text{Cu}_2\text{ZnSnS}_4$ võresse ja $\text{Cu}_2\text{Zn}_{1-x}\text{Cd}_x\text{SnS}_4$ tahke lahuse tekkimine, milles Cd sisaldus on piiratud kasutatud CdI_2 hulga ja süntees-kasvatuse temperatuuriga. Cd inkorporeerumise protsessi aktivatsioonienergiaks hinnati $17.5 \pm 2 \text{ kJ mol}^{-1}$. Leiti, et $\text{Cu}_2\text{Zn}_{1-x}\text{Cd}_x\text{SnS}_4$ moodustumist võib kirjeldada kahe-astmelise protsessina: esmalt tekivad $\text{Zn}_{1-x}\text{Cd}_x\text{S}$ ja Cu_2SnS_3 , mis omavahel moodustavad $\text{Cu}_2\text{Zn}_{1-x}\text{Cd}_x\text{SnS}_4$. DTA kõverate võrdlemisel leiti, et kõikide uuritud kvaasi-binaarsete süsteemide (lähteühend-sulandaja) ühine joon on, et (a) segude (CdI_2 segus S, ZnS, Cu_2S või SnS) sulamistemperatuurid on madalamad kui puhtal soolal, mis on indikaatoriks mõningasele lähteühendi lahustumisele CdI_2 -s; (b) kohe vahetult pärast endotermilist sulamisprotsessi algust ilmub eksotermiline efekt, mis alandab CdI_2 sulamisprotsessi entalpiat, näidates keemilist aktiivsust segudes olevate ühendite vahel vahetult pärast sula faasi teket; (c) $\text{CdI}_2+\text{Cu}_2\text{S}$ ja CdI_2+SnS segudes avastati CdS ja erinevate joodi sisaldavate ühendite (SnI_4 , Sn_2SI_2 , CuI, ja $\text{Cu}_2\text{Cd}_3\text{I}_4\text{S}_2$) teke ja CdI_2+ZnS segus $\text{Zn}_{1-x}\text{Cd}_x\text{S}$ teke. Võttes arvesse eksperimentaalselt leitu ja kirjandusest teadaolevat fakti, et CdI_2 säilitab sulamisel oma $[\text{CdI}_4]^{2-}$ anioon-struktuuri, kus väikesed Cd^{2+} ioonid asetsevad tetraheedselt koordineeritud kohtades, pakutakse töös välja versioon, et erinevate jodiidide ja CdS teke on võimalik, kui Cd^{2+} ioonid asenduvad lahustunud Zn, Sn või Cu ionidega. CdS teke on eelduseks $\text{Zn}_{1-x}\text{Cd}_x\text{S}$ tekkele ja Cd haaramisele nelikühendi võresse. ZnS lahustumine sulas CdI_2 -s on limiteerivaks teguriks Cd inkorporeerumisele $\text{Cu}_2\text{ZnSnS}_4$ võresse ja $\text{Cu}_2\text{Zn}_{1-x}\text{Cd}_x\text{SnS}_4$ tekkele. Cu_2SnS_3 tekke-entalpia CdI_2 -($\text{Cu}_2\text{S}+\text{SnS}+\text{S}$) segus oli $13 \pm 2 \text{ kJ mol}^{-1}$ ja $\text{Cu}_2\text{Zn}_x\text{Cd}_{1-x}\text{SnS}_4$ tekkereaktsiooni entalpia sulas CdI_2 -s leiti olevat $8 \pm 2 \text{ kJ mol}^{-1}$. Tööst selgus, et moodustuvate $\text{Cu}_2\text{Zn}_{1-x}\text{Cd}_x\text{SnS}_4$ kristallide kuju ja suurust saab muuta varieerides sünteesiprotsessi tingimusi. Nii väiksemate CdI_2 koguste kasutamisel kui ka kõrgematel temperatuuridel moodustuvad ümarama kujuga kristallid. Monotera-membraanides kasutatavate kristallide (50-100 μm) saagis on suurem, kui kasutada väiksemaid koguseid CdI_2 -sulandajat.

ABSTRACT

This thesis is focused on the studies of chemical processes in the synthesis-growth of $\text{Cu}_2\text{ZnSnS}_4$ (CZTS) in molten CdI_2 with the aim to produce single absorber materials for monograin layer solar cells. The direct band gap, high absorption coefficient and low cost and earth-abundant non-toxic constituent elements make CZTS attractive as absorber material for solar cells. $\text{Cu}_2\text{ZnSnS}_4$ -type materials in thin film solar cells have shown record efficiency of 12.6 %.

Monograin powder growth is one of the cheapest synthesis methods, allowing production of materials where every grain can be formed and grown as a single crystalline particle. So far, 9.5 % of certified efficiency has been reached for $\text{Cu}_2\text{ZnSn}(\text{Se}, \text{S})_4$ monograin layer solar cells by Crystalsol OÜ; due to the specific structure, the power conversion efficiency of the active material is around 13%. The chemical interactions between precursor compounds for CZTS synthesis and CdI_2 in molten phase have not been studied yet. Therefore, the thesis is centered on possible chemical reactions between molten CdI_2 and individual binary compounds - Cu_2S , ZnS , SnS - followed by studies on more complicated mixtures for synthesis of Cu_2SnS_3 (CTS) and CZTS in CdI_2 with the aim to fully understand the formation pathway of CZTS in molten CdI_2 .

By variation of synthesis-growth conditions, the possibilities to change the properties of produced powders were studied. Different analytical methods were used: differential thermal analysis (DTA) for the detection of temperatures of processes accompanied with thermal effects and for the determination of enthalpies of these processes, scanning electron microscopy (SEM) was used for morphology studies, energy dispersive spectroscopy (EDX) for elemental composition, Raman spectroscopy and X-ray diffraction (XRD) for phase determination. The probability of possible chemical reactions was evaluated by calculations of Gibbs free energy change using "Database of HSC Chemistry Ver. 6.0". DTA studies were performed in vacuum-sealed quartz ampoules adopted for the used DTA set-up. For DTA calibrations, the same CdI_2 flux salt as reference material was used because the traditionally used reference materials were unstable or gave low signal in quartz ampoules. After the detection of temperatures of thermal effects by DTA, larger identical samples were prepared for each detected effect. These samples were heated for 4 hours at slightly higher temperatures than the occurrence of thermal effects for discovering possible phase changes. Using the experimental approach described above and the complex of analytical methods, the formation enthalpy values of Cu_2SnS_3 and $\text{Cu}_2\text{ZnSnS}_4$ were experimentally determined.

In the present thesis, different aspects that determine the path of synthesis of the CZTS compound and the shape of crystals were found. The synthesis of CZTS monograin powders in CdI_2 resulted in the formation of solid solutions of $\text{Cu}_2\text{Zn}_x\text{Cd}_{1-x}\text{SnS}_4$ with limited Cd content. The amount of Cd incorporated from CdI_2 into forming $\text{Cu}_2\text{Zn}_{1-x}\text{Cd}_x\text{SnS}_4$ increased as the synthesis-growth process temperature was raised and the amount of CdI_2 grew. The activation energy of

the Cd incorporation process was estimated as $17.5 \pm 2 \text{ kJ mol}^{-1}$. $\text{Cu}_2\text{Zn}_{1-x}\text{Cd}_x\text{SnS}_4$ formation in molten CdI_2 can be described as a two-stage process: firstly, $\text{Zn}_{1-x}\text{Cd}_x\text{S}$ and Cu_2SnS_3 form in molten CdI_2 ; secondly, $\text{Zn}_{1-x}\text{Cd}_x\text{S}$ and Cu_2SnS_3 react to form $\text{Cu}_2\text{Zn}_{1-x}\text{Cd}_x\text{SnS}_4$. By studies of mixtures of individual precursors with CdI_2 we found chemical possibilities for the intermediate formation of $\text{Zn}_{1-x}\text{Cd}_x\text{S}$ taking into account our experimental findings: (a) CdI_2 mixed with different precursors - S, ZnS, Cu_2S or SnS - melts at temperatures lower than pure CdI_2 , showing some solubility of the precursors in molten CdI_2 ; (b) the formation of liquid phase of CdI_2 was accompanied with exothermic processes manifested by sudden decrease in the fusion enthalpy of CdI_2 mixtures with precursors; (c) CdS and different iodine-containing compounds - SnI_4 , Sn_2SI_2 , CuI, and $\text{Cu}_2\text{Cd}_3\text{I}_4\text{S}_2$ - were formed in $\text{CdI}_2+\text{Cu}_2\text{S}$ and CdI_2+SnS and a solid solution of $\text{Zn}_{1-x}\text{Cd}_x\text{S}$ in CdI_2+ZnS .

Combining our experimental findings with the knowledge from literature that molten phase of CdI_2 retains its solid closely packed anion structure of $[\text{CdI}_4]^{2-}$ in which the small Cd^{2+} ions occupy tetrahedrally coordinated sites, we propose that the formation of different iodides and CdS can occur due to the displacement of Cd^{2+} ions by Zn^{2+} (or by Sn and Cu ions) dissolved in CdI_2 . The formation of CdS is the presupposition for $\text{Zn}_{1-x}\text{Cd}_x\text{S}$ formation. The solubility of ZnS in the liquid phase of CdI_2 is proposed to be a limiting factor in the CdS formation and due to this also the incorporation of Cd into CZTS crystals is limited. The formation of Cu_2SnS_3 from $\text{Cu}_2\text{S}+\text{SnS}+\text{S}$ in CdI_2 gave an enthalpy value of $13 \pm 2 \text{ kJ mol}^{-1}$ while the reaction of formation $\text{Cu}_2\text{Zn}_x\text{Cd}_{1-x}\text{SnS}_4$ in the liquid phase of CdI_2 takes place with the experimentally determined enthalpy of $8 \pm 2 \text{ kJ mol}^{-1}$. The low formation enthalpy of $\text{Cu}_2\text{Zn}_x\text{Cd}_{1-x}\text{SnS}_4$ compared to high formation enthalpy of the ternary Cu_2SnS_3 confirm that the solid solution $\text{Cu}_2\text{Zn}_x\text{Cd}_{1-x}\text{SnS}_4$ is formed from the reaction between Cu_2SnS_3 and $\text{Zn}_{1-x}\text{Cd}_x\text{S}$. It was found that the shape and size of crystals can be modified by changing the synthesis conditions. Using smaller flux concentrations and higher temperatures less faceted and more rounded crystals can be grown. The yield of powder grains usable in monograin membranes with a size of 50-100 μm was higher as the flux concentration decreased

REFERENCES

1. Jimbo, K., Kimura, R., Kamimura, T., Yamada, S., Maw, W.S., Araki, H., Oishi, K., Katagiri, H. *Thin Solid Films*, **515** (2007) 5997-5999.
2. Wang, W., Winkler, M. T., Gunawan, O., Gokmen, T., Todorov, T. K., Zhu, Y., Mitzi, D. B. *Advanced Energy Materials*, **4** (2014) 1-5.
3. Ito, K.; Nakazawa, T. *Japanese Journal of Applied Physics*, **27** (1988) 2094–2097.
4. Shockley W, Queisser H J. *Journal of Applied Physics*, **32** (1961) 510-519.
5. Levi, D., Sarah, K. National Renewable Energy Laboratory (NREL), (www.nrel.gov/pv/assets/images/efficiency-chart.png).
6. Green, M.A., Emery, K., Hishikawa, Y., Warta, W., Dunlop E.D. *Solar Cell Efficiency Tables (Version 45). Progress In Photovoltaics: Research and Applications*, **23** (2015) 1-9.
7. Mellikov, E., Altosaar, M., Krunks, M., Krustok, J., Varema, T., Volobujeva, O., Grossberg, M., Kaupmees, L., Dedova, T., Timmo, K. and Ernits, K. *Thin Solid Films*, **516** (2008) 7125-7134.
8. Meissner D. *Materials and Processes for Energy: Communicating Current Research and Technological Developments*, (2013) 114-125.
9. Kauk-Kuusik, M., Timmo, K., Danilson, M., Altosaar, M., Grossberg, M., Ernits K. *Applied Surface Science*, **357** (2015) 795-798.
10. Klavina, I., Kaljuvee, T., Timmo, K., Raudoja, J., Traksmaa, R., Altosaar, M. and Meissner, D. *Thin Solid Films*, **519** (2011) 7399-7402.
11. Leinemann, I., Timmo, K., Grossberg, M., Kaljuvee, T., Tõnsuaadu, K., Traksmaa, R., Meissner D. *Journal of Thermal Analysis and Calorimetry*, **119** (2015) 1555-1564.
12. Leinemann, I., Zhang, W., Kaljuvee, T., Tõnsuaadu, K., Traksmaa, R., Raudoja, J., Meissner D. *Journal of Thermal Analysis and Calorimetry*, **118** (2014) 1313-1321.
13. Pope C H. *Solar Heat: Its Practical Applications*, CH Pope. (1903).
14. Craddock D. *Renewable Energy Made Easy: Free Energy From Solar, Wind, Hydropower, and Other Alternative Energy Sources*. Atlantic Publishing Company, (2008).
15. Chiadini, F., Fiumara, V., Scaglione, A., Pulsifer, D.P., Martín-Palma, R.J., Pantano, C.G. and Lakhtakia, A. *Optics and Photonics News*, **22** (2011) 38.
16. Platzter, M.D. *US Solar Photovoltaic Manufacturing: Industry Trends, Global Competition, Federal Support Washington, DC: Congressional Research Service*, **6** (2012) 1-32
17. Matroni, D.R. *Photovoltaic System Acceptability in The Future (Doctoral dissertation, Worcester Polytechnic Institute)*, (2011).
18. Pipkin, F.M. *Advances in atomic and molecular physics*, **14** (1979) 281-340.
19. Treble, F. *Milestones In The Development of Crystalline Silicon Solar Cells. Renewable Energy*, **15**(1998) 473-478.
20. Xing, Y., Han, P., Wang, S., Liang, P., Lou, S., Zhang, Y., Hu, S., Zhu, H., Zhao, C. and Mi, Y. *Renewable and Sustainable Energy Reviews*, **51** (2015) 1697-1708.
21. Brendel, R. *Japanese Journal of Applied Physics*, **40** (2001) 4431.

22. Romeo, N., Bosio, A., Tedeschi, R. and Canevari, V. *Materials Chemistry and Physics*, **66** (2000) 201-206.
23. Fang, Z., Wang, X.C., Wu, H.C. and Zhao, C.Z. *International Journal of Photoenergy*, (2011) 1-8.
24. Oladeji, I.O., Chow, L., Liu, J.R., Chu, W.K. Bustamante, A.N.P., Fredricksen, C. and Schulte, A.F. *Thin Solid Films*, **359** (2000) 154-159.
25. Todorov, T.K., Reuter, K.B. and Mitzi, D.B. *Advanced Materials*, **22** (2010) 156-159.
26. Tanaka, T., Nagatomo, T., Kawasaki, D., Nishio, M., Guo, Q., Wakahara, A., Yoshida, A. and Ogawa, H. *Journal of Physics and Chemistry of Solids*, **66** (2005) 1978–1981.
27. Friedlmeier, T.M., Wieser, N., Walter, T., Dittrich, H. and Schock, H.W. In *Proceedings of the 14th European Conference of Photovoltaic Science and Engineering and Exhibition*, (1997) 1242
28. Wang, H. *International Journal of Photoenergy*, **2011** (2011). 801292
29. Katagiri, H., Jimbo, K., Maw, W.S., Oishi, K., Yamazaki, M., Araki, H. and Takeuchi, A. *Thin Solid Films*, **517** (2009) 2455–2460.
30. Salomé, P.M.P., Malaquias, J., Fernandes, P.A., Ferreira, M.S., Da Cunha, A.F., Leitao, J.P., González, J.C. and Matinaga, F.M. *Solar Energy Materials and Solar Cells*, **101** (2012).
31. Su, Z., Yan, C., Sun, K., Han, Z., Liu, F., Liu, J., Lai, Y., Li, J. and Liu, Y. *Applied Surface Science*, **258** (2012) 7678-7682.
32. Vanalakar, S.A., Shin, S.W., Agawane, G.L., Suryawanshi, M.P., Gurav, K.V., Patil, P.S., Kim, J.H. *Ceramics International*, **40** (2014) 15097-15103.
33. Malerba C. *Material and Device Characterization (Doctoral dissertation, University of Trento)*, (2014).
34. Okano, M., Phuong, L.Q. and Kanemitsu, Y., *Physica Status Solidi (B)*, **252** (2015) 1219-1224.
35. Guo, Q., Ford, G. M., Yang, W. C., Walker, B. C., Stach, E. A., Hillhouse, H. W., and Agrawal R. *Journal of the American Chemical Society*, **132** (2010) 17384-17386.
36. Regulacio, M.D. and Han, M.Y. *Accounts of Chemical Research*, **49** (2016) 511-519.
37. Repins, I., Vora, N., Beall, C., Wei, S.H., Yan, Y., Romero, M., Teeter, G., Du, H., To, B., Young, M., Noufi, R. *Kesterites and Chalcopyrites: A Comparison of Close Cousins. In: MRS Proceedings*, **1324** (2011)
38. Mellikov, E., Hiie, J. and Altosaar, M. *International Journal of Materials and Product Technology*, **(3-4)** (2007) 291-311.
39. Mellikov, E., Altosaar, M., Kauk, M., Timmo, K, Meissner D., Grossberg, M., Krustok, J., and Volobujeva, O. (*In Copper Zinc Tin Sulfide-Based Thin Film Solar Cells*) *John Wiley and Sons*, (2015) 289-309.
40. Colombara, D., Delsante, S., Borzone, G., Mitchels, J.M., Molloy, K.C., Thomas, L.H., Mendis, B.G., Cummings, C.Y., Marken, F. and Peter, L.M. *Journal of Crystal Growth*, **364** (2013) 101-110.
41. Keszei, B., Szabó, G., Vandlik, J., Pogány, L., and Oszlányi G. *Journal of the Less Common Metals*, **155** (1989) 229-234.
42. Itô K. *Diffusion Processes. John Wiley and Sons, Inc.*, (1974).
43. Mellikov, E., Meissner, D., Varena, T., Altosaar, M., Kauk, M., Volobujeva, O., Raudoja, J., Timmo, K., and Danilson, M. *Solar Energy Materials and Solar*

- Cells*, **93** (2009) 65-68.
44. Seidell, A. *Solubilities of Inorganic and Organic Compounds C. 2. D. Van Nostrand Company*, (1919) 655.
 45. Solubility of KI in water". Hazard.com. 1998-04-21. (Retrieved 2016-08-09).
 46. Subhadra. DBSLSKG. *Alkali Halides: A Handbook of Physical Properties, 2017-09-02*.
 47. pubchem.ncbi.nlm.nih.gov/compound/sodium_iodide, (retrived on 2016-08-09).
 48. NIOSH Pocket Guide to Chemical Hazards -0087". *National Institute for Occupational Safety and Health (NIOSH)*, (Retrieved on 2016-08-09).
 49. Pradyot, P., *Handbook of Inorganic Chemicals. McGraw-Hill*, 2002, (Retrieved on 2016-08-09).
 50. Forty, A.J. *The London, Edinburgh, and Dublin Philosophical Magazine and Journal of Science*, **43** (1952) 72-81.
 51. Te Velde, T.S. Philips Corp, *Electrical Monograin Layers Having a Radiation Permeable Electrode. U.S. Patent 3,480,818. (1969)*.
 52. Jackson, A.J. and Walsh, A. *Journal of Materials Chemistry A*, **2** (2014) 7829-7836.
 53. Nagoya, A., Asahi, R., Wahl, R. and Kresse, G. *Physical Review B*, **81** (2010) 113202.
 54. Olekseyuk, I.D., Dudchak, I.V. and Piskach, L.V. *Journal of Alloys and Compounds*, **368** (2004) 135-143.
 55. Chakrabarti, D.J. and Laughlin, D.E. *Bull Alloy Phase Diagrams*, **4** (1983) 254-271.
 56. Parasyuk, O.V., Voronyuk, S.V., Gulay, L.D., Davidyuk, G.Y., and Halka V O. *Journal of Alloy and Compound*, **348** (2003) 57-64.
 57. Abrikosov, N.H., Bankina, V.F., Poretskaya, L.V., Skudnova, E.V. and Chizhevskaya, S.N. *Semiconductor Chalcogenides and Alloys on The Base of Thermal, Nauka, Moscow*, (1975) 220.
 58. Bletskan, D.I., *Journal of Ovonic Research*, **1** (2005) 47-52.
 59. Lindwall, G., Shang, S., Kelly, N. R., Anderson, T., and Liu Z.K. *Solar Energy*, **125** (2016) 314-323.
 60. Kniep, R., Mootz, D., Severin, U. and Wunderlich, H. *Acta Crystallographica Section B: Structural Crystallography and Crystal Chemistry*, **38** (1982) 2022–2023.
 61. Burton, L.A., Colombara, D., Abellon, R.D., Grozema, F.C., Peter, L.M., Savenije, T.J., Dennler, G. and Walsh, A. *Chemistry of Materials*, **25** (2013) 4908–4916.
 62. Piskach, L.V., Parasyuk, O.V. and Olekseyuk, I.D. *Journal of Alloys and Compounds*, **279** (1998) 142-152.
 63. Frost, R.L., Williams, P.A., Martens, W., Leverett, P., and Kloprogge, J.T. *American Mineralogist*, **89** (2004) 1130-1137.
 64. Thongtem, T., Phuruangrat, A. and Thongtem, S. *Current Applied Physics*, **9** (2009) 195-200.
 65. Thongtem, T., Phuruangrat, A., and Thongtem, S. *Journal of Materials Science*, **42** (2007) 9316-9323.
 66. Fernandes, P.A., Salomé, P.M.P. and Da Cunha, A.F. *Journal of Physics D: Applied Physics*, **43** (2010) 215403.
 67. Fernandes, P.A., Salomé, P.M.P. and Da Cunha, A.F. *Journal of Alloys and Compounds*, **509** (2011) 7600-7606.

68. Kumar, P., and Nagarajan, R. *Inorganic Chemistry*, **50** (2011) 9204-9206.
69. Munce, C.G., Parker, G.K., Holt, S.A. and Hope, G.A. *Physicochemical and Engineering Aspects*, **295** (2007) 152-158.
70. Parkin, I.P., Price, L.S., Hibbert, T.G. and Molloy, K.C. *Journal of Materials Chemistry*, **11** (2001) 1486-1490.
71. Berg, D.M., Djemour, R., Gütay, L., Siebentritt, S., Dale, P.J., and Fontane, X. *Applied Physics Letters*, **100** (2012) 192103.
72. Price, L.S., Parkin, I.P., Hardy, A.M., Clark, R.J., Hibbert, T.G., and Molloy, K.C. *Chemistry of Materials*, **11** (1999) 1792-1799.
73. Ballentyne, D.W.G. and Ray, B. *Physica*, **27** (1961) 337-341.
74. Fedorov, V.A., Ganshin, V.A. and Korkishko, Y.N. *Materials Research Bulletin*, **28** (1993) 59-66.
75. Chen, W.W., Zhang, J.M., Ardell, A.J., and Dunn, B. *Materials Research Bulletin*, **23** (1988) 1667-1673.
76. Parasyuk, O.V., Piskach, L.V., Romanyuk, Y.E., Olekseyuk, I.D., Zarembo, V.I., and Pekhnyo, V.I. *Journal of Alloys and Compounds*, **397** (2005) 85-94.
77. Fiechter, S., Martinez, M., Schmidt, G., Henrion, W., and Tömm, Y. *Journal of Physics and Chemistry of Solids*, **64** (2003) 1859-1862.
78. Mizetskaya, I.B., Oleinik, G.S., and Trishchuk, L.I. *Izvestija Akademii Nauk SSSR, Neorganicheskie Materialy*, **18** (1982) 1792-1794.
79. Sobott Robert, J.G, GH Teh; Neues Abh. **1** (1977) 21.
80. Moh, G.H. *Chem. Erde.*, **34** (1975).1-61
81. Nekrasov, I.Ya., Sorokin, V.I., Osadchij, E.G., and Tixomirova, V.I. *Journal of alloys and compounds*, **6** (1977) 200.
82. Boero, F., Delsante, S., Colombara, D., and Borzone, G. *Materials Letters*, **145** (2015) 145-149.
83. Muska, K., Kauk, M., Altosaar, M., Pilvet, M., Grossberg, M. and Volobujeva, O. *Energy Procedia*, **10** (2011) 203-207.
84. Chaplygin, I.V., Mozgova, N.N., Mokhov, A.V., Koporulina, E.V., Bernhardt, H.J. and Bryzgalov, I.A. *The Canadian Mineralogist*, **45** (2007) 709-722.
85. Crovetto, A., Chen, R., Ettliger, R.B., Cazzaniga, A.C., Schou, J., Persson, C. and Hansen, O. *Solar Energy Materials and Solar Cells*, **154** (2016) 121-129.
86. Alias, M.F.A., Naji, I.S., Taher, B.Y., Al-Douri, A.A.J. *Journal of Non-Oxide Glasses*, **8** (2016) 93-97.
87. Scragg, J.J., Ericson, T., Kubart, T., Edoff, M., Platzer-Björkman, C. *Chemistry of Materials*, **23** (2011) 4625-4633.
88. Dimitrievska, M., Fairbrother, A., Fontané, X., Jawhari, T., Izquierdo-Roca, V., Saucedo, E. and Pérez-Rodríguez, A. *Applied Physics Letters*, **104** (2014) 021901.
89. Fontané, X., Calvo-Barrio, L., Izquierdo-Roca, V., Saucedo, E., Pérez-Rodríguez, A., Morante, J.R., Berg, D.M., Dale, P.J. and Siebentritt, S. *Applied Physics Letters*, **98** (2011) 181905.
90. Redinger, A., Berg, D.M., Dale, P.J. and Siebentritt, S. *Journal of the American Chemical Society*, **133** (2011) 3320-3323.
91. Kimura, T. *In: Advances in Ceramics-Synthesis and Characterization, Processing and Specific Applications. InTech*, (2011).
92. German, R.M., Suri, P. and Park, S.J. *Journal of Material Science*, **44** (2009) 1-39.
93. Timmo, K., Altosaar, M., Raudoja, J., Mellikov, E., Varema, T., Danilson, M.

- and Grossberg, M. *Thin Solid Films*, **515** (2007) 5887-5890.
94. Kauk, M., Altosaar, M., Raudoja, J., Timmo, K., Varema, T., Danilson, M., Grossberg, M. and Mellikov, E. In : *Physica Status Solidi Conferences*, **5** (2008) 609.
 95. Timmo, K., Altosaar, M., Kauk, M., Raudoja, J. and Mellikov, E. *Thin Solid Films*, **515** (2007) 5884-5886.
 96. Porter, D.A., Easterling, K.E. and Sherif, M. *Phase Transformations in Metals and Alloys, (Revised Reprint)*. CRC press, (2009).
 97. Lovette, M.A., Browning, A.R., Griffin, D.W., Sizemore, J.P., Snyder, R.C. and Doherty, M.F. *Industrial and Engineering Chemistry Research*, **47** (2008) 9812-9833.
 98. Weber, A., Mainz, R. and Schock, H.W. *Journal of Applied Physics*, **107** (2010) 013516.
 99. Scragg, J.J., Choubrac, L., Lafond, A., Ericson, T. and Platzer-Björkman, C. *Applied Physics Letters*, **104** (2014) 41911.
 100. Just, J., Lützenkirchen-Hecht, D., Frahm, R., Schorr, S. and Unold, T. *Applied Physics Letters*, **99** (2011) 262105.
 101. Li, Q., Meng, H., Zhou, P., Zheng, Y., Wang, J., Yu, J., Gong J. *ACS Catalysis*, **3** (2013) 882-889.
 102. Zhang, Q., Deng, H., Chen, L., Yu, L., Tao, J., Sun, L., Yang, P. and Chu, J. *Journal of Alloys and Compounds*, **695** (2017) 482-488.
 103. Grossberg, M., Raadik, T., Raudoja, J., Krustok, J. *Current Applied Physics*, **14** (2014) 447-450.
 104. Fu, J., Tian, Q., Zhou, Z., Kou, D., Meng, Y., Zhou, W., Wu, S. *Chemistry of Materials*, **28** (2016) 5821-5828.
 105. Kaur, K., Kumar, N., Kumar M. *Journal of Material Chemistry A*, **5** (2017) 3069–3090.
 106. www.chemicalland21.com.
(chemicalland21.com/lifescience/phar/Potassium%20iodide.htm).
 107. George, J. Janz. "*Molten Salts Handbook*." (1967) 31-37.
 108. Thiers, E. *Heat transfer interface. U.S. Patent Application*, 13/521,879, (2011).
 109. Kanatzidis, M.G., Pöttgen, R. and Jeitschko, W. *Angewandte Chemie International Edition*, **44** (2005) 6996-7023.
 110. Johnson, M., Baryshev, S.V., Thimsen, E., Manno, M., Zhang, X., Veryovkin, I. V., Aydil, E.S. *Energy and Environmental Science*, **7** (2014) 1931-1938.
 111. Altosaar, M., Raudoja, J., Timmo, K., Danilson, M., Grossberg, M., Krustok, J. Mellikov, E. *Physica Status Solidi A*, **205** (2008) 167-170.
 112. Matsushita, H., Ichikawa, T., Katsui, A. *Journal of Material Science*, **40** (2005) 2003-2005.
 113. Perry, D.L. *Handbook of Inorganic Compounds*. CRC press; (2016).
 114. Patnaik, P. *Handbook of Inorganic Chemicals*, New York: McGraw-Hill, **529** (2003).
 115. Wells, A.F., *Structural Inorganic Chemistry*. Oxford University Press, (2012).
 116. Greenwood, N.N. and Earnshaw, A., *Chemistry of The Elements*. Pergamon Press; Oxford (UK), (1984).
 117. Guen, L. and Glaunsinger, W.S. *Journal of Solid State Chemistry*, **35** (1980) 10–21.
 118. Chen, S., Gong, X.G., Walsh, A. and Wei, S.H. *Applied Physics Letters*, **96** (2010) 21902.

119. Pilvet, M., Kauk-Kuusik, M., Altosaar, M., Grossberg, M., Danilson, M., Timmo, K., Mere, A. and Mikli, V. *Thin Solid Films*, **582** (2015) 180-3.
120. Nkwusi, G., Leinemann, I., Raudoja, J., Grossberg, M., Altosaar, M., Meissner, D., Traksmaa, R. and Kaljuvee, T. *In: Conf. of Young Scientists on Energy Issues, Kaunas*, **2** (2012) 24-25.
121. Fontané, X., Izquierdo-Roca, V., Saucedo, E., Schorr, S., Yukhymchuk, V.O., Valakh, M.Y., Pérez-Rodríguez, A. and Morante, J.R. *Journal of Alloys and Compounds*, **539** (2012) 190-194.
122. Valakh, M.Y., Kolomys, O.F., Ponomaryov, S.S., Yukhymchuk, V.O., Babichuk, I.S., Izquierdo-Roca, V., Saucedo, E., Perez-Rodríguez, A., Morante, J.R., Schorr, S. and Bodnar, I.V. *Physica Status Solidi (RRL)-Rapid Research Letters*, **7** (2013) 258-261.
123. Nakashima, S.I., Yoshida, H., Fukumoto, T. and Mitsuishi, A. *Journal of the Physical Society of Japan*, **31** (1971) 1847.
124. Coble, R.L. *Journal of Applied Physics*, **32** (1961) 787-792.
125. Thirumal, M., Jain, P. and Ganguli, A.K. *Materials Chemistry and Physics*, **70** (2001) 7-11.
126. Yoon, K.H., Cho, Y.S. and Kang, D.H. *Journal of Materials Science*, **33** (1998) 2977-2984.
127. Hiie, J., Altosaar, M. and Mellikov, E. *In Solid State Phenomena*, **67** (1999) 303-308.
128. Sun, C. and Xue, D. *CrystEngComm.*, **16** (2014) 2129.
129. Timmo, K., Kauk-Kuusik, M., Altosaar, M., Raudoja, J., Raadik, T., Grossberg, M., Varema, T., Pilvet, M., Leinemann, I., Volobujeva, O. and Mellikov, E. *In Proceedings of The 28th European Photovoltaic Solar Energy Conference*, (2013). 2385
130. Chikanov, V.N. *Russian Journal of Inorganic Chemistry*, **51** (2006) 1132–1138.
131. Flynn, J.H. and Wall, L.A. *Journal of Polymer Science Part C: Polymer Letters*, **4** (1966) 323-328.
132. Kuncewicz-Kupczyk, W., Kapala, J., Roszak, S. and Miller, M. *The Journal of Chemical Physics*, **108** (1998) 7743-7746.
133. Kaupp, M. and von Schnering, H.G. *Inorganic Chemistry*, **33** (1994) 4718-4722.
134. Konings, R.J.M., Booij, A.S. and Cordfunke, E.H.P. *Vibrational Spectroscopy*, **2** (1991) 251-255.
135. Kaiho, T. *Iodine Chemistry and Applications. John Wiley and Sons*, (2014).
136. Corbett, J.D., Winbush, S von, and Albers, F.C. *Journal of the American Chemical Society*, **79** (1957) 3020-3024.
137. Klavina, I., Raudoja, J., Altosaar, M., Mellikov, E., Meissner, D. and Kaljuvee, T. *In: Conf. of Young Scientists on Energy Issues Kaunas, Lithuania, (2010)*.
138. Leinemann, I., Raudoja, J., Grossberg, M., Altosaar, M., Meissner, D., Traksmaa, R. and Kaljuvee, T. *In: Conference of Young Scientists on Energy Issues Kaunas (CD pub): (2011)1-8*.
139. Börnstein L. *Thermodynamic Properties of Inorganic Material, Scientific Group Thermodata Europe (SGTE)*. (1999).
140. Donald, K.J., Hargittai, M. and Hoffmann, R. *Chemistry-A European Journal*, **15** (2009) 158-177.
141. Barin, I. *Thermochemical Data of Pure Substances, Thermochemical Data of Pure Substances. Wiley-VCH. (HSC software)*, (1997).
142. Zeidler, A., Chirawatkul, P., Salmon, P.S., Usuki, T., Kohara, S., Fischer, H.E.

- and Howells, W.S. *Journal of Non-Crystalline Solids*, **407** (2015) 235-245.
143. Gurvich, L.V., Veyts, I.V. and Alcock, C.B. *Thermodynamic Properties of Individual Substances: Elements O, H (D, T), F, Cl, Br, I, He, Ne, Ar, Kr, Xe, Rn, S, N, P and Their Compounds. pt. 1. Methods and Computation.etc. pt., 2* (1989).
144. Glushko, V.P. *Thermocenter of The Russian Academy of Sciences." IVTAN Association, Izhorskaya*, **13** (1994) 127412.
145. Gaune-Escard, M. *Springer Science and Business Media*, **52** (2012).
146. Russell, T.D. *The Journal of Physical Chemistry*, **90** (1986) 6590-6594.
147. Allen, D.A., Howe, R.A., Wood, N.D. and Howells, W.S. *The Journal of Chemical Physics*, **94** (1991) 5071-5076
148. Hurtado, I. and Neuschütz, D. *Landolt-Börnstein-Thermodynamic Properties of Inorganic Materials-Group IV (19A). (HSC 6.0 Software)*,(1999).
149. Schurr, R., Hölzing, A., Jost, S., Hock, R., Voß, T., Schulze, J., Kirbs, A., Ennaoui, A., Lux-Steiner, M. *Thin Solid Films*, **517** (2009) 2465-2468.
150. Knacke, O., Kubaschewski, O. and Hesselmann, K. *Thermochemical Properties of Inorganic Substances, Springer, Berlin*, (1991).

Appendix A

Article I

Nkwusi, G., Leinemann, I., Raudoja, J., Mikli, V., Kärber, E., Altosaar, M. Impact of growth-synthesis conditions on $\text{Cu}_2\text{Zn}_{1-x}\text{Cd}_x\text{SnS}_4$ monograin material properties. *Superlattices and Microstructures*, **98** (2016) 400- 405.



Impact of growth-synthesis conditions on $\text{Cu}_2\text{Zn}_{1-x}\text{Cd}_x\text{SnS}_4$ monograin material properties



G. Nkwusi*, I. Leinemann, J. Raudoja, V. Mikli, E. Karba, M. Altsaar

Institute of Materials Science, Tallinn University of Technology, Ehitajate tee 5, 19086, Tallinn, Estonia

ARTICLE INFO

Article history:

Received 29 May 2016

Received in revised form 31 August 2016

Accepted 1 September 2016

Available online 3 September 2016

Keywords:

$\text{Cu}_2\text{Zn}_{1-x}\text{Cd}_x\text{SnS}_4$

Monograin

CdI_2

Growth-synthesis

ABSTRACT

This paper presents the impact of growth conditions on the properties of copper zinc cadmium tin sulfide ($\text{Cu}_2\text{Zn}_{1-x}\text{Cd}_x\text{SnS}_4$) monograin powder synthesized in molten CdI_2 . We studied the effects of synthesis time and flux amount on the properties of the monograin powder. Our results showed that we could control the phase composition, grain size and the morphology of the as grown $\text{Cu}_2\text{Zn}_{1-x}\text{Cd}_x\text{SnS}_4$ powder by changing the synthesis conditions. We found that in comparison with other used fluxes (KI, NaI), monograin powders synthesized in molten CdI_2 were less faceted and more round shaped. The average grain size increased as the flux amount decreased. The optimum synthesis time to obtain usable grain size with 50–100 μm was found to be 160 h with CdI_2 flux amount, providing the ratio of the volumes of CdI_2/CZTS is 0.5.

© 2016 Elsevier Ltd. All rights reserved.

1. Introduction

It is generally difficult to grow high-quality single crystals of the CZTS-type compounds from their melt, because most of the compounds grow through a peritectic reaction or have a solid-state phase transition during the cooling process [1,2]. The monograin technology was developed as a possible alternative to thin film technology with its solar cell efficiency at about 9.4% based on CZTS powders synthesized in KI as flux [3–6]. In monograin technology (MGL), we explore the use of suitable flux to aid the growth of single crystalline CZTS powders known as monograin powders [7]. These powders are embedded into a thin layer of epoxy resin to form a monolayer [8]. A narrow size fraction of the powder grains, usually between 30 and 100 μm , is used. This implies that for a perfect monograin layer, the shape of the grains is very important. Spherical grains give higher possibility to form a perfect monolayer and prevent stacking of grains when compared to the grains with tetrahedral pyramidal structure with higher packing density [9]. Timmo et al. showed that the solubility of the synthesized material in the flux could affect the shape of growing grains [10]. In MGL, the synthesis-growth process is carried out in a closed ampoule and proceeds via isothermal conditions with the flux salt being saturated by dissolving precursors. Hence, the only driving force for crystal growth in this technology is the difference in surface energy of crystals of different sizes. The dissolution and crystal growth processes go on concurrently; the smaller crystals dissolve in flux and deposit onto surfaces of bigger crystals through mass transport (diffusion) in the molten phase that surrounds every crystal. The dissolution is more intensive in places where the surface energy is higher (grain borders, tips) and deposit onto plain surfaces (facets). If the solubility of compounds in the flux increases (by increasing temperature or by using flux material which permits high solubility of the precursors in a bigger

* Corresponding author.

E-mail address: godswillnkwusi@yahoo.com (G. Nkwusi).

amount), the dissolution process can prevail and crystals' borders take more rounded shape. At equilibrium, the dissolution-deposition rates are equal to each other and crystals tend to attain equilibrium shape. The equilibrium can be related to the volume of the growth solution and the time of growth [11,12]. In the review paper of M. A. Lovette et al. [12], the formation of a solid polyhedron with volume V from a fluid phase was described by the Gibbs-Thomson formula for the change of free Gibbs energy ΔG . Although Gibbs was the first to develop the criteria for equilibrium crystal shapes, he recognized that crystal shapes are usually determined by kinetics rather than by thermodynamics alone. In the synthesis-growth process, solid, powdery precursors are used. Their solubility in molten salts differs from each other, but is comparatively low [10]. When the mixtures are heated up and the molten phase starts to form but the dissolution of solids in the liquid flux has not reached the equilibrium state, the primary solid particles can sinter together. When the amount of liquid phase increases, it could penetrate into capillaries, repelling the weakly joined particles from each other. In our previous work [13], we confirmed the formation of solid solution of $\text{Cu}_2\text{Zn}_{1-x}\text{Cd}_x\text{SnS}_4$ (CZCdTS) when CZTS was synthesized in CdI_2 as a flux. Maris et al. studied (CuS, ZnS, CdS, SnS) in a molten KI [14], but the impact of growth-synthesis conditions on $\text{Cu}_2\text{Zn}_{1-x}\text{Cd}_x\text{SnS}_4$ monograin material properties was not reported. In this work, we investigated how the shape of the crystals of synthesized CZCdTS monograin powders can be controlled by the amount of low melting CdI_2 used as flux. We considered the use of CdI_2 as flux due to the future possibility to monitor KI doping when used as a flux among other reasons and to achieve a much lower synthesis temperature (below 750°C in the case of KI and NaI). In addition, we study the influence of different preparation conditions such as synthesis time and the flux amount on the composition, material properties and morphology of the as grown CZTS monograin powders. We gave Special attention to the changes in the macrostructure of re-crystallized powder crystals and to the incorporation of Cd from CdI_2 into the crystals of CZTS.

2. Experimental

All samples were synthesized from binary precursor compounds of CuS, SnS and ZnS in molten CdI_2 as flux material. Flux material and precursors were mixed and ground in an agate mortar, mixtures were degassed and sealed into quartz ampoules as described in Ref. [4]. The concentration of flux salt in synthesis mixtures was varied so that the ratio of volumes of the liquid flux (V_{CdI_2}) to solid precursors for CZTS (V_{CZTS}) $V_{\text{CdI}_2}/V_{\text{CZTS}} = 5, 3, 1, 0.5$ (if the ratio $V_{\text{CdI}_2}/V_{\text{CZTS}} = 1$, it is marked as C1) 0.5 was considered as the to avoid sintering at lower $V_{\text{CdI}_2}/V_{\text{CZTS}}$ ratio. We carried out the time dependent experiments at 650°C only for 24, 160 and 300 h. Currently, CZTS is synthesis in our Laboratory at 750°C in molten KI, 650°C was chosen for CdI_2 considering that it has a lower melting temperature compare to KI and based our previous report in Ref. [15]. After heating, the samples were quenched rapidly to room temperature in cold water. All synthesized powders were washed with de-ionized water to separate the monograins from the flux. We used sieving analysis to study the size distribution of grains and the yield of powders usable for making monograin layers. Low temperature (10 K) photoluminescence (PL) measurements were carried out to monitor the change in the band gap energy values of the formed monograins due to Cd incorporation. The 441 nm laser line with 100 mW intensity was used for the excitation and the PL spectra were detected using InGaAs detector. The morphology was studied with the scanning electron microscope (SEM) and chemical composition of the synthesized powders was analyzed using energy dispersive X-ray spectroscopy (EDX) (SEM-AsB and by 20 keV EDX) on Zeiss HR SEM ULTRA 55. The phases present in the powders was studied by room temperature (RT) micro-Raman spectroscopy using a Horiba LabRam HR800 high-resolution spectrometer with a multichannel CCD detection system in backscattering configuration with incident laser light of 532 nm focused on a $1\text{-}\mu\text{m}$ spot of the studied sample.

3. Results and discussions

3.1. Impact of flux concentration and synthesis time on the grain size and yield of powders

By sieving the powders into different size fractions, the amount of fractions with grain size $\geq 45\ \mu\text{m}$ (usable in monograin solar cells, grain size lower than $\geq 45\ \mu\text{m}$ may be too small to obtain a uniform unstacked layer) [8] was determined. In Fig. 1a, the synthesized powder with size $\geq 45\ \mu\text{m}$, decreases as the flux amount increases from 0.5C1–5C1 at 650°C and for 24, 160 and 300 h respectively. It is understandable if we consider that by increasing the amount of liquid phase, the diffusion between different crystals takes more time and the amount dissolved in the molten phase of flux increases. However, the lowest used amount of CdI_2 (0.5 C1) (see left side in Fig. 1), results in grains with sizes over $45\ \mu\text{m}$ in bigger amount than could be expected from the small linear decrease when $C_1 \geq 1$ (right part in Fig. 1a). This phenomenon could be understandable if to take into account that the single grain growth limit is roughly determined as $V_{\text{Liquid}}/V_{\text{Solid}} \geq 0.5$ [16] Therefore the amount of bigger grains increases for $C = 0.5$ in comparison with bigger used flux amounts (>0.5). In addition, at $C_1 < 0.5$, there is insufficient amount of flux to aid the growth process and sintering may begin to occur As the density of CZTS is not determined for higher temperatures, the amounts for initial liquid to solid volume ratio <0.5 could result in both the single grain growth and some sintering process occurring at the same time and at $C_1 < 0.5$, even greater sintering may occur which may affect the quality of the CZTS monograin powder. Fig. 1a also confirmed that the grain size increases as the temperature increases [17]. In addition, the yield of the total amount of CZTS monograins decreases as the flux amount increases and vice versa, it increases as the growth time increases (see Fig. 1b). From Fig. 1b, it is seen that the total yield of powder is bigger than the amount of input precursors for synthesis, particularly for heating times 160 and 300 h. The increase in the total amount of yield over the summarized amount of precursors can take place due to the replacement of Zn by Cd (with higher molar mass

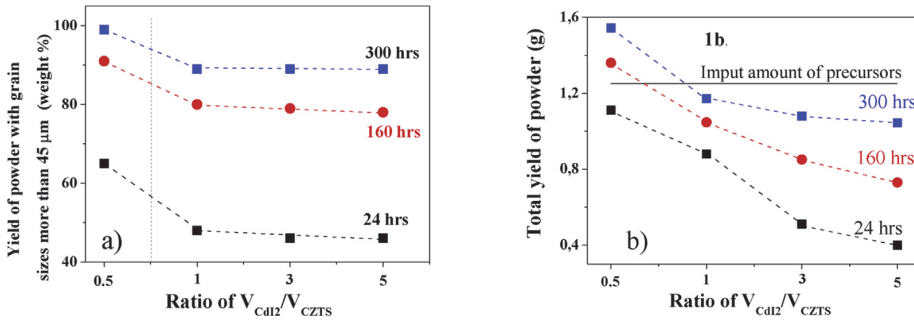


Fig. 1. Yield of powder fractions with grain size bigger than 45 μm (1a) and total yield of powders (1b) synthesized at 650 $^{\circ}\text{C}$ with different amounts of CdI_2 . The input amount of precursors is constant and shown as a horizontal solid line in 1b). Heating time 24, 160 and 300 h.

than Zn) in the crystal lattice of formed CZCdTS compound while CdI_2 is the only source of Cd. During the growth process, the concentration gradient drives the mass transfer of the crystal constituents from the fluid phase to the crystal phase. The mass flux at the growth interface depends on the direction-dependent concentration gradient [17] and the larger the flux amount the slower and less chance of higher agglomeration and vice versa, this leads to smaller grains that can be easily washed off during separation of monograin powder from the flux. Summarizing, from Fig. 1, it can be recognized that the grain size increases by synthesis time, but decreases with the increasing flux amount.

3.2. Impact of flux amount and synthesis-growth time on grain morphology

SEM images of individual CZCdTS crystals are presented in Fig. 2 (synthesized at 650 $^{\circ}\text{C}$). It can be seen that the grains produced by the smaller flux amount and are less faceted and have a more rounded shape. With increasing time as well as with the increasing flux amount, faceted crystals became more obvious. The most round shaped grains were formed in the samples with the lowest amount of CdI_2 heated for 160 h. Longer time (300 h) promotes the faceting. However, in crystals heated for 300 h, there can be observed also secondary agglomeration – the crystals are formed from different blocks. The

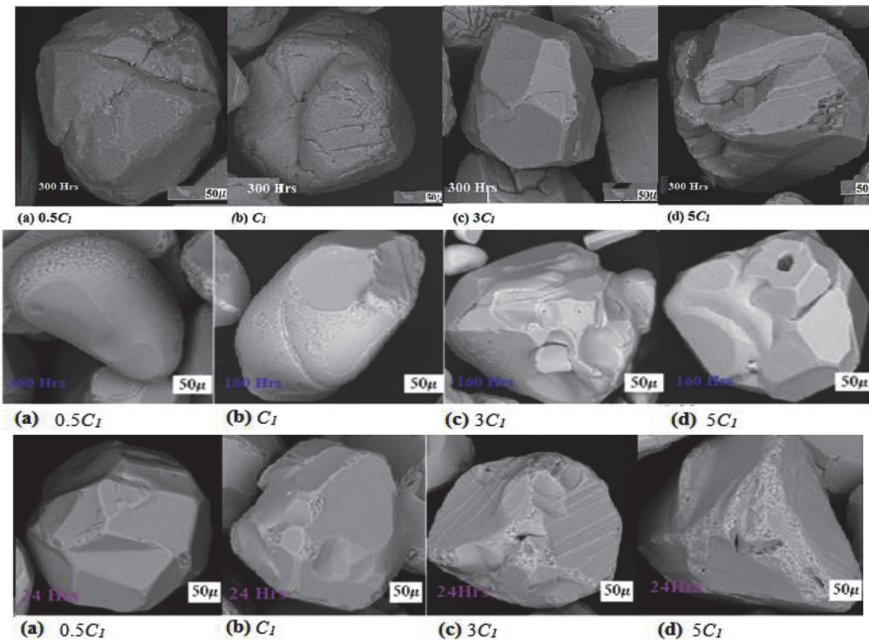


Fig. 2. SEM images of individual CZCdTS powder grains synthesized at $T = 650$ $^{\circ}\text{C}$ for 300 (upper row), 160 (middle row) and 24 (lower row) hours with increasing (from left to right) amount of CdI_2 . C_I corresponds to $V_{CdI_2}/V_{CZTS} = 1$.

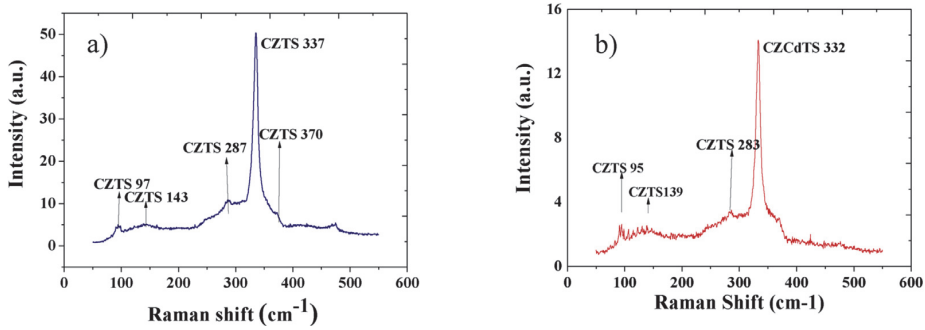


Fig. 3. Raman spectra of powder crystals synthesized at 650 °C for 300 h; a) with amount of $\text{CdI}_2/\text{CZTS} = 0.5$ and b) $\text{CdI}_2/\text{CZTS} = 5$. The Raman peaks at 337 cm^{-1} and 332 cm^{-1} are the expected peak positions respectively for pure CZTS and CdCdTS as shown in the graphs.

primary sintering effect at the lowest used flux amounts ($0.5C_1$) seems to be helpful for getting rounder and compact grains after long time of crystallization (160 and 300 h). All the samples synthesized at 650 °C shows that the grains are less faceted and bigger and the yield is higher as the flux concentration decreases.

3.3. Composition of materials

3.3.1. Raman spectroscopy

Raman spectra of powder crystals synthesized at 650 °C for 300 h are presented in Fig. 3. Raman spectra of the sample held for 300 h at 650 °C with the lowest amount of CdI_2 reveal the most intensive Raman peak at 337 cm^{-1} which is close to the most intensive Raman peak position of pure CZTS at 338 cm^{-1} [15] while the most intensive Raman peak of the sample with the highest amount of CdI_2 is at 332 cm^{-1} where is also the most intensive Raman peak of pure $\text{Cu}_2\text{CdSnS}_4$ - 332 cm^{-1} [18]. Raman peaks of samples with intermediate amounts of CdI_2 C_1 and $3C_1$ are at 333 cm^{-1} and 335 cm^{-1} respectively. In Ref. [20] there was shown that increasing Cd content in the $\text{Cu}_{1.85}(\text{Cd}_x\text{Zn}_{1-x})_{1.1}\text{SnS}_{4.1}$ monograin powders grown in KI decreased linearly the peak position of A1 Raman mode from 338 to 332 cm^{-1} in the interval of x values from 0 to 0.4, then, with higher Cd content the A1 peak position did not shift.

3.3.2. EDX analysis

The composition of the synthesized CZTS monograin powders was determined by EDX method. The common formula of product powders is the same for all samples with deviation in the range of limits for EDX and can be expressed as $\text{Cu}_{1.9\pm 0.01}\text{Zn}_{1-x}\text{Cd}_x\text{SnS}_{3.97\pm 0.04}$ with variable Cd content (x values). The values of x depending on heating conditions are given in Table 1. Table 1 also gives the compositions of $\text{Zn}_{1-x}\text{Cd}_x\text{S}$ (found by XRD) in washed powder samples. As it can be seen, the Cd concentration in $\text{Cu}_2\text{Zn}_{1-x}\text{Cd}_x\text{SnS}_4$ and in $\text{Zn}_{1-x}\text{Cd}_x\text{S}$ increases with increasing amount of CdI_2 in synthesis. The incorporation of Cd into $\text{Cu}_2(\text{ZnCd})\text{SnS}_4$ through the intermediate reaction of $\text{Zn}_{1-x}\text{Cd}_x\text{S}$ is by the formation of $\text{CdI}^+(\text{g})$ which also increases with temperature [19]. In Fig. 4. It is seen that as the flux amount increases the, [Cd] also increases. However, from Table 1, we can conclude that 24 h is not enough long time to reach the equilibrium due to the inconsistency in the obtained data.

3.3.3. Photoluminescence

The PL spectra of CZTS monograin powder samples grown in CdI_2 for 160 h with ratios of $V_{\text{CdI}_2}/V_{\text{CZTS}} = 5$ and 0.5 at $T = 650$ °C show PL band maxima at 1.05 eV and 1.07 eV respectively (see Fig. 5). Single broad and asymmetric PL bands have been reported for pure CZTS at 1.27 eV and 1.3 eV due to BI-recombination (Band-Impurity) and attributed to a deep acceptor defect [20], also PL bands at 1.39 eV (Band-to-tail) and 1.53 eV (Band-to-band) have been observed for CZTS [21]. In

Table 1

Composition of CdCdTS and $\text{Zn}_{1-x}\text{Cd}_x\text{S}$ for different flux concentrations and heating time as determined by EDX ($T = 650$ °C).

$V_{\text{CdI}_2}/V_{\text{CZTS}}$	Heating time (hours)					
	24		160		300	
	Value of x in $\text{Cu}_{1.9\pm 0.01}(\text{Zn}_{1-x}\text{Cd}_x)\text{SnS}_{3.97\pm 0.04}$			Value of x in $\text{Zn}_{1-x}\text{Cd}_x\text{S}$		
0.5	0.15	0.18	0.16			
1	0.15	0.26	0.22	0.1	0.25	0.15
3	0.25	0.28	0.28		0.22	0.22
5	0.3	0.35	0.35		0.35	0.39

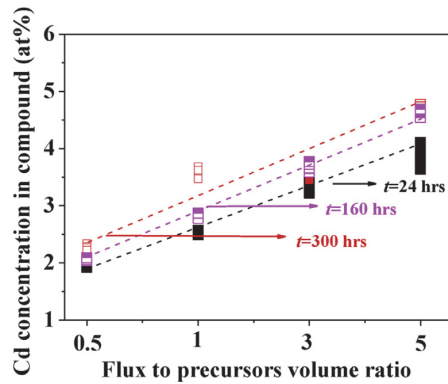


Fig. 4. Cd concentration in powders synthesized in different amounts of CdI_2 for different time at $T = 650^\circ\text{C}$ as determined by EDX analysis.

our work, we found that the CZCdTS PL band position varied slightly from 1.05 eV for 5C_1 to 1.07 eV for 0.5C_1 . The PL band of pure $\text{Cu}_2\text{CdSnS}_4$ is measured at 1.1 eV [21]. In the paper of M. Pilvet et al. [14] a shift of the PL band of $\text{Cu}_{1.85}(\text{Cd}_x\text{Zn}_{1-x})_{1.1}\text{SnS}_{4.1}$ ($0 \leq x \leq 1$) monograin powders (grown in KI) towards lower energies with increasing Cd content was observed in the region $0 \leq x < 0.4$. Therefore, we attribute the shift in PL band maximum to the Cd incorporation into the crystal lattice of CZTS. Fig. 5 presents the PL spectra of CZTS synthesized for 160 h at 650°C with ratios of $V_{\text{CdI}_2}/V_{\text{CZTS}}$ 0.5 and 5. The Cd content of each sample as determined by EDX is shown in Table 1.

All the used analytical methods confirm that during the synthesis of CZTS in CdI_2 as flux Cd incorporates from CdI_2 into the crystal lattice of CZTS resulting in the formation of solid solutions with a common formula of $\text{Cu}_{1.9 \pm 0.01}\text{Zn}_{1-x}\text{Cd}_x\text{SnS}_{3.97 \pm 0.04}$. In the work of Pilvet et al. [14] it was shown that by using CdS and ZnS as precursors the hole row of solid solutions of $\text{Cu}_{1.85}(\text{Cd}_x\text{Zn}_{1-x})_{1.1}\text{SnS}_{4.1}$ ($0 \leq x \leq 1$) can be synthesized. In our system the Cd content is limited by the amount of CdI_2 . In Ref. [15] we found that the Cd concentration in formed CZCdTS increased with temperature and it could be expressed as $[\text{Cd}] \sim e^{-\Delta E/kT}$, where the activation energy of the process $\Delta E = 17.5 \pm 2$ kJ/mol. In this work we found that the Cd concentration in formed CZCdTS and in $\text{Zn}_{1-x}\text{Cd}_x\text{S}$ increases with increasing amounts of CdI_2 in synthesis. The formation of $\text{Zn}_{1-x}\text{Cd}_x\text{S}$ seems to be the rate-determining step for the Cd incorporation into the crystal lattice of the CZTS monograins. Cd incorporation is dependent on temperature and on the amount of CdI_2 , but not influenced by heating time. The direct exchange reaction between solid ZnS and CdI_2 resulting in the formation of CdS and ZnI_2 is thermodynamically impossible because $\Delta G > 0$ [22,23]. We detected by DTA analysis a much lower endothermal effect of melting of the precursor mixture of $\text{Zn} + \text{CdI}_2$ in comparison with pure CdI_2 [18]. That can be explained by the occurrence of some simultaneous compensating exothermal process. We detected also some lowering of melting temperature, that can may due to the dissolution of ZnS in molten CdI_2 . Therefore, we believe that the formation of CdS and $\text{Zn}_{1-x}\text{Cd}_x\text{S}$ is enabled by dissolution of some ZnS in molten CdI_2 . It is well known that the amount of dissolved solute is dependent on the amount of solvent and temperature as seen in the case of Cd content in $\text{Zn}_{1-x}\text{Cd}_x\text{S}$ and also Cd content in formed CZCdTS monograins which was found to be dependent on temperature and on the amount of used CdI_2 as solvent in the present work.

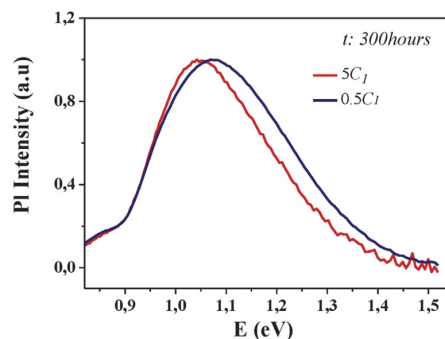


Fig. 5. Low temperature ($T = 10$ K) PL spectra of CZTS monograin powders grown at 650°C for 160 h in CdI_2 with 5C_1 and 0.5C_1 .

4. Conclusions

The impact of different technological conditions such as flux concentration, synthesis temperature and time on the properties of the synthesized CZTS monograins was studied. We found that the grains produced with smaller flux concentrations and at higher temperature are less faceted and have a more rounded shape. With increasing time as well as with increasing flux concentrations, faceted crystals became more obvious. The most round shaped grains were formed in the samples with the lowest amount of CdI₂. It was found that the yield of usable powder grains with a size of 50–100 μm was higher as the flux concentration decreased. Optimum synthesis conditions were found as time 160 h at 650 °C with CdI₂ flux concentration providing $V_{\text{CdI}_2}/V_{\text{CZTS}} = 0.5$. EDX results showed the all the powders were Cu₂Zn_{1-x}Cd_xSnS₄ solid solutions. The Cd incorporation into the crystals of the monograin powders was found to be dependent on the flux concentration but not on time. Cd content in synthesized powders was in the range of 1.9–4.8 at % with the used $V_{\text{CdI}_2}/V_{\text{CZTS}}$ ratios in between 0.5 and 5 at 650 °C.

Acknowledgments

This work was supported by institutional research funding IUT 19-28 of the Estonian Ministry of Education and Research and by the European Union through the European Regional Development Fund, Project TK141. Funding for facilities used in this research was provided by the core infrastructure support IUT-T4 of the Estonian Ministry of Education and Research.

References

- [1] I.D. Olekseyuk, I.V. Dudchak, L.V. Piskach, Phase equilibria in the Cu₂S–ZnS–SnS₂ system, *Journal Alloy. Compds.* 368 (1) (2004) 135–143.
- [2] I.V. Dudchak, L.V. Piskach, Phase equilibria in the Cu₂SnSe₃–SnSe₂–ZnSe system, *J. Alloy. Compd.* 351 (1) (2003) 145–150.
- [3] M. Altosaar, J. Raudoja, K. Timmo, M. Danilson, M. Grossberg, J. Krustok, E. Mellikov, Cu₂Zn_{1-x}Cd_xSn (Se_{1-y}S_y)₄ solid solutions as absorber materials for solar cells, *Phys. status solidi (a)* 205 (no. 1) (2008) 167–170.
- [4] E. Mellikov, M. Altosaar, M. Krunks, et al., Research in solar cell technologies at Tallinn University of technology, *Thin Solid Films* 516 (20) (2008) 7125–7134.
- [5] E. Mellikov, J. Hiie, M. Altosaar, Powder materials and technologies for solar cells, *Int. J. Mater. Prod. Technol.* 28 (3–4) (2007) 291–311.
- [6] M. Kauk-Kuusik, K. Timmo, M. Danilson, M. Altosaar, M. Grossberg, K. Ernits, p–n junction improvements of Cu₂ZnSnS₄/CdS monograin layer solar cells, *Appl. Surf. Sci.* 357 (2015) 795–798.
- [7] I. Klavina, T. Kaljuvee, K. Timmo, et al., Study of Cu₂ZnSnSe₄ monograin formation in molten KI starting from binary chalcogenides, *Thin Solid Films* 519 (21) (2011) 7399–7402.
- [8] E. Mellikov, D. Meissner, T. Varema, M. Altosaar, M. Kauk, O. Volobujeva, M. Danilson, Monograin materials for solar cells, *Sol. Energy Mater. Sol. Cells* 93 (1) (2009) 65–68.
- [9] D. Meissner, *Photovoltaics Based on Semiconductor Powders. Materials and Processes for Energy: Communicating Current Research and Technological Developments*, 2013.
- [10] K. Timmo, M. Altosaar, M. Kauk, J. Raudoja, E. Mellikov, CuInSe₂ monograin growth in the liquid phase of potassium iodide, *Thin Solid Films* 515 (15) (2007) 5884–5886.
- [11] D.A. Porter, K.E. Easterling, M. Sherif, *Phase Transformations in Metals and Alloys*, (Revised Reprint), CRC press, 2009.
- [12] M.A. Lovette, A.R. Browning, D.W. Griffin, J.P. Sizemore, R.C. Snyder, M.F. Doherty, *Cryst. Shape Eng.* 805 (2008).
- [13] G. Nkwusi, I. Leinemann, J. Raudoja, V. Mikli, M. Kauk-Kuusik, M. Altosaar, E. Mellikov, Synthesis of Cu₂(ZnCd)SnS₄ absorber material for monograin membrane applications, in: *MRS Proceedings*, vol. 1638, Cambridge University Press, 2014 pp. mrsf13-1638.
- [14] M. Pilvet, M. Kauk-Kuusik, M. Altosaar, M. Grossberg, M. Danilson, K. Timmo, V. Mikli, Compositionally tunable structure and optical properties of Cu_{1.85}(Cd_xZn_{1-x})_{1.1}SnS_{4.1} (0 ≤ x ≤ 1) monograin powders, *Thin Solid Films* 582 (2015) 180–183.
- [15] G. Nkwusi, I. Leinemann, J. Raudoja, M. Grossberg, M. Altosaar, D. Meissner, T. Kaljuvee, Formation of copper zinc tin sulfide in cadmium iodide for monograin membrane solar cells, in: *Conf. of Young Scientists on Energy Issues*, Kaunas, vol. 2, 2012, pp. 24–25.
- [16] J. Hiie, M. Altosaar, E. Mellikov, Comparative study of isothermal grain growth of CdS and CdTe in the presence of halide fluxes, in: *Solid State Phenomena*, vol. 67, Trans Tech Publications, 1999, pp. 303–308.
- [17] C. Sun, D. Xue, Chemical bonding theory of single crystal growth and its application to φ 3" YAG bulk crystal, *CrystEngComm* 16 (11) (2014) 2129.
- [18] K. Timmo, M. Kauk-Kuusik, M. Altosaar, J. Raudoja, T. Raadik, M. Grossberg, E. Mellikov, Novel Cu₂CdSnS₄ and Cu₂ZnGeSe₄ absorber materials for monograin layer solar cell application, in: *Proceedings of the 28th European Photovoltaic Solar Energy Conference*, France, Paris, 2013, September, p. 2385.
- [19] Nkwusi, G., Leinemann, I., Altosaar, M., The Processes and Enthalpies in Synthesis of Cu₂ZnSnS₄ in Molten CdI₂.
- [20] M. Grossberg, T. Raadik, J. Raudoja, J. Krustok, Photoluminescence study of defect clusters in Cu₂ZnSnS₄ polycrystals, *Curr. Appl. Phys.* 14 (3) (2014) 447–450.
- [21] M. Grossberg, J. Krustok, J. Raudoja, T. Raadik, The role of structural properties on deep defect states in Cu₂ZnSnS₄ studied by photoluminescence spectroscopy, *Appl. Phys. Lett.* 101 (10) (2012) 102102.
- [22] W. Kunczewicz-Kupczyk, J. Kapala, S. Roszak, M. Miller, The thermodynamic properties of the gaseous dimer of CdI₂, *J. Chem. Phys.* 108 (18) (1998) 7743–7746.
- [23] Landolt-Börnstein, *Thermodynamic Properties of Inorganic Material*, Sci Gr Thermodata Eur (SGTE). Berlin-Heidelberg, Springer-Verlag, 1999. Sci Gr Thermodata Eur (SGTE), Berlin-Heidelberg, Springer-Verlag, 1999.

Article II

Nkwusi, G., Leinemann, I., Altosaar, M. The Processes and Enthalpies in Synthesis of $\text{Cu}_2\text{ZnSnS}_4$ in Molten CdI_2 . *International Advanced Research Journal of Science, Engineering and Technology*, **3** (2016) 113-119.

The Processes and Enthalpies in Synthesis of $\text{Cu}_2\text{ZnSnS}_4$ in Molten CdI_2

Godswill Nkwusi¹, Inga Leinemann¹, Mare Altosaar¹

Institute of Materials Science, Tallinn University of Technology, Estonia¹

Abstract: Synthesis of $\text{Cu}_2\text{ZnSnS}_4$ (CZTS) in molten CdI_2 for solar cell absorber layer in monograin powder form is studied. The aim is to understand the chemical reactions and to describe the conditions for the synthesis of CZTS starting from binary compound precursors. It is found that the formation of $\text{Cu}_2\text{ZnSnS}_4$ proceeds mainly in the liquid phase of CdI_2 where CdS and $\text{Zn}_{1-x}\text{Cd}_x\text{S}$ form and initiate the formation of $\text{Cu}_2\text{Zn}_{1-x}\text{Cd}_x\text{SnS}_4$. The formed phases in the mixtures of CdI_2 with precursor compounds detected by XRD and Raman analyses are presented. The formation enthalpy for Cu_2SnS_3 and $\text{Cu}_2\text{ZnSnS}_4$ are $13 \pm 2 \text{ kJmol}^{-1}$ and $8 \pm 2 \text{ kJmol}^{-1}$ respectively.

Keyword: $\text{Cu}_2\text{ZnSnS}_4$, $\text{Cu}_2\text{Zn}_{1-x}\text{Cd}_x\text{SnS}_4$, Monograin powder, Enthalpies.

I. INTRODUCTION

CZTS monograin layer solar cells have shown power conversion efficiency of 9.4 % (measured from the active area of solar cell) [1]. Monograin technology (MGT) explores the use of suitable flux to aid the growth of single crystalline CZTS powder particles. As the monograin powder growth is carried out at high temperatures in a molten salt, the semiconductor compound crystals are doped with the constituent elements of the used salts (KI, NaI) at the level of their solubility at synthesis temperature. The solubility of precursor compounds in KI was determined as follows: 3.6 mole% CuSe, 0.27 mole% SnSe and 0.086 mole% ZnSe [2].

The solubility of $\text{Cu}_2\text{ZnSnSe}_4$ in KI was 0.61 mole% [2]. In addition, the doping of the synthesized monograin powder with Na and K, also with Cl, has a rather big influence on the monograin absorber material properties [3-4].

Using CdI_2 as a flux in monograin powder growth allows to produce a material without K/Na doping and to study the influence of intentional Na and/or K doping of CZTS. I. Leinemann (Klavina), studied the formation of CZTSe in NaI and KI and determined CZTSe formation reactions enthalpies [5-6]. It was also found that in the synthesis of $\text{Cu}_2\text{ZnSnSe}_4$ in CdI_2 , Cd from CdI_2 incorporated into the crystals of CZTSe forming a solid solution of $\text{Cu}_2\text{Zn}_{1-x}\text{Cd}_x\text{SnSe}_4$, however, the formation of $\text{Cu}_2\text{ZnSnS}_4$ in CdI_2 and the reaction enthalpies have not been studied yet.

In this report, we present the reaction path of CZTS synthesis in CdI_2 starting from binary compound precursors. In this study, various mixtures of the individual precursors with CdI_2 , as well as the precursor mixtures for the synthesis of CZTS in CdI_2 were used. We also report the chemical reactions and their enthalpies occurring in the growth process. All chemical reactions and enthalpy calculations are based on DTA-DSC analysis data and on phase changes determined by XRD and Raman analyses.

II. EXPERIMENTAL

Copper Zinc Tin Sulphide (CZTS) monograin powder was synthesized from a mixture of precursors ($\text{Cu}_2\text{S}+\text{SnS}+\text{ZnS}+\text{S}$) in the presence of molten phase of CdI_2 . Separate quasi-binary mixtures ($\text{Cu}_2\text{S}+\text{CdI}_2$), ($\text{ZnS}+\text{CdI}_2$), ($\text{SnS}+\text{CdI}_2$) ($\text{S}+\text{CdI}_2$), also mixture for ternary Cu_2SnS_3 (CTS) compound ($\text{Cu}_2\text{S}+\text{SnS}+\text{S}+\text{CdI}_2$) were studied as described in [7]. An empty quartz ampoule was used as a reference for the DTA measurements. Pure CdI_2 was selected as the reference material for the DTA-DSC enthalpy calibrations for two reasons; firstly, the processes taking place in the synthesis occur in the same temperature region as the melting of CdI_2 and secondly, our experimentally determined melting point of CdI_2 coincide with the value found from literature ($T_{\text{melt}}=385^\circ\text{C}$) [8]. Our readings from DTA curves in $\mu\text{V.s}$ were converted to J/mol using the value of enthalpy of fusion of CdI_2 (15.31 kJ/mol [9]) considering that our experimental heat value for melting of CdI_2 is $666 \pm 2 \mu\text{Vs}$ which corresponds to $\approx 5.23 \text{ J}$ (constant for our calculations). The DTA heating's and cooling's were carried out in two runs. The obtained energy values were used for the evaluation of the enthalpies of the occurring processes with error margin estimated as 5 %, given as the largest deviation of the individual process value from the average value. The applied heating and cooling rates from room temperature to 800°C were 5 and 10°C per minute, respectively. After recording the thermal effects by DTA, the changes in the phase composition of different precursor mixtures with CdI_2 were determined by Raman and XRD analyses. For the phase analyses, separate mixture samples with bigger amounts but in the same molar proportions as for DTA were prepared for each thermal effect observed in the DTA curves. The samples were heated in closed quartz ampoules for 4 hours at temperatures slightly higher than the observed thermal effects in DTA curves. After heating, the bigger samples were quenched from the heating temperature to room temperature in cold water. The heated and quenched powder samples were analyzed by SEM, EDX, Raman and XRD methods both before and after separation of CdI_2 (by washing with deionized water).

Details of the used analytical set-ups are reported elsewhere [10,6].

III.RESULTS AND DISCUSSIONS

The melting temperatures of the studied mixtures ($\text{Cu}_2\text{S}+\text{CdI}_2$), ($\text{ZnS}+\text{CdI}_2$), ($\text{SnS}+\text{CdI}_2$), ($\text{Cu}_2\text{S}+\text{SnS}+\text{S}+\text{CdI}_2$) and ($\text{Cu}_2\text{S}+\text{SnS}+\text{ZnS}+\text{S}+\text{CdI}_2$), picked up from DTA curves, are presented in Figure 1. It can be seen that the melting of the precursor mixtures with CdI_2 takes place at lower temperatures than the melting temperature of pure CdI_2 (385 °C) [8]. The lowering of melting temperatures shows some solubility of the precursors in molten CdI_2 and/or the formation of new phases.

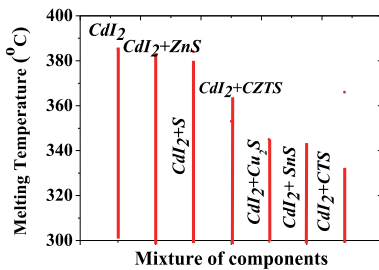


Fig 1. Melting temperatures of studied mixtures as determined from DTA curves

A. CdI_2

At temperatures above the melting point, CdI_2 exists in gaseous as monomeric $\text{CdI}_{2(g)}$ and dimeric $\text{Cd}_2\text{I}_{4(g)}$ forms [11-13]. According to Shushic et.al. and Corbett et.al. [14], molten CdI_2 has a brown colour, since a certain amount of free iodine is always in equilibrium with the melt [15]. Iodine is known as an oxidizing agent which may limit the reactions between CdI_2 and the precursors. The DTA probe of pure CdI_2 (see Figure 2) gave an endothermic effect at 385 °C in heating and an exothermic effect at 366 °C in cooling cycle which can be attributed to the melting and freezing of CdI_2 with enthalpy signal of $666 \pm 2 \mu\text{V.s}$. This signal is equal to 5.23J, as calculated from the obtained peak area for correspondent 0.00034 mole of CdI_2 in the ampoule (molar mass of $\text{CdI}_2=366.22 \text{ g/mol}$ and the molar fusion enthalpy value for pure CdI_2 is 15.31kJ/mol) .

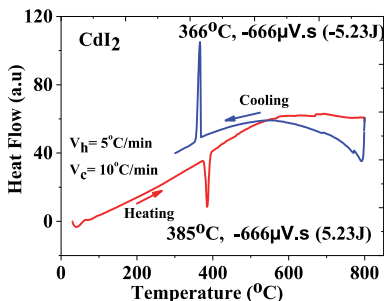


Fig 2. DTA curves of CdI_2

B. $\text{CdI}_2 + \text{Cu}_2\text{S}$

By phase analyses the sample of the mixture heated just above the melting temperature of CdI_2 revealed the formation of CuI , while Cu_2S had been transformed to $\text{Cu}_{1.96}\text{S}$ at 353 °C, correspondently to the Cu-S phase diagram [16]. In the DTA curves of the mixture of $\text{CdI}_2 + \text{Cu}_2\text{S}$ (see Figure 3), there is seen an endothermic melting effect at 353 °C and an exothermic effect of freezing of CdI_2 at 338 °C. We can observe a decrease in the energy value of melting process from 5.23 J (666 $\mu\text{V.s}$) for pure CdI_2 to 2.1 J (264 $\mu\text{V.s}$) in $\text{CdI}_2+\text{Cu}_2\text{S}$ mixture. This decrease can be ascribed to the simultaneous exothermic reactions occurring alongside the melting of CdI_2 . By XRD and Raman, different compounds - $\text{Cu}_{1.96}\text{S}$, CuI , $\text{Cu}_2\text{Cd}_3\text{I}_4\text{S}_2$, CdS and Cu_4Cd_3 - were found in $\text{CdI}_2+\text{Cu}_2\text{S}$ mixtures heated for 4 hours at temperature a little bit above the melting point of the mixture (353 °C) (see Tabel 1). This confirms the chemical interaction between the flux material and Cu_2S . By XRD and Raman analyses, we found that some of these processes occurring during the melting and freezing of the mixture ($\text{CdI}_2+\text{Cu}_2\text{S}$) are reversible: Cu_2S , as observed by XRD, transformed to $\text{Cu}_{1.96}\text{S}$ and re-transformed to Cu_2S by cooling down - that is in accordance with the report [16-17]. In the heating process, in addition to the main fusion peak at 353 °C there is seen another endothermic DTA peak at 400 °C. The phase analysis of the bigger sample heated and quenched at 420 °C shows that this peak corresponds to the decomposition of $\text{Cu}_2\text{Cd}_3\text{I}_4\text{S}_2$ with formation of CdS , CuI_2 and Cu_4Cd_3 (see equation (5) in the Tabel 1) with summary thermal effect of 77 mVs (0.6J).

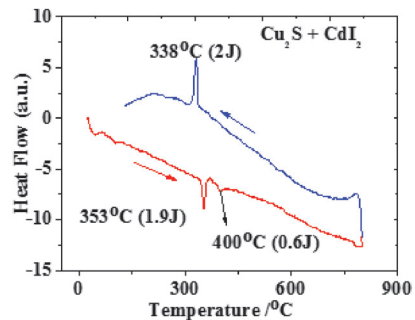


Fig 3: DTA curves of $\text{CdI}_2+\text{Cu}_2\text{S}$

C. $\text{CdI}_2 + \text{ZnS}$

The DTA heating and cooling curves of this mixture are presented in Figure 4. It shows an endothermic peak at 382 °C in the heating cycle, slightly lower than the melting temperature of pure CdI_2 ($T_{\text{melt}}=385^\circ\text{C}$) with the thermal effect of 2.7 J, that is much lower than in the melting of pure CdI_2 (5.23J). It means that some exothermic process compensates the endothermic melting effect. However, no new phases other than CdI_2 and ZnS were found by XRD and Raman in the sample heated and quenched at 385 °C, may be due to the low sensitivity of XRD. In the cooling curve two exothermic peaks at 354 °C and 338 °C are seen. This implies that CdI_2 in the mixture with ZnS melts close to the melting temperature of its pure form.

Table 1: The annealing conditions, determined phases, reactions and calculated ΔG values for CuS+CdI₂ quasi-binary system

Annealing conditions	Phases Raman and XRD	By and	Reactions	ΔG kJmol ⁻¹
Heated to 353°C, annealed for 4 hours	CuS, Cu _{1.96} S, CuI, Cu ₂ Cd ₃ I ₄ S ₂		(1) Cu ₂ S+CdI ₂ ←2CuI+CdS [18-20]	[18-49 T=300°C -31.5 T=400°C
			(2) CdS+Cu ₂ S+2CdI ₂ ↔Cu ₂ Cd ₃ I ₄ S ₂	Proposed
Heated to 400°C, annealed for 4 hours	CdS, Cu ₄ Cd ₃		(3) Cu ₂ S + CdI ₂ (g) = 2CuI + CdS [18,20]	-43.6 T=300°C -1.8 T=600°C
Heated to 800°C and cooled down to 330°C	CdS, Cu ₄ Cd ₃ , CuS, Cu ₂ Cd ₃ I ₄ S ₂ , CuI		(4) CuS+CdI ⁺ (g)→ CuI +CdS [18,21]	-152 T=300°C -84.7 T=800°C
			(5) 2Cu ₂ Cd ₃ I ₄ S ₂ ↔Cu ₄ Cd ₃ +2CdS+CdI ₂ +I ₂	Proposed

That can be an evidence about minimal interaction between each other, or some compensating process can interfere. The peak at 338°C corresponds to an energy signal of about 1.8J (234 μV.s) much lower than that of freezing of pure CdI₂. Analyses by XRD and Raman showed that there had been formed a solid solution of Zn_{1-x}Cd_xS in the mixture of ZnS + CdI₂ (see Table 2). As the formation of Zn_{1-x}Cd_xS presupposes the formation of CdS that incorporates into ZnS, the overall enthalpy of the process was found as 3.42J.

In Figure 4, the slight lowering of melting temperature of CdI₂ in the DTA curve and lowered melting effect suggests that there has been some interaction between the molten CdI₂ and ZnS. In equation (8), there exist a thermodynamical possibility for a possible reaction between ZnS and CdI⁺ for temperatures between 0 and 1000°C. In equation (6), the calculations of Gibbs energy change gave positive values for the reaction between solid CdI₂ and ZnS and therefore the CdS formation from solids is thermodynamically impossible. The probability of the reaction (6 and 11) should be therefore excluded. However, (see Table 2 and 5) we found Zn_{1-x}Cd_xS and Cu₂Zn_{1-x}Cd_xSnS₄ formed in the studied samples. Explanation for the possibility to form Zn_{1-x}Cd_xS in the mixture of liquid CdI₂ and solid ZnS could be therefore found by studying the properties of liquid and gaseous

phases of CdI₂. It is well known that many salts in their molten phase are in the form of ionic liquids, but not CdI₂. MX₂ salts retain their solid phase structure even in liquid phase, in which the small metal²⁺ ions occupy tetrahedrally coordinated sites in a closely packed anion structure, with strong intermediate range ordering [22-23]. Konigns et. al. in their work [13] studied the vapors over CdI₂(l) and they found it to consist of monomeric and dimeric molecules.

Also, measurements of the scattering of thermal neutrons in natural samples of molten ZnCl₂, ZnBr₂ and ZnI₂ confirmed a structural model in which the small Zn²⁺ ions occupy tetrahedrally coordinated sites in a closely packed anion structure, with strong intermediate range ordering [24-26]. Therefore, in the cooling process, some ZnS that had been dissolved in the molten phase and reacted with CdI⁺ forming CdS and ZnI₂ (see reaction 8), precipitates from the melt as solid solution of Zn_{1-x}Cd_xS at 354°C. Probably ZnI₂-CdI₂ liquid solution freezes at 338°C. According to Chikanov et.al, in ZnI₂-CdI₂ mixtures there form continuous row of solid solutions [27]. After opening the ampoule, ZnI₂ could not be detected by phase analyses due to its very high hygroscopicity. So, the possible explanation for the Zn_xCd_{1-x}S formation can be given through the formation of CdI⁺ in the equations (9) and (10).

D. CdI₂ + SnS

The melting was observed at 345°C (see Figure 5), at much lower temperature than for pure CdI₂. This fact suggests to a higher solubility/interaction of SnS in CdI₂. XRD and Raman studies of the bigger samples: (a) heated to 800 °C and cooled down to 350°C and then quenched to room temperature and (b) cooled down to 250°C from 800°C before quenching rapidly; revealed that SnI₄, Sn₂Si₂ and CdS had been formed (shown in Table 3). The final freezing of SnS+CdI₂ mixture can be detected in the cooling curve at 300°C (see Fig 5). The enthalpy observed in the cooling process is -6.23J. It can be attributed to the exothermic freezing of CdI₂ with cumulatively formed tin iodides and CdS as observed by phase analysi

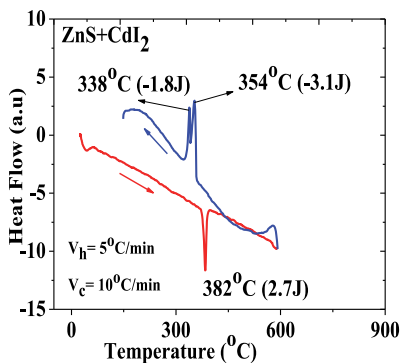


Fig 4: DTA curves of CdI₂+ZnS mixture

Table 2: The annealing conditions, determined phases, reactions and calculated ΔG values for ZnS+CdI₂ binary system

Annealing conditions	Phases by Raman and XRD	Reactions	ΔG kJmol ⁻¹
Annealed at 385°C and quenched to RT	ZnS, CdI ₂	(6) ZnS _(s) +CdI _{2(s,l)} → ZnI ₂ +CdS, [27]	44.1 T=0°C 51.8 T=800°C
		(7) ZnS+CdI _{2(g)} = ZnI ₂ +CdS. [27-29]	-8.3 T=300°C Positive above 300°C
Heated to 800°C, cooled down and quenched at 330°C to RT	Zn _{0.94} Cd _{0.06} , S ₆ , (Zn _{0.8} Cd _{0.2}) S, CdI ₂ , ZnS,	(8) ZnS + I ⁺ + CdI _(g) ⁺ → CdS+ZnI _{2(g)} +I _(g) [29]	-59.5 T=300°C -86.2 T=800°C
Heated to 800°C, cooled down to and quenched at 350°C RT		(9) ZnS+I ⁺ +CdI _(g) ⁺ → ZnS+CdI ₂ [27-29]	-186.7 T=300°C -113 T=800°C
		(10) ZnS+I ⁺ +CdI _(g) ⁺ →Zn _{1-x} C _x dS+1-xCdI ₂	Proposed
		(11) ZnS (s)+CdI ₂ (s) → Zn _{1-x} C _x dS (s)	Proposed

Table 3: The annealing conditions, determined phases, reactions and calculated ΔG values for SnS+CdI₂ binary system

Annealing conditions	Phases by Raman and XRD	Reactions	ΔG kJmol ⁻¹
Heated to 350 °C and quenched	CdI ₂ , CdS, SnI ₂ , Sn ₂ SI ₂	(12) SnS+CdI ₂ (g) = SnI ₂ +CdS [17,30]	-79.5 T ≥ 0 -9.6 T ≤ 500
		(13) 2SnS+I ₂ →Sn ₂ SI ₂ +S	proposed on phases observed
		(14) 2SnS+CdI ₂ →Sn ₂ SI ₂ +CdS	proposed on phases observed
		(15) CdI _{2(g)} +S → I ₂ + CdS,	-43.2 T=0°C 9.7 T=400°C
		(16) SnS _{2(g)} = SnS+ S [29-30]	-196.8 T=100°C -98.6 T=800°C
Heated to 800 °C and cooled down to 250°C	SnI ₄ , SnS, SnSI ₂ , CdS, SnI ₂	(17) SnI ₄ +2CdS=SnS+2CdI ₂ +S	-11.7 T=100°C -22.8 T=800°C
		(18) I ₂ + CdS =CdI _{2(g)} +S	26.5 T=100°C -50 T= 800°C
		(19) SnS ₂ + 2CdI _(g) ⁺ → 2CdS + SnI ₂ (SnSI ₂) [27]	-379 T=0°C -162.4 T=800°C
		(20) 2CdI _(g) ⁺ +2S= I ₂ + 2CdS	-368.9 T=0°C -132 T=800°C

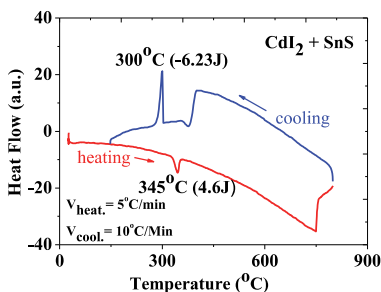


Fig 5: DTA curves of CdI₂+SnS mixture

E. Mixture for synthesis of Cu₂SnS₃ (CdI₂+SnS+Cu₂S+S)

In the mixture of (Cu₂S+SnS+S+CdI₂), we observed two endothermic peaks in the heating process with enthalpy

signals of 0.7J (88μV.s) and 2.0J (265 μV.s) at 339°C and 360°C respectively. The former is attributed to the melting of CdI₂ while the latter can be attributed to the transformation of Cu₂S to Cu_{1.96}S as it was observed already in (Cu₂S+CdI₂). In addition, SnS₂ was also found by XRD. XRD analysis of the mixture of (CdI₂+SnS+Cu₂S+S) heated just above the melting of CdI₂, revealed the formation of ternary compound Cu₂SnS₃. The low enthalpy signal can be attributed to the net effect of the endothermic melting of CdI₂ and the exothermic formation of SnS₂ and Cu₂SnS₃ alongside the other concurrent processes. The enthalpy of the cumulative formation process in the heating process can be given as (666μV.s - 88μV.s = 578μV.s) - this corresponds to 13±2kJmol⁻¹. In the cooling process, the observed exothermic enthalpy signal of 2.7J (343 μV.s) at 343 °C is lower than freezing of pure CdI₂, probably due to some dissolved compound, for example SnI₂ or SnI₄, in it. XRD

analysis of the sample mixture of $CdI_2 + SnS + Cu_2S + S$ heated to $800^\circ C$ and then cooled down to $300^\circ C$ before quenching rapidly to room temperature showed the presence of Cu_2SnS_3 . In the second heating/cooling process, we observed single endothermic /exothermic peaks for the melting and freezing of the mixture with close enthalpy signal values as observed in the first heating/cooling process. The reaction between $Cu_2S + SnS + S$ leads to the formation of ternary compounds Cu_2SnS_3 [31] and Cu_4SnS_6 [32] (see table 4) and the formation of the ternaries takes place during the melting of the flux (CdI_2) see figure 6.

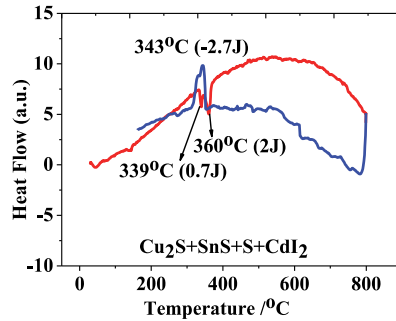


Fig 6: DTA curve of $CdI_2 + SnS + Cu_2S + S$ mixtures

Table 4: The annealing conditions, determined phases, reactions and calculated ΔG values for ($CdI_2 + SnS + Cu_2S + S$) ternary system

Annealing conditions	Phases by Raman and XRD	Reactions	$\Delta G \text{ kJmol}^{-1}$
Heated to $490^\circ C$	CdI_2 , Cu_2S ,	(21) $2CuS \rightarrow Cu_2S + S_{(l)}$ [27][33]	-4.48 $T = 500^\circ C$ -39.88 $T = 1000$
Heated to $560^\circ C$	SnS , Cu_2SnS_3	(22) $2SnS + 2S \rightarrow 2SnS_2$ (23) $2CuS + SnS \rightarrow Cu_2SnS_3$ [31][34]	-28.6 $T = 400^\circ C$ Proposed
Heated to $800^\circ C$ and cooled down to $300^\circ C$	CdI_2 , Cu_2S ,	(24) $2CuS + SnS \text{ (melt)} \rightarrow Cu_2SnS_3$	Proposed
Heated to $800^\circ C$ and cooled down to $470^\circ C$	SnS_2 , Cu_2SnS_3 , Cu_4SnS_6	(25) $2Cu_2S + SnS_2 + 2S \rightarrow Cu_4SnS_6$ [31]	Proposed

F. Mixture for quaternary CZTS compound, ($CdI_2 + SnS + Cu_2S + S + ZnS$).

The mixture of CdI_2 with the binary precursors in the required stoichiometric composition for the formation of Cu_2ZnSnS_4 , melts/solidifies at $366^\circ C/353^\circ C$ respectively with thermal effects of $2.4J$ ($308 \mu V.s$) in the endothermic and exothermic processes as seen in DTA curves (see Figure 7) accompanied by other multiple processes proceeding at the same time, considering the reduced enthalpy signal. In order to study the formed phases present in the quaternary system, mixtures of $CdI_2 + SnS + Cu_2S + S + ZnS$ were heated to $800^\circ C$ and cooled down to $600^\circ C$ and $350^\circ C$ respectively before quenching rapidly to room temperature. We found by XRD and Raman the formation Cu_2SnS_3 , $Cu_2ZnCdSnS_4$, Cu_2ZnSnS_4 and $Zn_{1-x}Cd_xS$, which confirms that the other (exo-endo) reactions also occur alongside in the molten phase of CdI_2 . In another sample heated to $500^\circ C$ and quenched to room temperature, CZTS was detected by Raman, which confirms that CZTS already begins to form starting from the formation of ternary Cu_2SnS_3 compound. Cu_2SnS_3 reacts with $Zn_xCd_{1-x}S$ (described for the mixture of ($ZnS + CdI_2$)) to form $Cu_2ZnCdSnS_4$ as the final product. The formation of CZTS in molten CdI_2 proceeds via a complex exothermic process with enthalpy signal of ($666 \mu V.s - 308 \mu V.s = 358 \mu V.s$) that corresponds to enthalpy value of $8 \pm 2 \text{ kJmol}^{-1}$. $Cu_2Zn_{1-x}Cd_xSnS_4$ is the prevailing phase with its characteristic Raman peaks at $166, 250, 286, 336, 374 \text{ cm}^{-1}$ in the unwashed sample.

CdI_2 with its Raman peak at 110 cm^{-1} and CuI at 145 cm^{-1} were detected only in unwashed samples but not in washed samples. CuI is soluble in KI or NaI solutions, as also reported in our previous report, allowing separation of single phase CZTS [35,7]. All phases detected by Raman and XRD and the proposed reaction path are summarized in Table 5. The formed solid solution of $Cu_2Zn_{1-x}Cd_xSnS_4$ was confirmed by EDX analysis and by the shift of Raman peak from 338 cm^{-1} to 332 cm^{-1} [36]. We propose that the formation of $Cu_2Zn_{1-x}Cd_xSnS_4$ solid solution proceeds via an intermediate reaction between $Zn_{1-x}Cd_xS$ and Cu_2SnS_3 equation (26) or directly by reaction (27) in the molten phase of CdI_2 .

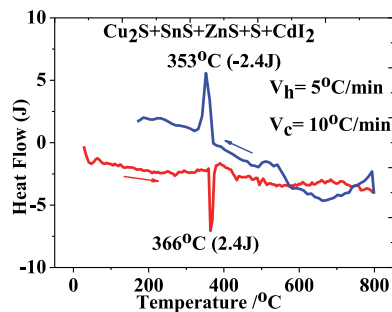


Fig 7. DTA curves of precursor mixtures $CdI_2 + SnS + Cu_2S + S + ZnS$

Table 5: The annealing conditions, determined phases, reactions and calculated ΔG values for $(\text{CdI}_2 + \text{SnS} + \text{Cu}_2\text{S} + \text{S} + \text{ZnS})$ quaternary system

Annealing conditions	Phases by Raman and XRD	Reactions	ΔG (kJ)
Heated to 800°C	$\text{Cu}_2\text{Zn}_{1-x}\text{Cd}_x\text{SnS}_4$	26 $\text{Cu}_2\text{SnS}_3 + \text{Zn}_{1-x}\text{Cd}_x\text{S} \rightarrow \text{Cu}_2\text{Zn}_{1-x}\text{Cd}_x\text{SnS}_4$	
Heated to 800°C and cooled to 600°C	CdI_2 , $\text{Cu}_2\text{-xS}$, Cu_2SnS_3 , $\text{Cu}_2\text{ZnCd}_{1-x}\text{SnS}_4$, SnI_4 ,	27 $\text{Cu}_2\text{S} + \text{SnS} + \text{Zn}_{1-x}\text{Cd}_x\text{S} + \text{S} \rightarrow \text{Cu}_2\text{Zn}_{1-x}\text{Cd}_x\text{SnS}_4$	Proposed
Heated to 800°C and cooled to 350°C	CdI_2 , CuI , SnI_4 , $\text{Cu}_2\text{ZnCd}_{1-x}\text{SnS}_4$		

In figure 8, on the base of the ΔG calculations for different reactions, we show that the most probable route to the formation of $\text{Cu}_2(\text{ZnCd})\text{SnS}_4$ through the intermediate formation of $\text{Zn}_{1-x}\text{Cd}_x\text{S}$ is by the formation of $\text{CdI}^+(\text{g})$. The chemical interaction between ZnS and solid CdI_2 at temperatures lower than 400°C is not favourable because the ΔG value is positive.

Therefore this rules out the possibility of formation of quaternary $\text{Cu}_2\text{Zn}_{1-x}\text{Cd}_x\text{SnS}_4$. As mentioned earlier, there exist a thermo-dynamical possibility for a possible reaction between ZnS and CdI^+ to form $(\text{Zn}_{(1-x)}\text{Cd}_x\text{S})$ at temperatures between 0 and 1000°C which is the only favourable path for the formation of $\text{Cu}_2(\text{ZnCd})\text{SnS}_4$.

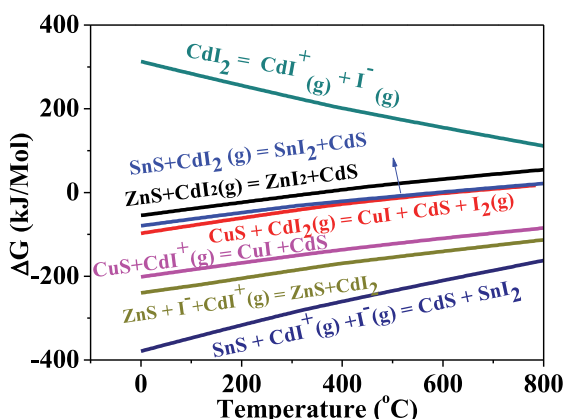


Fig 8: Calculated ΔG values for different reactions showing the possible reaction path for the synthesis of $\text{Cu}_2\text{ZnCdSnS}_4$ in molten CdI_2

IV. CONCLUSIONS

By studying mixtures of CdI_2 with individual precursors for synthesis of CZTS we found that CdI_2 mixed with S , ZnS , Cu_2S or SnS melts at temperatures lower than pure CdI_2 due to the freezing-point depression effect showing some solubility of the precursors in molten CdI_2 . CdS and different iodine-containing compounds (SnI_4 , Sn_2SI_2 , CuI , and $\text{Cu}_2\text{Cd}_3\text{I}_4\text{S}_2$) form in $\text{CdI}_2 + \text{Cu}_2\text{S}$ and $\text{CdI}_2 + \text{SnS}$. The overall enthalpy value of the processes in each case studied is formed via an exothermic process alongside the endothermic melting of the CdI_2 which gives rise to a lower melting temperature and enthalpy of fusion of the CdI_2 flux. CZTS formation in molten CdI_2 can be described as a two-stage process: first CdI^+ reacts with ZnS forming CdS , that after alloying with ZnS results in $\text{Zn}_{1-x}\text{Cd}_x\text{S}$. The amount of CdI^+ increases with temperature

with the released Iodine acting as an oxidizing agent which reacts with Cu_2S and SnS resulting in different iodine containing compounds. Secondly, Cu_2S and SnS react to form ternary Cu_2SnS_3 . The formation of Cu_2SnS_3 from $\text{Cu}_2\text{S} + \text{SnS} + \text{S}$ in CdI_2 gave an enthalpy value of $13 \pm 2 \text{ kJmol}^{-1}$. The $\text{Zn}_{1-x}\text{Cd}_x\text{S}$ and Cu_2SnS_3 combines to form a quaternary CZCdTS. The synthesis of CZTS monograin powders in CdI_2 results in the formation of solid solutions of $\text{Cu}_2\text{Zn}_x\text{Cd}_{1-x}\text{SnS}_4$ with limited Cd content. The reaction of formation $\text{Cu}_2\text{Zn}_x\text{Cd}_{1-x}\text{SnS}_4$ in the liquid phase of CdI_2 takes place with the experimentally determined enthalpy of $8 \pm 2 \text{ kJmol}^{-1}$. The low enthalpy of formation of $\text{Cu}_2\text{Zn}_x\text{Cd}_{1-x}\text{SnS}_4$ compared to high formation enthalpy of the ternary Cu_2SnS_3 could confirm that the solid $\text{Cu}_2\text{Zn}_x\text{Cd}_{1-x}\text{SnS}_4$ solution is formed from the reaction between Cu_2SnS_3 and $\text{Zn}_{1-x}\text{Cd}_x\text{S}$. The formation of CdI^+ in the liquid phase is proposed to be a limiting

factor in the CdS formation and due to this also the incorporation of Cd into CZTS crystals is limited

ACKNOWLEDGEMENT

This work was supported by institutional research funding IUT 19-28 of the Estonian Ministry of Education and Research and by the European Union through the European Regional Development Fund, Project TK141. Funding for facilities used in this research was provided by the core infrastructure support IUT-T4 of the Estonian Ministry of Education and Research.

REFERENCES

- [1] Kauk-Kuusik, M., Timmo, K., Danilson, M., Altosaar, M., Grossberg, M., & Ernits, K. (2015). p-n junction improvements of Cu₂ZnSnS₄/CdS monograin layer solar cells. *Applied Surface Science*, 357, 795-798.
- [2] Klavina, I., Kaljuvee, T., Timmo, K., Raudoja, J., Traksmaa, R., Altosaar, M., & Meissner, D. (2011). Study of Cu₂ ZnSnSe₄ monograin formation in molten KI starting from binary chalcogenides. *Thin Solid Films*, 519(21), 7399-7402.
- [3] Timmo, K., Altosaar, M., Raudoja, J., Mellikov, E., Varema, T., Danilson, M., & Grossberg, M. (2007). The effect of sodium doping to CuInSe₂ monograin powder properties. *Thin solid films*, 515(15), 5887-5890.
- [4] Kauk, M., Altosaar, M., Raudoja, J., Timmo, K., Varema, T., Danilson, M., ... & Mellikov, E. (2008, February). The influence of doping with donor type impurities on the properties of CuInSe₂. In *Physica Status Solidi C Conferences* (Vol. 5, No. 2, p. 609). John Wiley & Sons, Ltd.
- [5] I. Leinemann, J. Raudoja, M. Grossberg, M. Altosaar, D. Meissner, R. Traksmaa, and T. Kaljuvee, Comparison of Copper Zinc Tin Selenide Formation In Molten Potassium Iodide and Sodium Iodide As Flux Material. 2011.
- [6] I. Klavina, J. Raudoja, M. Altosaar, E. Mellikov, D. Meissner. CZTS (Cu₂ZnSnSe₄) crystal growth for use in monograin membrane solar cells. *CYSENI 2010*, May 27–28, Kaunas, Lithuania. ISSN 1822-7554
- [7] Nkwusi, G., Leinemann, I., Raudoja, J., Grossberg, M., Altosaar, M., Meissner, D., ... & Kaljuvee, T. (2012). Formation of copper zinc tin sulfide in cadmium iodide for monograin membrane solar cells. In *Conf. of Young Scientists on Energy Issues*, Kaunas (Vol. 2, pp. 24-25)...
- [8] Pfenig, B. W. (2015). *Principles of Inorganic Chemistry*. John Wiley & Sons.
- [9] CRC PRESS LLC. Standard Thermodynamic Properties of Chemical Substance (continued). *CRC Handb Chem Phys*. 2012;13(4):5.4 - 5.41, (http://www.update.uu.se/~jolkkonen/pdf/CRC_TD.pdf) retrieved on 11/04/2016.
- [10] Nkwusi, G., Leinemann, I., Raudoja, J., Mikli, V., Kauk-Kuusik, M., Altosaar, M., & Mellikov, E. (2014). Synthesis of Cu₂(ZnCd)SnS₄ Absorber Material for Monograin Membrane Applications. In *MRS Proceedings* (Vol. 1638, pp. mrsf13-1638). Cambridge Universi.
- [11] Kaupp, M., & von Schnering, H. G. (1994). Ab Initio Comparison of the (MX)₂ Dimers (M= Zn, Cd, Hg; X= F, Cl, H) and Study of Relativistic Effects in Crystalline HgF₂. *Inorganic Chemistry*, 33(21), 4718-4722.
- [12] Topor, L., & Moldovea. I. (1974). Vapor-pressures of molten CdBr₂, CdI₂, MgBr₂ and molecular association in gaseous phase. *revue roumaine de Chimie*, 19(6), 985-990.
- [13] Konings, R. J. M., Booi, A. S., & Cordfunke, E. H. P. (1991). High-temperature infrared study of the vaporization of CsI, CdI₂ and Cs₂CdI₄. *Vibrational spectroscopy*, 2(4), 251-255.
- [14] Corbett, J. D., von Winbush, S., & Albers, F. C. (1957). The Solubility of the Post-Transition Metals in their Molten Halides. *Journal of the American Chemical Society*, 79(12), 3020-3024.
- [15] M. V. Šušić, S. V. Mentus, Cyclic voltammetry of molten CdI₂ and Cd-CdI₂. *Bulletin Tome LXVIII: Classe Des Sciences Naturelles Et* Mathematiques, Academie Serbe des sciences et des arts, Nr 19 - 1979, Beograd.
- [16] Dumon, A., Lichanot, A., & Gromb, S. (1974). Study of Cu-S Phase-Diagram in Compositional Area Cu₂, 000S-Cu1, 960S. *Journal De Chimie Physique et de Physico-Chimie Biologique*, 71(3), 407-414.
- [17] Buerger, N. W. (1939). The Polymorphism of Cu₂S, and the Relations Between the Solid Phases in the System Cu₂S-CuS. *The Journal of Chemical Physics*, 7(11), 1067-1068.
- [18] Börnstein, L. (1999). *Thermodynamic Properties of Inorganic Material*, Scientific Group Thermodata Europe (SGTE).
- [19] SGTE 94, Scientific Group Thermodata Europe, Grenoble Campus, 1001 Avenue Centrale, BP 66, F-38402 Saint Martin d'Hères, France, 1994 (HSE software).
- [20] Donald, K. J., Hargittai, M., & Hoffmann, R. (2009). Group 12 dihalides: structural predilections from gases to solids. *Chemistry-A European Journal*, 15(1), 158-177.
- [21] Barin I: *Thermochemical Data of Pure Substances*, Part II, VCH Verlags Gesellschaft, Weinheim, 1993 (HSC software).
- [22] Russell, T. D. (1986). Vapor-phase composition above the cadmium iodide-sodium iodide and the thorium tetra-iodide-sodium iodide systems. *The Journal of Physical Chemistry*, 90(24), 6590-6594.
- [23] Allen, D. A., Howe, R. A., Wood, N. D., & Howells, W. S. (1991). Tetrahedral coordination of Zn ions in molten zinc halides. *The Journal of chemical physics*, 94(7), 5071-5076.
- [24] Zeidler, A., Chirawatkul, P., Salmon, P. S., Usuki, T., Kohara, S., Fischer, H. E., & Howells, W. S. (2015). Structure of the network glass-former ZnCl₂: From the boiling point to the glass. *Journal of Non-Crystalline Solids*, 407, 235-245.
- [25] Özen, A. S., Akdeniz, Z., Ruberto, R., Pastore, G., & Tosi, M. P. (2014). The origins of tetrahedral coordination in molten and glassy ZnCl₂ and other group-2B metal dihalides. *Physics Letters A*, 378(4), 431-433.
- [26] Glushko, V. P. (1994). Thermocenter of the Russian Academy of Sciences. *IVTAN Association, Izhorskaya*, 13(19), 127412.
- [27] Glushko Thermocenter of the Russian Academy of Sciences, *IVTAN Association, Izhorskaya* 13/19, 127412 Mos-cow, Russia, 1996 .
- [28] Landolt-Börnstein: *Thermodynamic Properties of Inorganic Material*,. *Sci Gr Thermodata Eur (SGTE)*, Berlin-Heidelberg, Springer-Verlag,. 1999 (HSC 6.0 software).
- [29] <http://zonvark.wustl.edu/geopig/index.html>, Everett Shock, Department of Earth and Planetary Sciences, Washington University, One Brookings Drive, St Louis MO, 63130-4899, <http://www.earthsci.unibe.ch/t>, <http://www.nmt.edu>.
- [30] Gurvich, L.V., Veitz, I.V., et al. *Thermodynamic Properties of Individual Substances*. Fourth edition in 5 volumes, Hemisphere Pub Co. NY, L., Vol 1 in 2 parts, 1989, etc. (= TSVI 82).
- [31] Oleksejuk, I. D., Dudchak, I. V., & Piskach, L. V. (2004). Phase equilibria in the Cu₂S-ZnS-SnS₂ system. *Journal of alloys and compounds*, 368(1), 135-143.
- [32] Schurr, R., Hölzing, A., Jost, S., Hock, R., Voß, T., Schulze, J., ... & Kötschau, I. (2009). The crystallisation of Cu₂ZnSnS₄ thin film solar cell absorbers from co-electroplated Cu-Zn-Sn precursors. *Thin Solid Films*, 517(7), 2465-2468.
- [33] Knacke O., Kubaschewski O., Hesselman K., *Thermochemical properties of inorganic substances*, 2nd ed., Springer-Verlag, Berlin, pp.1114-2412, 1991.
- [34] Fiechter, S., Martinez, M., Schmidt, G., Henrion, W., & Tomm, Y. (2003). Phase relations and optical properties of semiconducting ternary sulfides in the system Cu-Sn-S. *Journal of Physics and Chemistry of Solids*, 64(9), 1859-1862.
- [35] Altosaar, M., Jagomägi, A., Kauk, M., Krunks, M., Krustok, J., Mellikov, E., & Varema, T. (2003). Monograin layer solar cells. *Thin Solid Films*, 431, 466-469.
- [36] Timmo, K., Kauk-Kuusik, M., Altosaar, M., Raudoja, J., Raadik, T., Grossberg, M., & Mellikov, E. (2013, Septem-ber). Novel Cu₂CdSnS₄ and Cu₂ZnGeSe₄ absorber materials for monograin layer solar cell application. In *Proceed-ings of the 28th European Photovo.*

Article III

Nkwusi, G., Leinemann, I., Raudoja, J., Mikli, V., Kauk-Kuusik, M. Altsaar, M., Mellikov E. (2014). Synthesis of $\text{Cu}_2(\text{ZnCd})\text{SnS}_4$ Absorber Material for Monograin Membrane Applications.– [CD-ROM] *MRS Proceedings 2014: 2013 MRS Fall Meeting. SCHOLARONE Manuscripts, (Symposium W – Next-Generation Inorganic Thin-Film Photovoltaics)*, 1638.



Synthesis of Cu₂(ZnCd)SnS₄ Absorber Material for Monograin Membrane Applications

Journal:	2013 MRS Fall Meeting
Manuscript ID:	MRSF13-1638-W09-24.R2
Manuscript Type:	Symposium W
Date Submitted by the Author:	10-Feb-2014
Complete List of Authors:	Nkwusi, Godswill Leinemann, Inga; Tallinn University of Technology, Material Science Raudoja, Jaan; Tallinn University of Technology, Material Science Mikli, Valdek; Tallinn University of Technology, Material Science Kauk-Kuusik, Marit; Tallinn University of Technology, Material Science Altosaar, Mare; Tallinn University of Technology, Material Science Mellikov, Enn; Tallinn University of Technology, Material Science
Keywords:	crystal growth, flux growth, powder processing

Synthesis of $\text{Cu}_2(\text{ZnCd})\text{SnS}_4$ Absorber Material for Monograin Membrane Applications

Godswill Nkwusi¹, Inga Leinemann¹, Jaan Raudoja¹, Valdek Mikli¹, Marit Kauk-Kuusik¹ Mare
Altosaar¹, Enn Mellikov¹

Department of Materials Science, Tallinn University of Technology,
Ehitajate tee 5, 19086 Tallinn, Estonia

ABSTRACT

CZTS monograin powder samples were synthesized in CdI_2 as flux material. The obtained materials were analysed by EDX, SEM, and Raman methods. It was found that Cd from flux was incorporated into the formed compound leading to the formation of solid solution $\text{Cu}_2\text{Zn}_{1-x}\text{Cd}_x\text{SnS}_4$. The content of Cd in the compound was studied in the dependence of synthesis temperature and time. It was found that Cd content in the formed $\text{Cu}_2\text{Zn}_{1-x}\text{Cd}_x\text{SnS}_4$ did not depend on synthesis duration at constant temperature and increased with temperature. The activation energy of the Cd incorporation process was estimated as 17.5 ± 2 kJ/mol.

Keyword: CZTS, monograin powder, CdI_2 flux, Cd incorporation

INTRODUCTION

Kesterite structured $\text{Cu}_2\text{ZnSnS}_4$ (CZTS) as an absorber material for solar cell is a promising semiconductor for low-cost and sustainable energy production [1-5]. Thin film technology of quaternary CZTS solar cell has been widely studied over the last decade with the contribution of different authors aimed at understanding the best preparation conditions and to improve the solar cell efficiency, that is currently 11.1 % for $\text{Cu}_2\text{ZnSn}(\text{S}, \text{Se})_4$ synthesized in hydrazine [6]. Monograin technology has been developed as a possible alternative to thin film technology with current CZTS monograin layer (MGL) solar cell efficiency of over 8%. In the monograin technology, synthesis and isothermal recrystallization of polycrystalline powders in the presence of the liquid phase of a suitable solvent (flux) in sufficient amount, aids the formation of powders with single crystalline structure of powder grains [2].

CZTS in monograin form has been grown in different flux materials such as KI, NaI and CdI_2 [7-10]. Cadmium Iodide (CdI_2) had been used as a low temperature flux in our previous report [11]. It was confirmed that CZTS monograin powder can be grown in molten CdI_2 at lower temperatures relative to the melting temperature of KI [12]. According to *Klavina I, et al.*, it is known that during the synthesis of CZTS in CdI_2 as flux, Cd incorporates into the crystals of CZTS forming a solid solution of $\text{Cu}_2(\text{CdZn})\text{SnS}_4$. However, how to reach single phase absorber material in monograin powder form and how to avoid the formation of by-products was not discussed. Also, the incorporation of Cd from CdI_2 into CZTS crystals affects the properties of solar cell absorber materials. Therefore, the regularities and extent of Cd incorporation into CZTS have been studied in this report. The influence of synthesis temperature and time on the Cd incorporation into CZTS is reported. Finally, based on the obtained experimental data the activation energy of the Cd incorporation was determined.

EXPERIMENTAL DETAILS

Copper Zinc Tin Sulfide (CZTS) monograin powder was synthesised from precursors Cu_2S , SnS , ZnS and S in molten CdI_2 as flux material taken in mass ratio of CZTS/ CdI_2 equal to 1:1. The precursor binaries and CdI_2 were mixed by grinding in an agate mortar, degassed and encapsulated into quartz ampoules. The formation reaction of CZTS from precursors in liquid flux at high temperature was described in [11]. Samples were quenched rapidly to the room temperature in cold water. The formed powder particles were separated from flux material by washing with deionized water. The amount of Cd incorporated into CZTS was studied as depending on synthesis temperature and time: samples were heated for 15 hours at 280°C, 370°C, 500°C, 600°C, 700°C and 780°C and at 600°C for 6, 22, 32 and 60 hours. The ratios of metals in the mix of binary precursors was chosen as $[\text{Cu}]/([\text{Zn}]+[\text{Sn}]) = 0.92$ and $[\text{Zn}]/[\text{Sn}] = 1.03$, considering that the best solar cell efficiencies could be achieved with single phase CZTS without the presence of secondary phases in the range of compositions $[\text{Cu}]/([\text{Zn}]+[\text{Sn}])$ $0.82 \leq x \leq 0.93$ and $([\text{Zn}]/[\text{Sn}] \geq 1.03$ [13-15]. All compositional analyses were carried out using energy dispersive X-ray spectroscopy (EDS). Cd incorporated into the crystals was determined from polished crystals. The EDS analysis was made at least from 10 crystals of an analysed sample. The phases formed in the annealed samples were determined by the Raman spectra recorded using a Horiba LabRam HR high resolution spectrometer equipped with a multichannel CCD detection system in backscattering configuration. Incident laser light of 532 nm was focused on different $1 \mu\text{m}^2$ spots of the studied sample and an average of five readings were taken for every sample to obtain an average result of the sample.

RESULTS AND DISCUSSION

Temperature dependence

At 280°C, much below the melting point of CdI_2 , the formation of quaternary compound was not detected. As the temperature increases up to 370°C, just below the melting temperature of pure CdI_2 , the formation of CZTS begins. At this temperature the Raman spectra confirm the presence of different secondary phases coexisting with CZTS as it was shown already in [11]. Cd concentration in CZTS crystals grown in CdI_2 at different temperatures is presented in Figure 1. With increasing annealing temperature, Cd content in formed CZTS increases reaching the maximum average value 2.75 at% at 780°C.

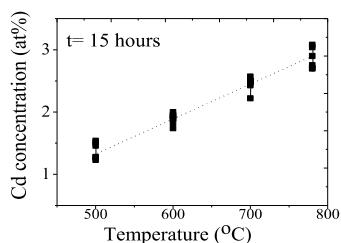


Figure 1. Cd content incorporated into CZTS from CdI₂ flux as a function of heating temperature.

Time dependence

Cd concentration in CZTS grown at 600 °C for different annealing times is presented in Figure 2. It is obvious that annealing for 6 hours leads to the large dispersion in measurement data attributable to the non-equilibrium status of the system. After heating for 22 hours the Cd concentration in grown CZTS crystals reaches the equilibrium concentration at 600 °C.

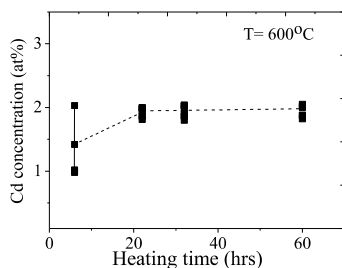


Figure 2: Time dependency of Cd incorporation into CZTS from CdI₂ flux.

Figure 3 shows the SEM images of samples synthesized at 600°C for different times starting from 6 hours up to 60 hours. It is obvious that as the synthesis time increases, the grain size increases. At the same time there is no remarkable changes in the morphology of crystals.

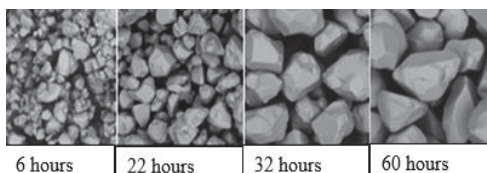


Figure 3: SEM images of powder samples synthesized at 600 °C for different synthesis time: 6 hours; 22 hours; 32 hours and 60 hours.

Phase Composition

In Figure 4a and 4b, Raman spectra of the various powder samples are presented. The spectra are very similar to each other and no other peaks than those belonging to CZTS can be recognized. The most intense Raman peak of pure CZTS is at 338 cm⁻¹ [2, 11]. It is seen that this Raman peak in our samples is shifted to lower values. In the Raman spectrum of pure Cu₂CdSnS₄ the most intense Raman peak is at 332 cm⁻¹ [17]. The shift in Raman spectra is the sign that solid solution of Cu₂Zn_{1-x}Cd_xSnS₄ is formed in our powder samples.

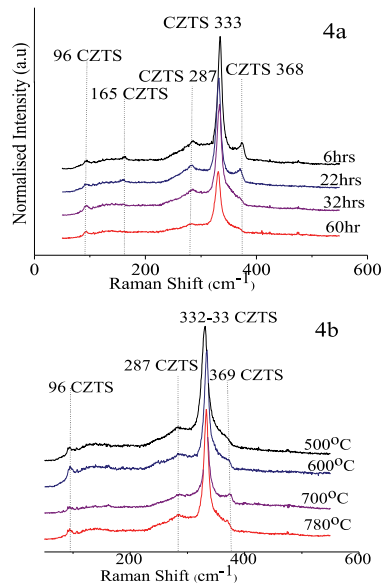


Figure 4: Raman spectra of samples with different preparation conditions; (4a) Raman spectra of samples synthesized at 600°C for different times (4b) Raman spectra of samples synthesized for 15 hours at different temperatures.

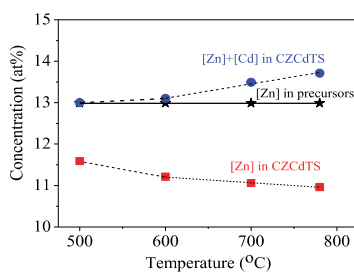


Figure 5: Variation of Zn concentration in the $\text{Cu}_2\text{Zn}_{1-x}\text{Cd}_x\text{SnS}_4$ powders synthesized in CdI_2 at different temperatures.

In Figure 5, the changes of Zn concentration in powders grown at different temperatures are presented. It can be seen that [Zn] in the CZTS powders is reduced if compared with the Zn content in precursors and it decreases with temperature and with increasing Cd content, which can be attributed to the replacement of Zn by Cd. In addition, the sum of Zn and Cd contents also increases with increasing temperature. The ratio of [Zn]/[Sn] decreases while the ratio [Cu]/[Sn] increases due to the decrease in [Zn] in the final powder. It was confirmed by our group that the

syntheses of $\text{Cu}_2\text{Zn}_{1-x}\text{Cd}_x\text{SnS}_4$ solid solutions in potassium iodide using CdS as Cd source could increase the level of incorporation of Cd into CZTS depends only on the initial $[\text{Cu}]/[\text{Sn}]$ ratio and not on the $[\text{Zn}]/[\text{Sn}]$ ratio [14]. It was also suggested that the decrease in Cu content in the precursors should lead to an increase in the substitution of Zn atoms by Cd atoms [14], therefore a decrease in $[\text{Zn}]$ can be attributed to the atomic substitution of Cd at Zn site from CdI_2 . The single phase solid solution of $\text{Cu}_2\text{Zn}_{1-x}\text{Cd}_x\text{SnS}_4$ forms starting from 500°C. As the direct exchange reaction between ZnS and CdI_2 resulting in the formation of CdS and ZnI_2 is thermodynamically impossible, then the formation of solid solution $\text{Cu}_2\text{Zn}_{1-x}\text{Cd}_x\text{SnS}_4$, (Cd incorporation at the Zn site) can take place due to some fragmentation of CdI_2 dimeric molecules (Cd_2I_4) in its liquid or gaseous phase resulting in the release of CdI_2^+ and Cd_2I_3^+ ions, as it was shown for CdI_2 gaseous phase in [16]. Now the reaction $x\text{CdI}_2^+ + x\text{e}^- + \text{ZnS} = \text{Zn}_{1-x}\text{Cd}_x\text{S} + \text{ZnI}_2$ is possible. In the next step $\text{Zn}_{1-x}\text{Cd}_x\text{Se}$ reacting with Cu_2SnS_3 results in the formation of $\text{Cu}_2\text{Zn}_{1-x}\text{Cd}_x\text{SnS}_4$ [11].

Activation energy of the process

In Figure 5 the Arrhenius plot of Cd concentration in formed $\text{Cu}_2\text{Zn}_{1-x}\text{Cd}_x\text{SnS}_4$ is shown. The formation of solid solution of $\text{Cu}_2\text{Zn}_{1-x}\text{Cd}_x\text{SnS}_4$ was reported earlier in [11] and confirmed in the present study. By our considerations the only possible route for Cd incorporation is through the CZTS formation reaction in participation of more electronegative CdI_2^+ . The latter was found in the gaseous phase of CdI_2 by the mass spectrometric investigations with modified Knudsen cell–mass spectrometer by W. Kuncewicz-Kupczyk et al [16]. In their work, they confirmed the presence of CdI_2^+ , Cd^+ and I^- formed as fragment ions in the gaseous phase of $\text{CdI}_2(\text{g})$ consisting mainly of monomers $\text{CdI}_2(\text{g})$ and dimers $\text{Cd}_2\text{I}_4(\text{g})$ at 534 to 613 K.

The overall activation energy of the process estimated from the Arrhenius plot (see Figure 5) is 17.5 ± 2 kJ/mol.

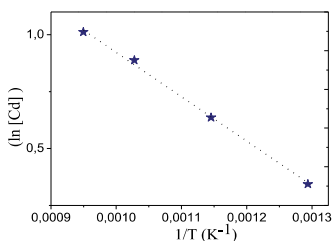


Figure 5: Arrhenius plot of $[\text{Cd}]$ in $\text{Cu}_2\text{Zn}_{1-x}\text{Cd}_x\text{SnS}_4$ powders grown in CdI_2 .

CONCLUSIONS

It was shown that in the synthesis process of CZTS in CdI_2 flux the amount of Cd, incorporated into CZTS from CdI_2 and resulting in the formation of solid solution of $\text{Cu}_2\text{Zn}_{1-x}\text{Cd}_x\text{SnS}_4$, changes from 1.3 at% at 500 °C to 2.75 at % at 780 °C. We found that Cd concentration in the formed $\text{Cu}_2\text{Zn}_{1-x}\text{Cd}_x\text{SnS}_4$ did not depend on synthesis time after reaching the equilibrium state at constant temperature and it increased with temperature. The activation energy of the Cd incorporation process was estimated as 17.5 ± 2 kJ/mol. Finally, it was found that the incorporation of Cd took place at the Zn site and depended on the Cu/Sn ratio and not on

the Zn/Sn ratio. Therefore a decrease of Cu content in the precursors would lead to an increase in the amount of Cd incorporated into $\text{Cu}_2\text{Zn}_{1-x}\text{Cd}_x\text{S}_4$ solid solution. The route of Cd incorporation into CZTS from CdI_2 was described as a CZTS formation process in participation of CdI_2^+ formed in molten phase of cadmium iodide due to the fragmentation of cadmium iodide molecules.

ACKNOWLEDGMENTS

This research was supported by the Doctoral Studies and Internationalization Program DoRa of the European Social Funds, Estonian Science Foundation grants G8964 and G9346, Project TK117 Estonian Centre of Excellence in Research, National R&D programs AR10128 and AR12128, the Estonian Ministry of Education and Research Contract No. SF0140099s08.

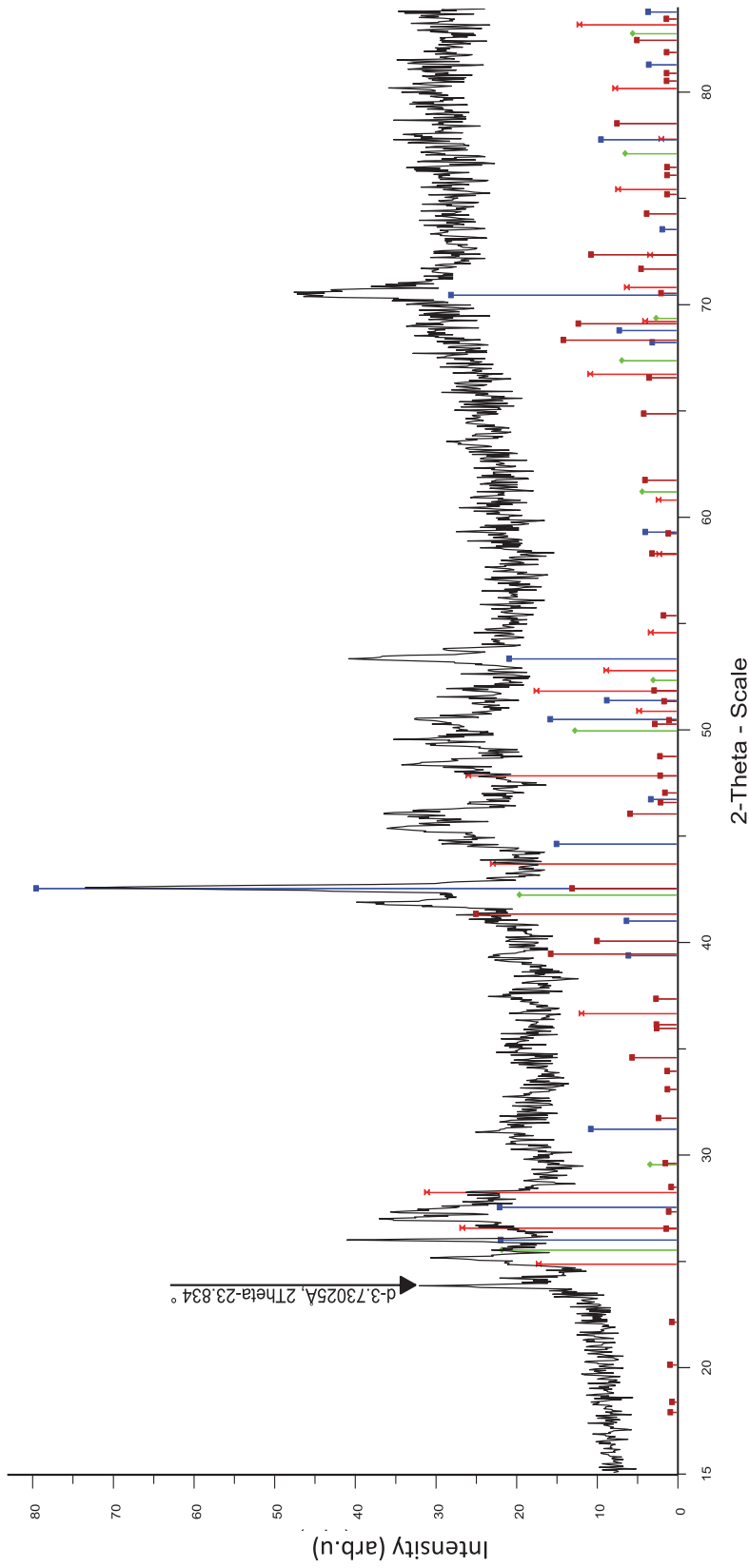
REFERENCES

- [1] A. Nagoya, R. Asahi, R. Wahl, and G. Kresse, " *Phys. Rev. B*, vol. 81, no. 11, p. 113-202, Mar. 2010.
- [2] M. Altosaar, J. Raudoja, K. Timmo, M. Danilson, M. Grossberg, J. Krustok, and E. Mellikov, *physica status solidi*, vol. 205, no. 1, pp. 167–170, Jan. 2008.
- [3] K. S. Seol, S.-Y. Lee, J.-C. Lee, H.-D. Nam, "Sol. Energy Mater. vol. 75, no. 155, p. 2003.
- [4] T. Maeda, S. Nakamura, and T. Wada, *Jpn. J. Appl. Phys.*, vol. 50, no. 4, p. 04, DP07, Apr. 2011.
- [5] A Nagoya, R Asahi and G Kresse, *J. Phys: Condens. Matter* 23 404203, 2011
- [6] K. Todorov, J. Tang, S. Bag, O. Gunawan, T. Gokmen, Y. Zhu, *Adv. Energy Mater.*, no. doi:10.1002/aenm.2012,00348.
- [7] I. Leinemann, J. Raudoja, M. Grossberg, M. Altosaar, D. Meissner, R. Traksmaa, and T. Kaljuvee, Conference of Young Scientists on Energy Issues, P.1 – 8, 1822-7554, 2011.
- [8] I. Klavina, T. Kaljuvee, K. Timmo, J. Raudoja, R. Traksmaa, M. Altosaar, Thin Solid Films," vol. Vol. 519,, no. p. 7399–7402.
- [9] E. Mellikov, J. Hiie, and M. Altosaar, *Int. J. Mater. Prod. Technol.*, vol. 28, no. 3/4, p. 291, 2007.
- [10] I. Klavina, J. Raudoja, M. Altosaar, E. Mellikov, D. Meissner, and T. Kaljuvee, Conf. of Young Scientists on Energy Issues Kaunas, Lithuania, P.VII 345 - VII 353, May 27-28, 2010.
- [11] G. Nkwusi, I. Leinemann, J. Raudoja, M. Grossberg, M. Altosaar, D. Meissner, R. Traksmaa, and T. Kaljuvee, Conf. of Young Scientists on Energy Issues, Kaunas, Vol. 2, P.II 38 - II 46, 1822-7554, May 24-25, 2012.
- [12] P. Patnaik, Handbook of Inorganic Chemicals, P. 150, 761, 0-07-049439-8, 2002
- [13] S. Chen, X. G. Gong, A. Walsh, and S.-H. Wei, *Appl. Phys. Lett.*, vol. 96, no. 2, p. 021902, 2010.
- [14] Pilvet M, Kauk-Kuusik M, Altosaar M, et al. *Thin Solid Films*. 2015;582:180-.
- [15] I. D. Olekseyuk, I. V. Dudchak, "," *J. Alloy. Compd.*, vol. Vol. 368., pp. 135–143, 2004.
- [16] W. Kunczewicz-Kupczyk, J. Kapała, S. Roszak, and M. Miller, *J. Chem. Phys.*, vol. 108, no. 18, p. 7743, 1998.
- [17] K. Timmo et al, unpublished work, Tallinn University of technology, 2013.

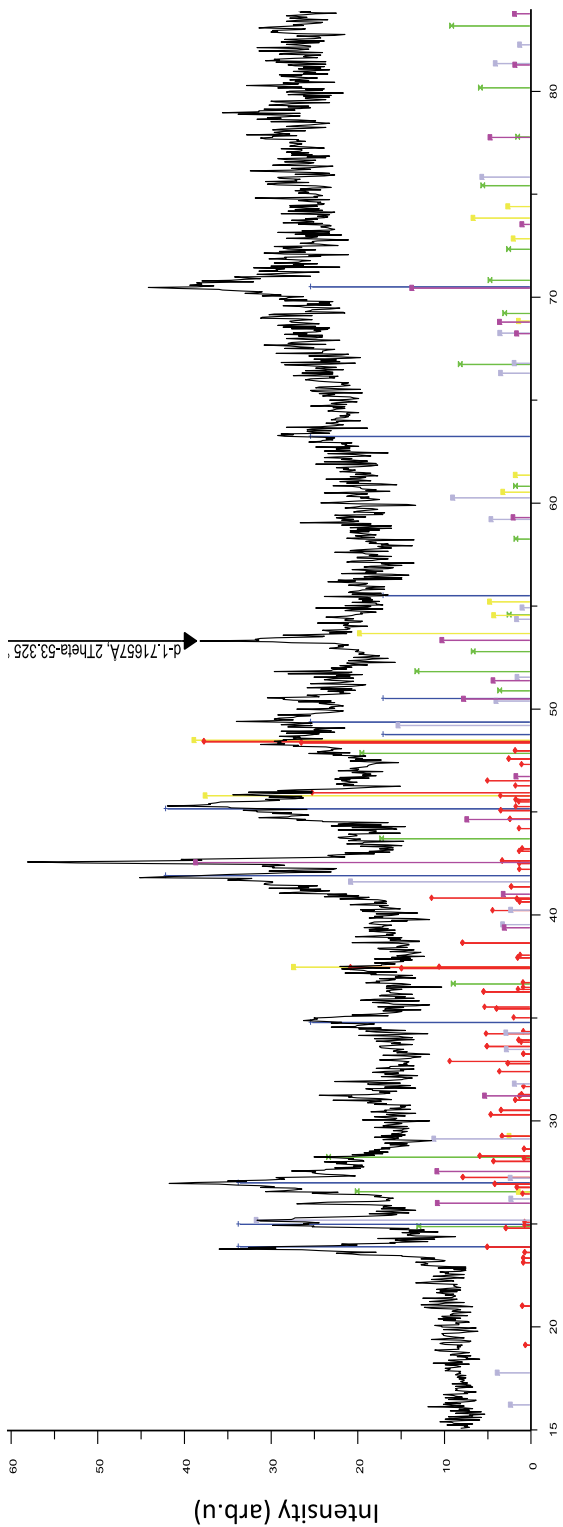
Appendix B

XRD pattern of studied mixtures: $\text{Cu}_2\text{S} + \text{CdI}_2$, $\text{SnS} + \text{CdI}_2$, $\text{ZnS} + \text{CdI}_2$,
($\text{Cu}_2\text{S} + \text{SnS} + \text{S} + \text{CdI}_2$), ($\text{Cu}_2\text{S} + \text{SnS} + \text{ZnS} + \text{S} + \text{CdI}_2$).

Cu₂S+CdI₂ -330°C

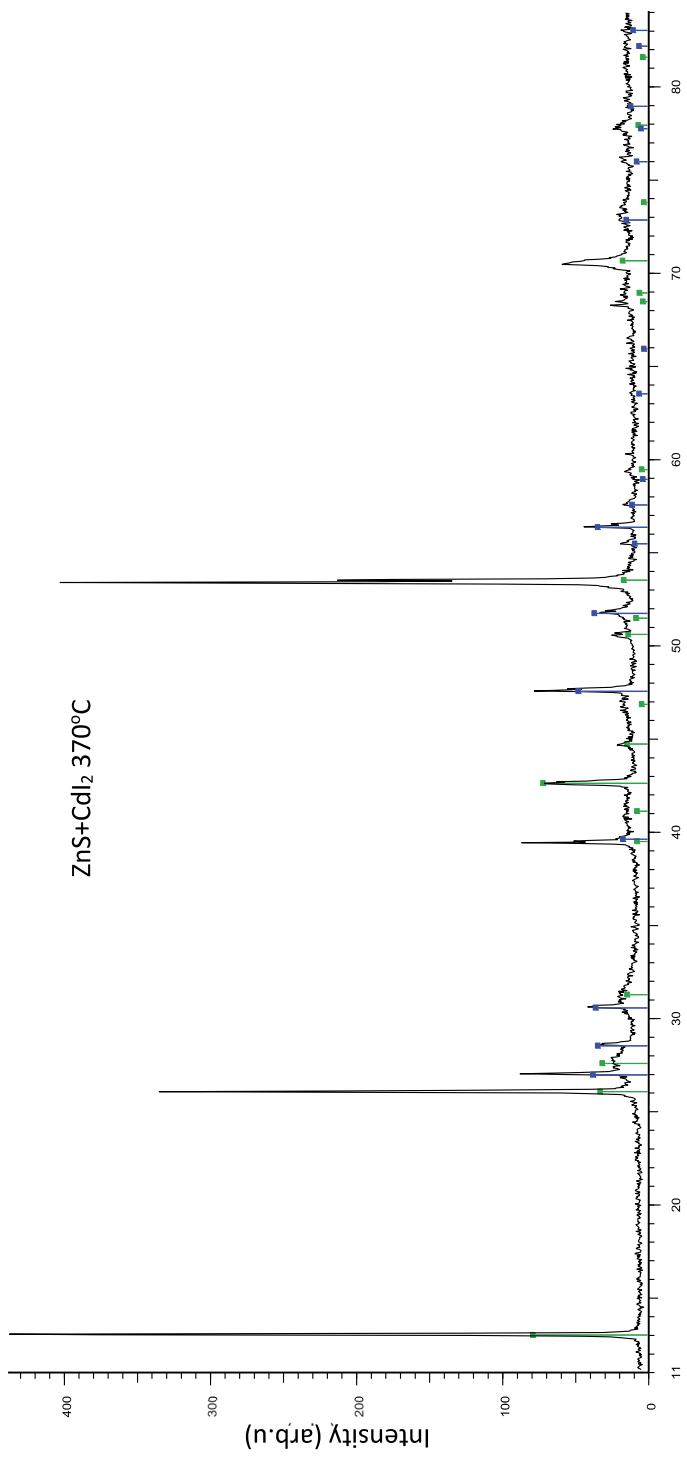


Cu₂S+CdI₂-353°C

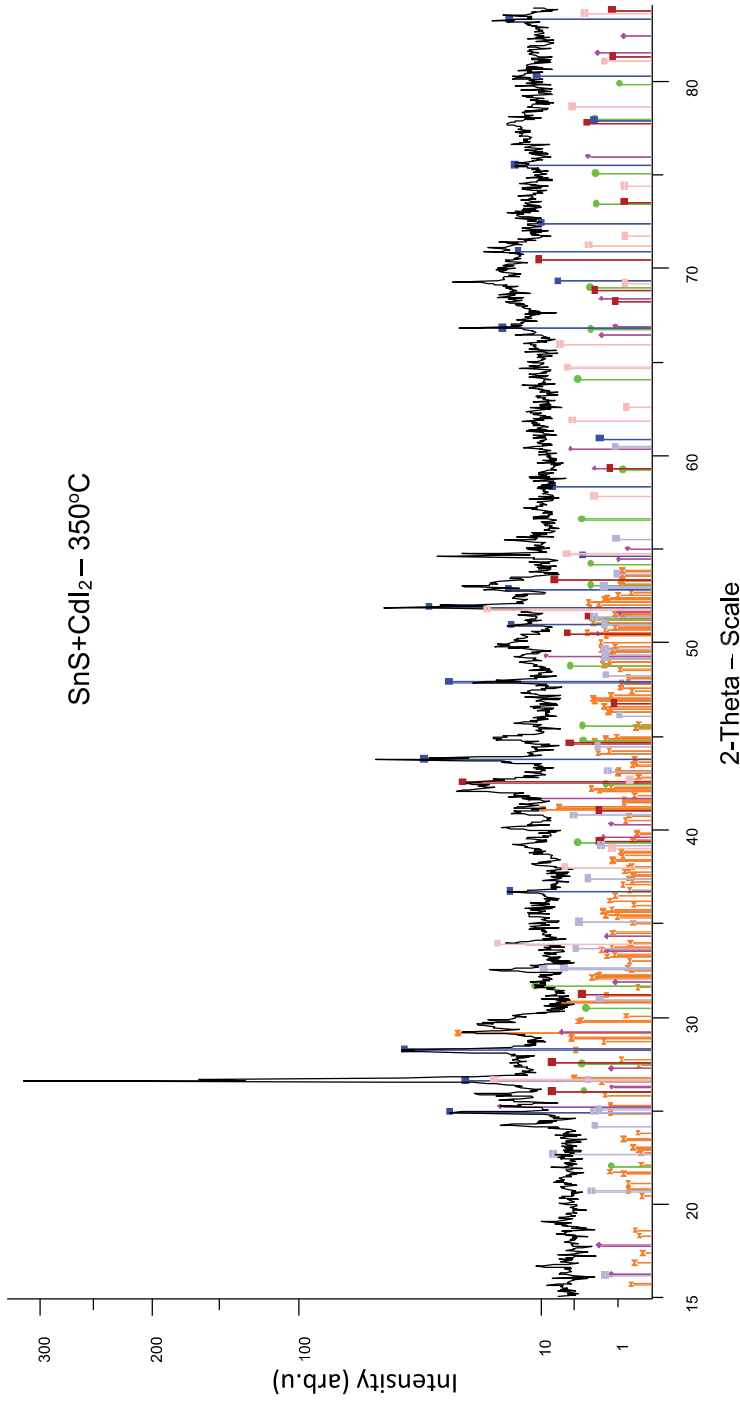


2-Theta - Scale

- File: Cu₂S+CdI₂-5,raw - Start: 15,000 ° - End: 84,000 ° - Step: 0,040 ° - Step time: 5, s - Creation: 31.01.2012 14:53:58 -
- 00-0033-0239 (1) - Cadmium Iodide - CdI₂ - Hexagonal - a 4,24810 - b 4,24810 - c 13,72650 - alpha 90,000 - beta 90,000 - gamma 120,000 - Primitive - P63mc (186) - 2 - 214,526 - I/c PDF 1. - S-Q 18,2 % - F30= 25(0)
- 00-041-1049 (1) - Greenockite, syn - CdS - Hexagonal - a 4,14092 - b 4,14092 - c 6,71980 - alpha 90,000 - beta 90,000 - gamma 120,000 - Primitive - P63mc (186) - 2 - 98,7885 - I/c PDF 1. - S-Q 10,9 % - F30= 317(0)
- 00-049-0660 (N) - Copper Sulfide-2 - Cu₂CS₂S - Hexagonal - a 3,06914 - b 4,30070 - c 7,14723 - alpha 90,000 - beta 90,000 - gamma 120,000 - Primitive - P63mc (186) - 2 - 11,6393 - I/c PDF 1 - S-Q 13,1 % - F30= 25(0)
- 00-028-0490 (1) - Chalcocite, syn - Cu₂S - Monoclinic - a 15,23500 - b 11,88500 - c 13,45600 - alpha 90,000 - beta 90,000 - gamma 120,000 - Primitive - P21/c (14) - 48 - 2191,49 - I/c PDF 1. - S-Q 17,8 % - F30= 17(0)



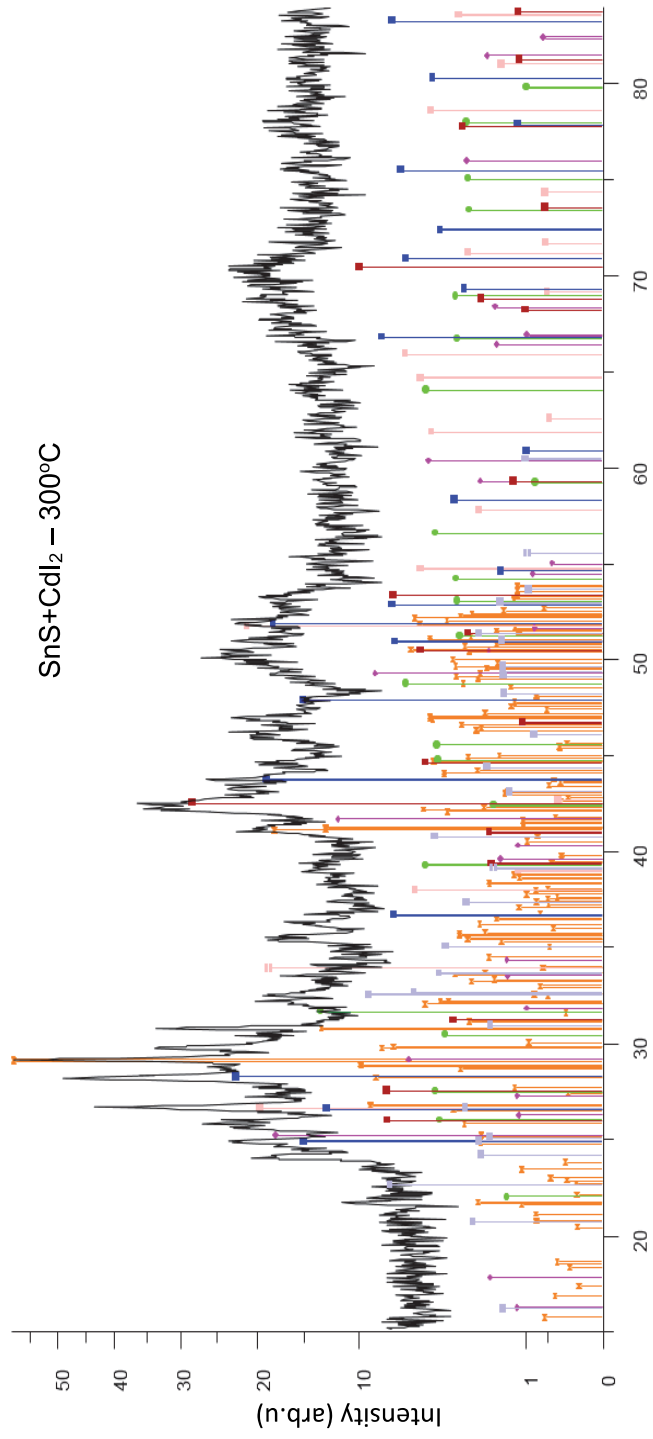
▲ File: ZnS-CdI2 - Q370°C.raw - Start: 11.078 ° - End: 84.058 ° - Step: 0.040 ° - Step time: 5. s - Creation: 27.02.2012 17:14:01 -
■ 00-033-0239 () - Cadmium Iodide - CdI₂ - Hexagonal - a 4.23925 - b 4.23925 - c 13.68074 - alpha 90.000 - beta 90.000 - gamma 120.000 - Primitive - P63mc (186) - 2 - 212.S21 - JIC PDF 1. - S-Q 62.7 % - F30= 25(0)
■ 00-005-0492 (A) - Wurtzite-2H, syn - ZnS - Hexagonal - a 3.82000 - b 3.82000 - c 6.26000 - alpha 90.000 - beta 90.000 - gamma 120.000 - Primitive - P63mc (186) - 2 - 79.1101 - JIC PDF 1. - S-Q 37.3 % - F30= 28(0)



SnS+CdI₂ — 350°C

- File: SnS+CdI2 (Cooled down to 350°C).raw - Start: 15.020 ° - End: 84.015 ° - Step: 0.040 ° - Step time: 5. s - Creation: 19.01.2012 14:31:37 -
- 04-012-7383 (A) - Tin Iodide Sulfide - Sn₂S₂I₂ - Orthorhombic - a 17.44700 - b 25.33400 - c 4.39100 - alpha 90.000 - beta 90.000 - gamma 90.000 - Primitive - Pnam (62) - 12 - 1940,83 - I/lc PDF 7.2 - S-Q 3.2 % -
 - 00-006-0232 (*) - Tin Iodide - SnI₄ - Cubic - a 12.25254 - b 12.25254 - c 12.25254 - alpha 90.000 - beta 90.000 - gamma 90.000 - Primitive - Pa-3 (205) - 8 - 1839,41 - I/lc PDF 1 - S-Q 13.8 % - F27= 21(0.0116,11
 - 00-001-0984 (A) - Herzenbergite, syn. - SnS - Orthorhombic - a 3.99000 - b 4.34000 - c 11.20000 - alpha 90.000 - beta 90.000 - gamma 90.000 - Primitive - Pmcn (62) - 4 - 193,946 - I/lc PDF 1 - S-Q 8.2 % - F22=
 - 00-006-0314 (A) - Greenockite, syn. - CdS - Hexagonal - a 4.13600 - b 4.13600 - c 6.71300 - alpha 90.000 - beta 90.000 - gamma 120.000 - Primitive - P63mc (186) - 2 - 96,4508 - I/lc PDF 1 - S-Q 37.5
 - 00-033-0239 (*) - Cadmium Iodide - CdI₂ - Hexagonal - a 4.24810 - b 4.24810 - c 13.72690 - alpha 90.000 - beta 90.000 - gamma 120.000 - Primitive - P63mc (186) - 2 - 214,526 - I/lc PDF 1 - S-Q 21.8 % - F30=

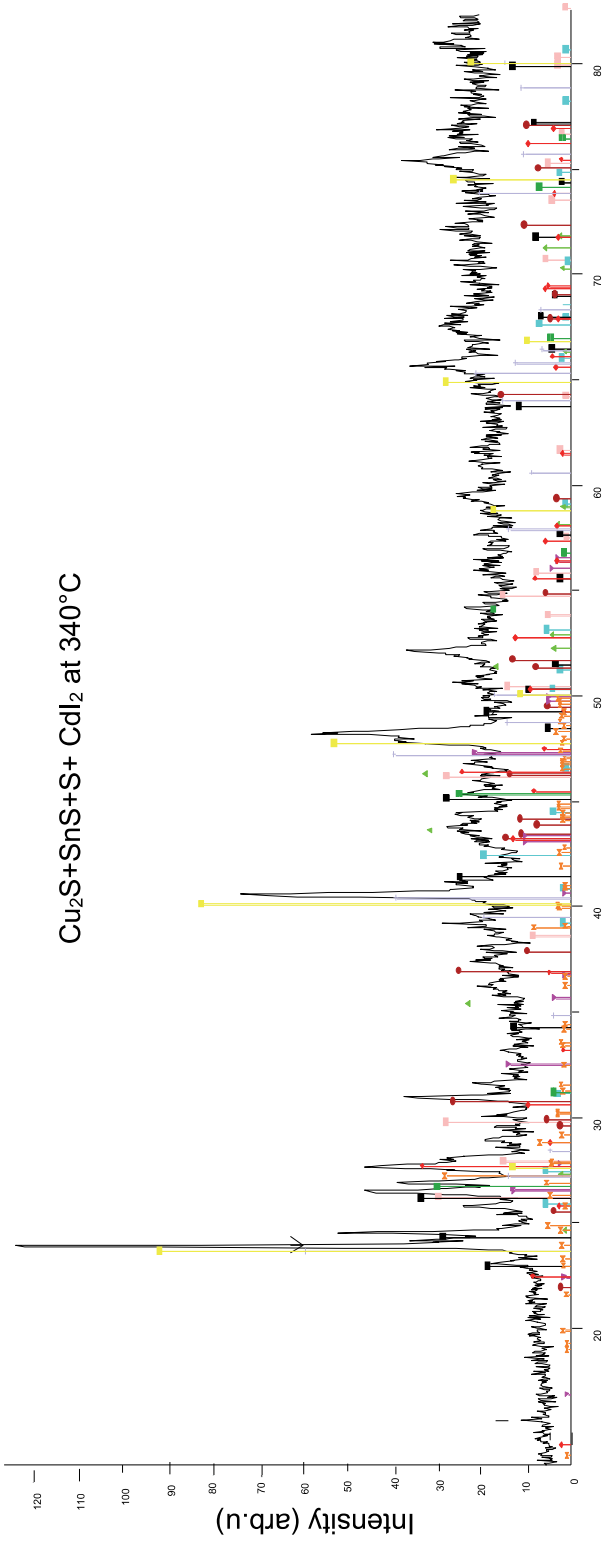
SnS+CdI₂ – 300°C



2-Theta - Scale

- File: SnS+CdI2 (cooled down to 300°C).raw - Start: 15.061° - End: 84.046° - Step: 0.040° - Step time: 5 s - Creation: 20.01.2012 13:23:54.
- 04-012-7393 (A) - Tin Iodide Sulfide - Sn2S3I2 - Orthorhombic - a 17.44700 - b 25.32400 - c 4.39100 - alpha 90.000 - beta 90.000 - gamma 90.000 - Primitive - Pnmm (62) - 12 - 1940 83 - Ilic PDF 7.2 - S-Q 7.4 % -
- 00-006-0232 (Y) - Tin Iodide - SnI4 - Cubic - a 12.25254 - b 12.25254 - c 12.25254 - alpha 90.000 - beta 90.000 - gamma 90.000 - Primitive - Pa-3 (205) - 8 - 1639 41 - Ilic PDF 1 - S-Q 16.2 % - FZ7= 21(0.0116, 11
- 00-001-0984 (A) - Heizenbergite - syn - Sns - Orthorhombic - a 3.9900 - b 4.3400 - c 11.2000 - alpha 90.000 - beta 90.000 - gamma 90.000 - Primitive - Pnch(G2) - 4 - 193 946 - Ilic PDF 1 - S-Q 12.0 % - FZ2
- 00-006-0314 (A) - Greenockite - syn - Cds - Hexagonal - a 4.13600 - b 4.13600 - c 6.71300 - alpha 90.000 - beta 90.000 - gamma 120.000 - Primitive - P63mc (186) - 2 - 99 4508 - Ilic PDF 1 - S-Q 20.4 % - F30=7
- 00-033-0239 (Y) - Cadmium Iodide - CdI2 - Hexagonal - a 4.24810 - b 4.24810 - c 13.72650 - alpha 90.000 - beta 90.000 - gamma 120.000 - Primitive - P63mc (186) - 2 - 214 526 - Ilic PDF 1 - S-Q 25.6 % - F30=

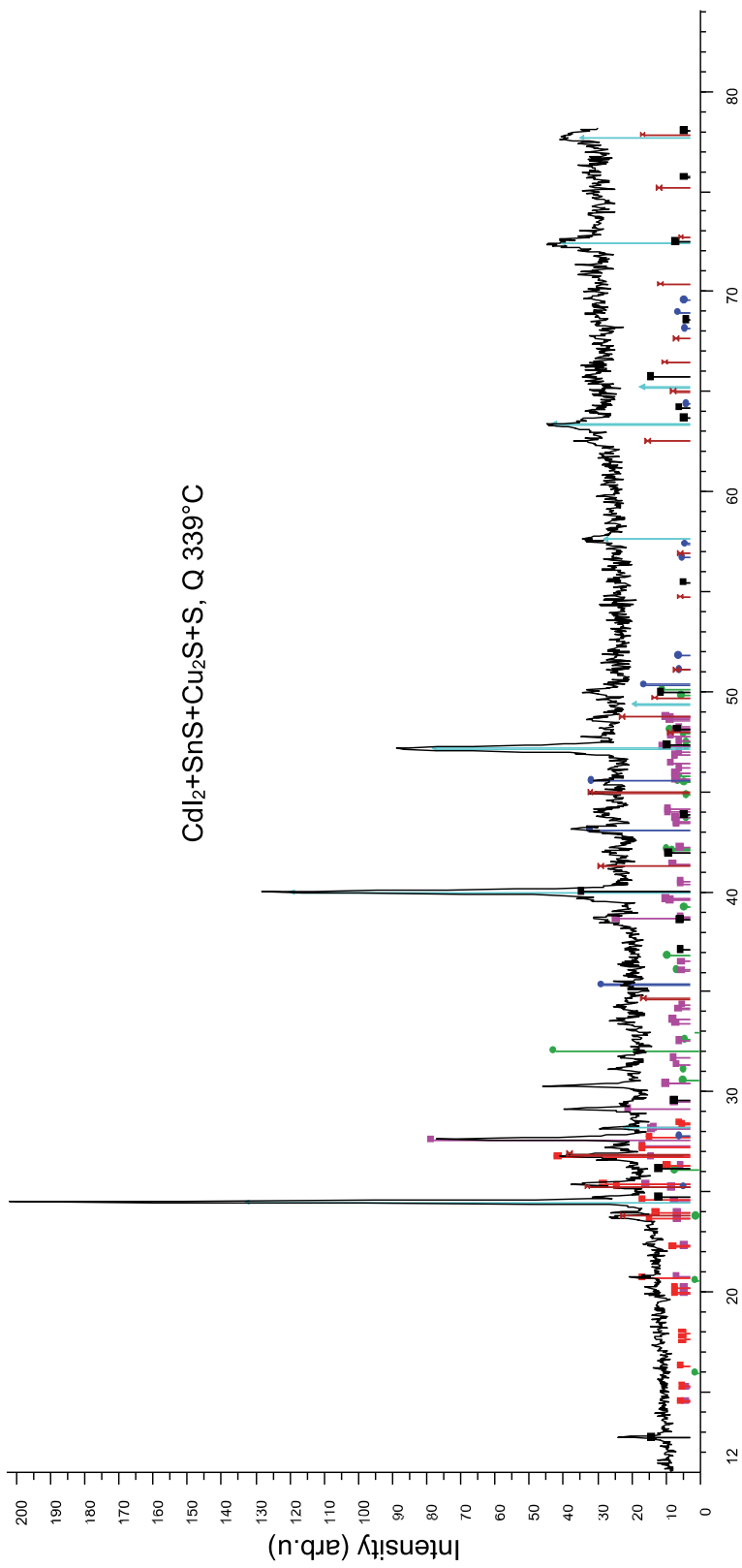
Cu₂S+SnS+S+ CdI₂ at 340 °C



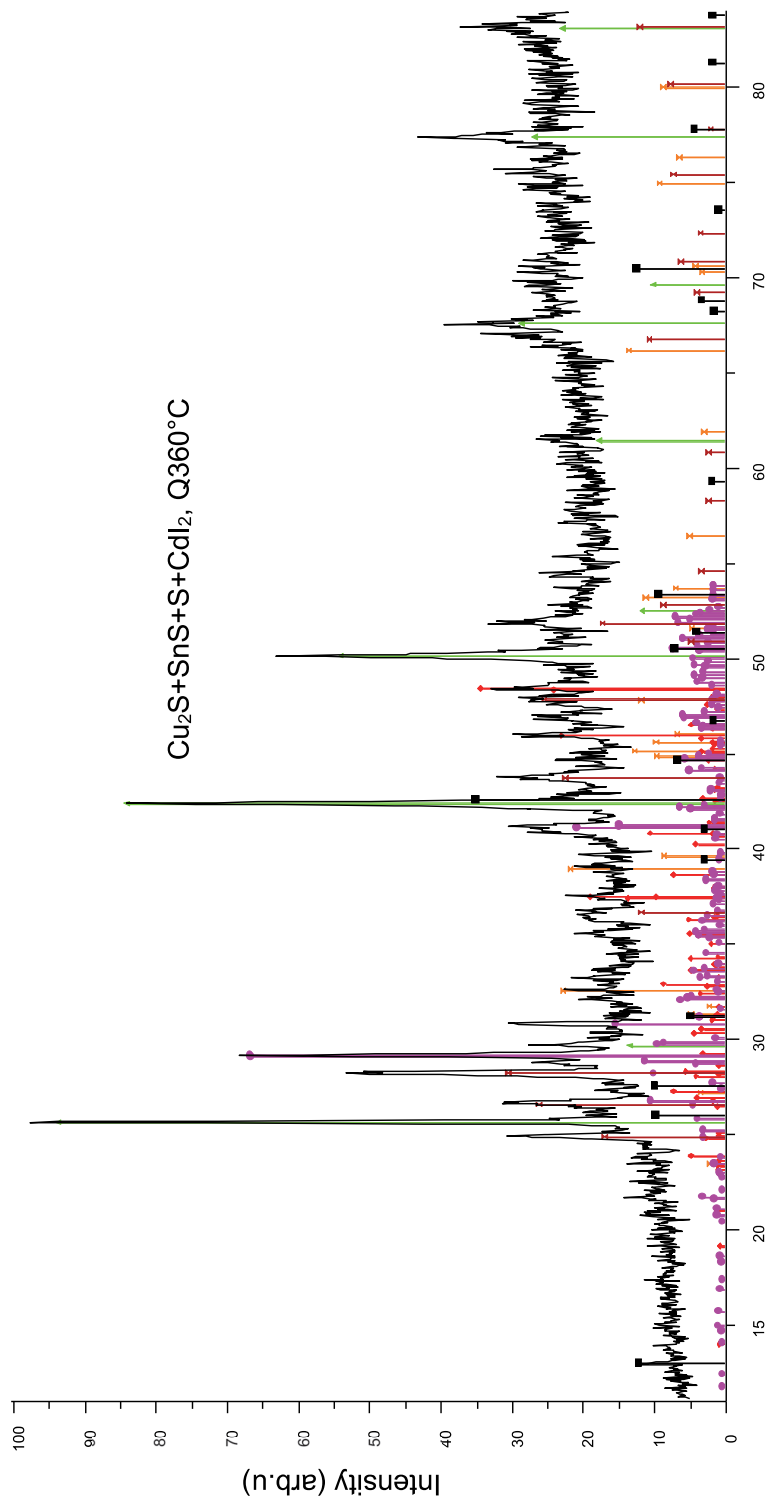
2-Theta – Scale

- File: Cu2S+SnS+S+CdI2 - (Cooled down to 340°C).raw - Start: 15.110 ° - End: 84.082 ° - Step time: 5. s - Creation: 23.02.2012 14:27:52
- 00-041-1049 (*) - Greenockite, syn - CdS - Hexagonal - a 4.11849 - b 4.11849 - c 6.71960 - alpha 90.000 - beta 90.000 - gamma 120.000 - Primitive - P63mc (186) - 2 - 98.7104 - I/lc PDF 1. - S-Q 10.9 % - F30=317(0).
- 00-033-0239 (*) - Cadmium Iodide - CdI2 - Hexagonal - a 4.24810 - b 4.24810 - c 13.72650 - alpha 90.000 - beta 90.000 - gamma 120.000 - Primitive - P63mc (186) - 2 - 214.526 - I/lc PDF 1. - S-Q 21.8 % - F30=
- 00-029-0578 (U) - Chalcocite-Q, syn - Cu1.96S - Tetragonal - a 4.04002 - b 4.04002 - c 11.28700 - alpha 90.000 - beta 90.000 - gamma 90.000 - beta 90.000 - gamma 120.000 - Primitive - P13212 (96) - 4 - 184.224 - I/lc PDF 1. - S-Q 10.0 % - F24=
- 00-026-1116 (C) - Copper Sulfide - Cu2S - Hexagonal - a 3.95110 - b 3.95110 - c 6.71920 - alpha 90.000 - beta 90.000 - gamma 120.000 - Primitive - P63/mmc (194) - 2 - 90.8415 - I/lc PDF 1. - S-Q 9.2 % - F20=305(
- 00-027-0198 (I) - Mohite, syn - Cu2SnS3 - Triclinic - a 6.64000 - b 11.51000 - c 19.93000 - alpha 90.000 - beta 109.750 - gamma 90.000 - Primitive - P1 (1) - 12 - 1433.58 - I/lc PDF 1. - S-Q 17.0 % - F27= 1(0)0616,4
- 00-036-0053 (I) - Copper Tin Sulfide - Cu4SnS6 - Rhombo. - a 3.74300 - b 3.74300 - c 32.99200 - alpha 90.000 - beta 90.000 - gamma 120.000 - Primitive - P63/mmc (194) - 2 - 90.8415 - I/lc PDF 1. - S-Q 9.2 % - F20=305(
- 00-006-0246 (*) - Marssite, syn - CuI - Cubic - a 6.01066 - b 6.01066 - c 6.01066 - alpha 90.000 - beta 90.000 - gamma 90.000 - Face-centered - F43m (216) - 4 - 217.153 - I/lc PDF 1. - S-Q 41.0 % - F20=124(0)0665.
- 00-027-0896 (I) - Tin Iodide Sulfide - SnI2S2 - Orthorhombic - a 17.42240 - b 25.34520 - c 4.34587 - alpha 90.000 - beta 90.000 - gamma 90.000 - Primitive - Pnam (62) - 12 - 1919.02 - I/lc PDF 1. - S-Q 12.1 % - F21=

Cd₁₂+SnS+Cu₂S+S, Q 339°C

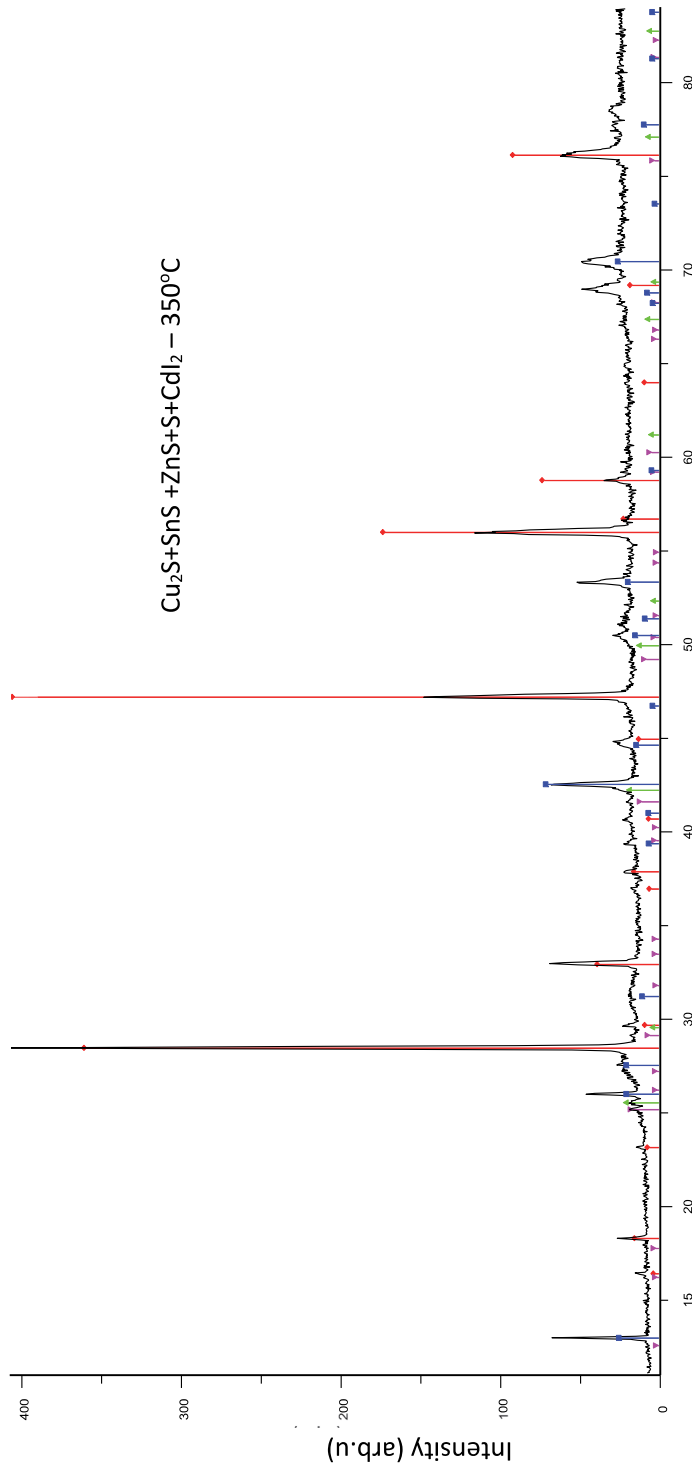


- File: Cd12+SnS+Cu2S+S - Q339°C.raw - Start: 11.045 ° - End: 84.034 ° - Step: 0.040 ° - Step time: 5. s - Creation: 23.02.2012 14:27:52 -
- 00-053-0526 (I) - Tin Sulfide - SnS - Orthorhombic - a 3.96030 - b 4.33120 - c 11.18020 - alpha 90.000 - beta 90.000 - gamma 90.000 - Primitive - Pcrmm (53) - 4 - 192.741 - Ilc PDF 1. - S-Q 13.3 % - F24= 40(0.0224,2
- 00-029-0578 (I) - Chalcocite-Q. syn - Cu1.96S - Tetragonal - a 4.04002 - b 4.04002 - c 11.28700 - alpha 90.000 - beta 90.000 - gamma 90.000 - gamma 90.000 - Primitive - P43212 (96) - 4 - 184.224 - Ilc PDF 1. - S-Q 10.0 % - F24=
- 00-027-0198 (I) - Mohite, syn - Cu2SnS3 - Triclinic - a 6.64000 - b 11.51000 - c 19.93000 - alpha 90.000 - beta 109.750 - gamma 90.000 - Primitive - P1 (1) - 12 - 1433.56 - Ilc PDF 1. - S-Q 17.0 % - F27= 1(0.0616,4
- 00-006-0246 (Y) - Marasite, syn - CuI - Cubic - a 6.01066 - b 6.01066 - c 6.01066 - alpha 90.000 - beta 90.000 - gamma 90.000 - Face-centered - F-43m (216) - 4 - 217.163 - Ilc PDF 1. - S-Q 41.0 % - F20=124(0.0085,
- 00-026-1116 (C) - Copper Sulfide - Cu2S - Hexagonal - a 3.95110 - b 3.95110 - c 6.71920 - alpha 90.000 - beta 90.000 - gamma 120.000 - Primitive - P63/mmc (194) - 2 - 90.8415 - Ilc PDF 1. - S-Q 9.2 % - F20=305(
- 00-041-1049 (Y) - Greenockite, syn - CdS - Hexagonal - a 4.11849 - b 4.11849 - c 6.71980 - alpha 90.000 - beta 90.000 - gamma 120.000 - Primitive - P63mc (186) - 2 - 98.7104 - Ilc PDF 1. - S-Q 10.9 % - F30=317(0,
- 00-033-0239 (Y) - Cadmium Iodide - CdI2 - Hexagonal - a 4.24810 - b 4.24810 - c 13.72850 - alpha 90.000 - beta 90.000 - gamma 120.000 - Primitive - P63mc (186) - 2 - 214.526 - Ilc PDF 1. - S-Q 10.0 % - F30= 25(0



- File: Cu2S+SnS+S+CdI2 - Q360°C.raw - Start: 11.063 ° - End: 84.047 ° - Step: 0.040 ° - Slip time: 5. s - Creation: 21.02.2012 17:39:31 - 270°C - 1
- 00-033-0239 (*) - Cadmium Iodide - CdI2 - Hexagonal - a 4.24810 - b 4.24810 - c 13.72650 - alpha 90.000 - beta 90.000 - gamma 120.000 - Primitive - P63mc (186) - 2 - 214.526 - I/IC PDF 1 - S-Q 15.5 % - F30= 250
 - 00-029-0578 (I) - Chalcocite-Cu, syn - Cu1.96S - Tetragonal - a 4.04002 - b 4.04002 - c 11.28700 - alpha 90.000 - beta 90.000 - gamma 90.000 - Primitive - P43212 (96) - 4 - 184.224 - I/IC PDF 1 - S-Q 10.0 % - F24=
 - 00-033-0490 (I) - Chalcocite-M - Cu2S - Monoclinic - a 15.23500 - b 11.88500 - c 13.49600 - alpha 90.000 - beta 116.260 - gamma 90.000 - Primitive - P21/c (14) - 48 - 2191.49 - I/IC PDF 1 - S-Q 15.2 % - F30= 177(0)
 - 00-006-0246 (*) - Marshite, syn - CuI - Cubic - a 6.05100 - b 6.05100 - c 6.05100 - alpha 90.000 - beta 90.000 - gamma 90.000 - Face-centered - F-43m (216) - 4 - 221.555 - I/IC PDF 1 - S-Q 41.7 % - F20=124(0.0085,
 - 04-012-7393 (A) - Tin Iodide Sulfide - Sn2S2 - Orthorhombic - a 17.44700 - b 25.33400 - c 4.39100 - alpha 90.000 - beta 90.000 - gamma 90.000 - Primitive - Pnam (62) - 12 - 1940.83 - I/IC PDF 7.2 - S-Q 4.2 % - F30
 - 00-041-1049 (*) - Greenockite, syn - CdS - Hexagonal - a 4.14092 - b 4.14092 - c 6.71980 - alpha 90.000 - beta 90.000 - gamma 120.000 - Primitive - P63mc (186) - 2 - 99.7885 - I/IC PDF 1 - S-Q 13.4 % - F30=317(0)

$\text{Cu}_2\text{S}+\text{SnS}+\text{ZnS}+\text{S}+\text{CdI}_2 - 350^\circ\text{C}$



File: Cu2S+SnS+ZnS+CdI2+S - Cooled 350°C.raw - Start: 11.031 ° - End: 84.023 ° - Step: 0.040 ° - Step time: 10. s - Creation: 29.02.2012 20:02:36 -
00-033-0239 (*) - Cadmium Iodide - CdI2 - Hexagonal - a 4.24810 - b 4.24810 - c 13.72650 - alpha 90.000 - beta 90.000 - gamma 120.000 - Primitive - P63mc (186) - 2 - 214,526 - I/c PDF 1 - S-O 11.0 % - F30=25(0
00-026-0575 (I) - Kesterite, syn - Cu2ZnSnS4 - Tetragonal - a 5.44283 - b 5.44283 - c 10.64600 - alpha 90.000 - beta 90.000 - gamma 90.000 - Body-centered - I-42m (121) - 2 - 321,365 - I/c PDF 1 - S-O 83.4 % - F1
00-006-0246 (*) - Marshite, syn - CuI - Cubic - a 6.05100 - b 6.05100 - c 6.05100 - alpha 90.000 - beta 90.000 - gamma 90.000 - Face-centered - F-43m (216) - 4 - 221,655 - I/c PDF 1 - S-O 3.0 % - F20=124(0.0085,2
00-006-0232 (*) - Tin Iodide - SnI4 - Cubic - a 12.27300 - b 12.27300 - c 12.27300 - alpha 90.000 - beta 90.000 - gamma 90.000 - Primitive - Pa-3 (205) - 6 - 1848,64 - I/c PDF 1 - S-O 2.6 % - F27=21(0.0116,113)

Appendix C

Curriculum Vitae

1. Personal data

First name and Surname	God'swill Chimezie Nkwusi
Date and place of birth	02.04.1982 Ilesha,
Nationality	Nigerian
Email	godswillnkwusi@yahoo.com

2. Education

Educational institution	Year	Education (field of studies/degree)
Tallinn University of Technology	2013-2017	Doctoral Study
Tallinn University of Technology/Tartu University	2011-2013	Masters Study/MSc. in Natural Science
University of California Berkeley	01.2013-06.2013	Visiting research student /Exchange program
Federal University of Agriculture Abeokuta	2001-2006	Bachelor Study/BSc. Chemistry
African Church Grammar School/Oyemekun Grammar School	1993-2000	Senior Secondary School Certificate
Arisoyin Primary School /IMG Ibadan	1987-1993	Primary School Leaving Certificate

3. Language competence/skills

Language	Level
English	Fluent
Igbo	Native
Yoruba,	Fluent
Hausa	Basic
Estonian	Basic

4. Special Course/Conferences/Scientific work

Period	Educational or Other Organisation
24.05.2012-25.05.2012	9th International Conference of Young Scientists on Energy Issues, Kaunas, May 24-25, 2012/Oral presentation
30.07.2012-17.08.2012	European Innovation Academy/Training
01.12.2013-06.12.2013	MRS Boston/Poster presentation
13.11.2014-14.11.2014	5 th European Kesterite Workshop, Tallinn, 13-14 November 2014
15.09.2014-18.09.2014	E-MRS Fall Meeting/Oral presentation

5. Professional Employment

Period	Organisation	Position
09.2016-	Euro Academy, Tallinn, Estonia	Lecturer/Environmental Chemistry
09.2014- 2017	EBS, Estonian Business School, Tallinn, Estonia	School Representative
08.2015-07.2017	Association of African Students Estonia-AASE	President
07.2013-12.2016	Tallinn University of Technology	Student Adviser/ Teaching Assistant
09.2011-12.2012	Arvato Bertelsmann/Microsoft, Tallinn, Estonia	Customer Support
07.2008-08.2011	CAP Plc/UAC/Akzo Nobel, Nigeria	Research and Development Chemist
02.2007-02.2008	UNAAD, University of ADO'EKITI, Nigeria	Teaching Assistant
04.2005-07.2005	GSK, Nigeria	Trainee Chemist

6. Defended thesis

Year	Topic	Supervisor
2013	Formation of $\text{Cu}_2\text{ZnSnS}_4$ in molten CdI_2 for monograin membrane solar cells/Masters' thesis	Ms Inga Leinemann
2006	Synthesis Characterization and Antibacterial Effect of Metal-antibiotic drug complexes/Bachelor thesis,	Dr Amolegbe

7. Main field of research and scientific work

Natural Sciences and Engineering; Process Technology and Materials Science; Material Technology; Materials Science and Technology.

List of publications

1. **Nkwusi, G.**, Leinemann, I., Raudoja, J., Mikli, V., Kärber, E., Altosaar, M. Impact of growth-synthesis conditions on $\text{Cu}_2\text{Zn}_{1-x}\text{Cd}_x\text{SnS}_4$ monograin material properties. *Superlattices and Microstructures*, **98** (2016) 400- 405.
2. **Nkwusi, G.**, Leinemann, I., Altosaar, M.. The Processes and Enthalpies in Synthesis of $\text{Cu}_2\text{ZnSnS}_4$ in Molten CdI_2 . *International Advanced Research Journal of Science, Engineering and Technology* **3** (2016), 113- 119.
3. **Nkwusi, G.**, Adeaga, S.; Ayejuyo, S., Annuk, A.. Climate Change; Farmers' Awareness, Perceptions and Responses in Lagos State. *Journal Applied Ecology and Environmental Sciences*, **3** (2015) 95–99, 10.12691/aees-3-4-1.
4. **Nkwusi, G.**; Leinemann, I.; Raudoja, J.; Mikli, V.; Kauk-Kuusik, M.; Altosaar, M.; Mellikov, E. Synthesis of $\text{Cu}_2(\text{ZnCd})\text{SnS}_4$ Absorber Material for Monograin Membrane Applications. *MRS Proceedings / Volume 1638 / 2014: 2013 MRS Fall Meeting*. Scholarone Manuscripts, 1638. (1638 - Symposium W – Next-Generation Inorganic Thin-Film Photovoltaics).
5. **Nkwusi, G.**, Leinemann, I.; Grossberg, M.; Kaljuvee, T.; Traksmaa, R.; Altosaar, M.; Meissner, D. Formation of Copper Zinc Tin Sulfide in Cadmium Iodide for Monograin Membrane Solar Cells. *Conference Proceedings of the 9th International Conference of Young Scientists on Energy Issues*, Kaunas, May 24-25, 2012. II 38–II 46.

ELULOOKIRJELDUS

1. Isikuandmed

Ees- ja perenimi	God'swill Chimezie Nkwusi
Sünniaeg, -koht	02.04.1982, Ilesha
Rahvus	nigeerlane
E-mail	godswillnkwusi@yahoo.com

2. Haridus

Õppeasutus	Õppeaeg	Haridus
Tallinna Tehnikaülikool	2013-2017	Doktoriõpe
Tallinna Tehnikaülikool /Tartu Ülikool	2011-2013	Magistriõpe/loodusteaduste magister
California Berkeley Ülikool	01.2013- 06.2013	Vahetusüliõpilane/vahetusprogramm
Abeokuta Põllumajandusülikool	2001-2006	Bakalaureuseõpe/keemia bakalaureusekraad
Aafrika Kiriklik Gümnaasium /Oyemekuni Gümnaasium	1993-2000	Keskharidus
Arisoyin algkool /IMG Ibadan	1987-1993	Algharidus

3. Keelteoskus/tase

Keel	Tase
Inglise keel	kõrgtase
Igbo keel	emakeel
Yoruba keel	kõrgtase
Hausa keel	algtase
Eesti keel	algtase

4. Täiendusõpe/konverentsid/teadustööd

Periood	Organisatsioon
24.05.2012-25.05.2012	9. rahvusvaheline noorteadlaste konverents Conference of Young Scientists on Energy Issues, Kaunas, 24.-25. mai 2012/suuline ettekanne
30.07.2012-17.08.2012	Euroopa Innovatsiooniakadeemia/Koolitus
01.12.2013-06.12.2013	MRS Boston/Poster ettekanne
13.11.2014-14.11.2014	5 th European Kesterite Workshop, Tallinn, 13-14 November 2014, posterettekanne
15.09.2014-18.09.2014	E-MRS Fall Meeting/ suuline ettekanne

5. Teenistuskäik

Töötamise aeg	Tööandja	Ametikoht
09.2016-	Euroakadeemia, Tallinn, Eesti	Lektor/keskonnakeemia
09.2014- 2017	EBS, Tallinn, Eesti	Esindaja
08.2015-07.2017	Aafrika Üliõpilaste Ühing Eestis - AASE	President
07.2013-12.2016	Tallinna Tehnikaülikool	Üliõpilaste nõustaja/õppeassistent
09.2011-12.2012	Arvato Bertelsmann/Microsoft, Tallinn, Estonia	Klienditugi
07.2008-08.2011	CAP Plc/UAC/Akzo Nobel, Nigeria	Uurimis- ja arenduskeemik
02.2007-02.2008	UNAAD, ADO'EKITI Ülikool, Nigeria	Õppeassistent
04.2005-07.2005	GSK, Nigeria	Keemia praktikant

6. Kaitstud lõputööd

Aasta	Teema	Juhendaja
2013	Cu_2ZnSnS_4 moodustumine sula CdI_2 keskkonnas./ Magistritöö	Ms Inga Leinemann
2006	Metall-antibiootik ravim-komplekside süntees, karakteriseerimine ja antibakteriaalne toime/Bakalaureuse lõputöö	Dr Amolegbe

7. Uurimis- ja teadustöö alad

Loodusteadused ja inseneeria, protsessitehnoloogia ja materjaliteadus, materjalitehnoloogia, päikeseenergia materjalide süntees ja uurimine.

Teaduspublikatsioonide nimekiri

1. **Nkwusi, G.**, Leinemann, I., Raudoja, J., Mikli, V., Kärber, E., Altosaar, M. Impact of growth-synthesis conditions on $\text{Cu}_2\text{Zn}_{1-x}\text{Cd}_x\text{SnS}_4$ monograin material properties. *Superlattices and Microstructures*, **98** (2016) 400- 405.
2. **Nkwusi, G.**, Leinemann, I., Altosaar, M.. The Processes and Enthalpies in Synthesis of $\text{Cu}_2\text{ZnSnS}_4$ in Molten CdI_2 . *International Advanced Research Journal of Science, Engineering and Technology* **3** (2016), 113- 119.
3. **Nkwusi, G.**, Adeaga, S.; Ayejuyo, S., Annuk, A.. Climate Change; Farmers' Awareness, Perceptions and Responses in Lagos State. *Journal Applied Ecology and Environmental Sciences*, **3** (2015) 95–99, 10.12691/aees-3-4-1.
4. **Nkwusi, G.**; Leinemann, I.; Raudoja, J.; Mikli, V.; Kauk-Kuusik, M.; Altosaar, M.; Mellikov, E. Synthesis of $\text{Cu}_2(\text{ZnCd})\text{SnS}_4$ Absorber Material for Monograin Membrane Applications. *MRS Proceedings / Volume 1638 / 2014: 2013 MRS Fall Meeting*. Scholarone Manuscripts, 1638. (1638 - Symposium W – Next-Generation Inorganic Thin-Film Photovoltaics).
5. **Nkwusi, G.**, Leinemann, I.; Grossberg, M.; Kaljuvee, T.; Traksmaa, R.; Altosaar, M.; Meissner, D. Formation of Copper Zinc Tin Sulfide in Cadmium Iodide for Monograin Membrane Solar Cells. *Conference Proceedings of the 9th International Conference of Young Scientists on Energy Issues*, Kaunas, May 24-25, 2012. II 38–II 46.

**DISSERTATIONS DEFENDED AT
TALLINN UNIVERSITY OF TECHNOLOGY ON
NATURAL AND EXACT SCIENCES**

1. **Olav Kongas.** Nonlinear Dynamics in Modeling Cardiac Arrhythmias. 1998.
2. **Kalju Vanatalu.** Optimization of Processes of Microbial Biosynthesis of Isotopically Labeled Biomolecules and Their Complexes. 1999.
3. **Ahto Buldas.** An Algebraic Approach to the Structure of Graphs. 1999.
4. **Monika Drews.** A Metabolic Study of Insect Cells in Batch and Continuous Culture: Application of Chemostat and Turbidostat to the Production of Recombinant Proteins. 1999.
5. **Eola Valdre.** Endothelial-Specific Regulation of Vessel Formation: Role of Receptor Tyrosine Kinases. 2000.
6. **Kalju Lott.** Doping and Defect Thermodynamic Equilibrium in ZnS. 2000.
7. **Reet Koljak.** Novel Fatty Acid Dioxygenases from the Corals *Plexaura homomalla* and *Gersemia fruticosa*. 2001.
8. **Anne Paju.** Asymmetric oxidation of Prochiral and Racemic Ketones by Using Sharpless Catalyst. 2001.
9. **Marko Vendelin.** Cardiac Mechanoenergetics *in silico*. 2001.
10. **Pearu Peterson.** Multi-Soliton Interactions and the Inverse Problem of Wave Crest. 2001.
11. **Anne Menert.** Microcalorimetry of Anaerobic Digestion. 2001.
12. **Toomas Tiivel.** The Role of the Mitochondrial Outer Membrane in *in vivo* Regulation of Respiration in Normal Heart and Skeletal Muscle Cell. 2002.
13. **Olle Hints.** Ordovician Scolecodonts of Estonia and Neighbouring Areas: Taxonomy, Distribution, Palaeoecology, and Application. 2002.
14. **Jaak Nõlvak.** Chitinozoan Biostratigraphy in the Ordovician of Baltoscandia. 2002.
15. **Liivi Kluge.** On Algebraic Structure of Pre-Operad. 2002.
16. **Jaanus Lass.** Biosignal Interpretation: Study of Cardiac Arrhythmias and Electromagnetic Field Effects on Human Nervous System. 2002.
17. **Janek Peterson.** Synthesis, Structural Characterization and Modification of PAMAM Dendrimers. 2002.
18. **Merike Vaher.** Room Temperature Ionic Liquids as Background Electrolyte Additives in Capillary Electrophoresis. 2002.
19. **Valdek Mikli.** Electron Microscopy and Image Analysis Study of Powdered Hardmetal Materials and Optoelectronic Thin Films. 2003.
20. **Mart Viljus.** The Microstructure and Properties of Fine-Grained Cermets. 2003.
21. **Signe Kask.** Identification and Characterization of Dairy-Related *Lactobacillus*. 2003.
22. **Tiiu-Mai Laht.** Influence of Microstructure of the Curd on Enzymatic and Microbiological Processes in Swiss-Type Cheese. 2003.
23. **Anne Kuusksalu.** 2–5A Synthetase in the Marine Sponge *Geodia cydonium*. 2003.
24. **Sergei Bereznev.** Solar Cells Based on Polycrystalline Copper-Indium Chalcogenides and Conductive Polymers. 2003.

25. **Kadri Kriis.** Asymmetric Synthesis of C₂-Symmetric Bimorpholines and Their Application as Chiral Ligands in the Transfer Hydrogenation of Aromatic Ketones. 2004.
26. **Jekaterina Reut.** Polypyrrole Coatings on Conducting and Insulating Substrates. 2004.
27. **Sven Nõmm.** Realization and Identification of Discrete-Time Nonlinear Systems. 2004.
28. **Olga Kijatkina.** Deposition of Copper Indium Disulphide Films by Chemical Spray Pyrolysis. 2004.
29. **Gert Tamberg.** On Sampling Operators Defined by Rogosinski, Hann and Blackman Windows. 2004.
30. **Monika Übner.** Interaction of Humic Substances with Metal Cations. 2004.
31. **Kaarel Adamberg.** Growth Characteristics of Non-Starter Lactic Acid Bacteria from Cheese. 2004.
32. **Imre Vallikivi.** Lipase-Catalysed Reactions of Prostaglandins. 2004.
33. **Merike Peld.** Substituted Apatites as Sorbents for Heavy Metals. 2005.
34. **Vitali Syritski.** Study of Synthesis and Redox Switching of Polypyrrole and Poly(3,4-ethylenedioxythiophene) by Using *in-situ* Techniques. 2004.
35. **Lee Põllumaa.** Evaluation of Ecotoxicological Effects Related to Oil Shale Industry. 2004.
36. **Riina Aav.** Synthesis of 9,11-Secosterols Intermediates. 2005.
37. **Andres Braunbrück.** Wave Interaction in Weakly Inhomogeneous Materials. 2005.
38. **Robert Kitt.** Generalised Scale-Invariance in Financial Time Series. 2005.
39. **Juss Pavelson.** Mesoscale Physical Processes and the Related Impact on the Summer Nutrient Fields and Phytoplankton Blooms in the Western Gulf of Finland. 2005.
40. **Olari Ilison.** Solitons and Solitary Waves in Media with Higher Order Dispersive and Nonlinear Effects. 2005.
41. **Maksim Säkki.** Intermittency and Long-Range Structurization of Heart Rate. 2005.
42. **Enli Kiipli.** Modelling Seawater Chemistry of the East Baltic Basin in the Late Ordovician–Early Silurian. 2005.
43. **Igor Golovtsov.** Modification of Conductive Properties and Processability of Polyparaphenylene, Polypyrrole and polyaniline. 2005.
44. **Katrin Laos.** Interaction Between Furcellaran and the Globular Proteins (Bovine Serum Albumin β -Lactoglobulin). 2005.
45. **Arvo Mere.** Structural and Electrical Properties of Spray Deposited Copper Indium Disulphide Films for Solar Cells. 2006.
46. **Sille Ehala.** Development and Application of Various On- and Off-Line Analytical Methods for the Analysis of Bioactive Compounds. 2006.
47. **Maria Kulp.** Capillary Electrophoretic Monitoring of Biochemical Reaction Kinetics. 2006.
48. **Anu Aaspõllu.** Proteinases from *Vipera lebetina* Snake Venom Affecting Hemostasis. 2006.

49. **Lyudmila Chekulayeva.** Photosensitized Inactivation of Tumor Cells by Porphyrins and Chlorins. 2006.
50. **Merle Uudsemaa.** Quantum-Chemical Modeling of Solvated First Row Transition Metal Ions. 2006.
51. **Tagli Pitsi.** Nutrition Situation of Pre-School Children in Estonia from 1995 to 2004. 2006.
52. **Angela Ivask.** Luminescent Recombinant Sensor Bacteria for the Analysis of Bioavailable Heavy Metals. 2006.
53. **Tiina Lõugas.** Study on Physico-Chemical Properties and Some Bioactive Compounds of Sea Buckthorn (*Hippophae rhamnoides* L.). 2006.
54. **Kaja Kasemets.** Effect of Changing Environmental Conditions on the Fermentative Growth of *Saccharomyces cerevisiae* S288C: Auxo-accelerostat Study. 2006.
55. **Ildar Nisamedtinov.** Application of ^{13}C and Fluorescence Labeling in Metabolic Studies of *Saccharomyces* spp. 2006.
56. **Alar Leibak.** On Additive Generalisation of Voronoï's Theory of Perfect Forms over Algebraic Number Fields. 2006.
57. **Andri Jagomägi.** Photoluminescence of Chalcopyrite Tellurides. 2006.
58. **Tõnu Martma.** Application of Carbon Isotopes to the Study of the Ordovician and Silurian of the Baltic. 2006.
59. **Marit Kauk.** Chemical Composition of CuInSe₂ Monograin Powders for Solar Cell Application. 2006.
60. **Julia Kois.** Electrochemical Deposition of CuInSe₂ Thin Films for Photovoltaic Applications. 2006.
61. **Iiona Oja Ačik.** Sol-Gel Deposition of Titanium Dioxide Films. 2007.
62. **Tiia Anmann.** Integrated and Organized Cellular Bioenergetic Systems in Heart and Brain. 2007.
63. **Katrin Trummal.** Purification, Characterization and Specificity Studies of Metalloproteinases from *Vipera lebetina* Snake Venom. 2007.
64. **Gennadi Lessin.** Biochemical Definition of Coastal Zone Using Numerical Modeling and Measurement Data. 2007.
65. **Enno Pais.** Inverse problems to determine non-homogeneous degenerate memory kernels in heat flow. 2007.
66. **Maria Borissova.** Capillary Electrophoresis on Alkylimidazolium Salts. 2007.
67. **Karin Valmsen.** Prostaglandin Synthesis in the Coral *Plexaura homomalla*: Control of Prostaglandin Stereochemistry at Carbon 15 by Cyclooxygenases. 2007.
68. **Kristjan Piirimäe.** Long-Term Changes of Nutrient Fluxes in the Drainage Basin of the Gulf of Finland – Application of the PolFlow Model. 2007.
69. **Tatjana Dedova.** Chemical Spray Pyrolysis Deposition of Zinc Sulfide Thin Films and Zinc Oxide Nanostructured Layers. 2007.
70. **Katrin Tomson.** Production of Labelled Recombinant Proteins in Fed-Batch Systems in *Escherichia coli*. 2007.
71. **Cecilia Sarmiento.** Suppressors of RNA Silencing in Plants. 2008.
72. **Vilja Mardla.** Inhibition of Platelet Aggregation with Combination of Antiplatelet Agents. 2008.

73. **Maie Bachmann.** Effect of Modulated Microwave Radiation on Human Resting Electroencephalographic Signal. 2008.
74. **Dan Huvonen.** Terahertz Spectroscopy of Low-Dimensional Spin Systems. 2008.
75. **Ly Villo.** Stereoselective Chemoenzymatic Synthesis of Deoxy Sugar Esters Involving *Candida antarctica* Lipase B. 2008.
76. **Johan Anton.** Technology of Integrated Photoelasticity for Residual Stress Measurement in Glass Articles of Axisymmetric Shape. 2008.
77. **Olga Volobujeva.** SEM Study of Selenization of Different Thin Metallic Films. 2008.
78. **Artur Jogi.** Synthesis of 4'-Substituted 2,3'-dideoxynucleoside Analogues. 2008.
79. **Mario Kadastik.** Doubly Charged Higgs Boson Decays and Implications on Neutrino Physics. 2008.
80. **Fernando Perez-Caballero.** Carbon Aerogels from 5-Methylresorcinol-Formaldehyde Gels. 2008.
81. **Sirje Vaask.** The Comparability, Reproducibility and Validity of Estonian Food Consumption Surveys. 2008.
82. **Anna Menaker.** Electrosynthesized Conducting Polymers, Polypyrrole and Poly(3,4-ethylenedioxythiophene), for Molecular Imprinting. 2009.
83. **Lauri Ilison.** Solitons and Solitary Waves in Hierarchical Korteweg-de Vries Type Systems. 2009.
84. **Kaia Ernits.** Study of In₂S₃ and ZnS Thin Films Deposited by Ultrasonic Spray Pyrolysis and Chemical Deposition. 2009.
85. **Veljo Sinivee.** Portable Spectrometer for Ionizing Radiation "Gammamapper". 2009.
86. **Juri Virkepu.** On Lagrange Formalism for Lie Theory and Operadic Harmonic Oscillator in Low Dimensions. 2009.
87. **Marko Piirsoo.** Deciphering Molecular Basis of Schwann Cell Development. 2009.
88. **Kati Helmja.** Determination of Phenolic Compounds and Their Antioxidative Capability in Plant Extracts. 2010.
89. **Merike Sõmera.** Sobemoviruses: Genomic Organization, Potential for Recombination and Necessity of P1 in Systemic Infection. 2010.
90. **Kristjan Laes.** Preparation and Impedance Spectroscopy of Hybrid Structures Based on CuIn₃Se₅ Photoabsorber. 2010.
91. **Kristin Lippur.** Asymmetric Synthesis of 2,2'-Bimorpholine and its 5,5'-Substituted Derivatives. 2010.
92. **Merike Luman.** Dialysis Dose and Nutrition Assessment by an Optical Method. 2010.
93. **Mihhail Berezovski.** Numerical Simulation of Wave Propagation in Heterogeneous and Microstructured Materials. 2010.
94. **Tamara Aid-Pavlidis.** Structure and Regulation of BDNF Gene. 2010.
95. **Olga Bragina.** The Role of Sonic Hedgehog Pathway in Neuro- and Tumorigenesis. 2010.
96. **Merle Randrt.** Wave Propagation in Microstructured Solids: Solitary and Periodic Waves. 2010.

97. **Marju Laars.** Asymmetric Organocatalytic Michael and Aldol Reactions Mediated by Cyclic Amines. 2010.
98. **Maarja Grossberg.** Optical Properties of Multinary Semiconductor Compounds for Photovoltaic Applications. 2010.
99. **Alla Maloverjan.** Vertebrate Homologues of Drosophila Fused Kinase and Their Role in Sonic Hedgehog Signalling Pathway. 2010.
100. **Priit Pruunsild.** Neuronal Activity-Dependent Transcription Factors and Regulation of Human *BDNF* Gene. 2010.
101. **Tatjana Knjazeva.** New Approaches in Capillary Electrophoresis for Separation and Study of Proteins. 2011.
102. **Atanas Katerski.** Chemical Composition of Sprayed Copper Indium Disulfide Films for Nanostructured Solar Cells. 2011.
103. **Kristi Timmo.** Formation of Properties of CuInSe_2 and $\text{Cu}_2\text{ZnSn}(\text{S,Se})_4$ Monograin Powders Synthesized in Molten KI. 2011.
104. **Kert Tamm.** Wave Propagation and Interaction in Mindlin-Type Microstructured Solids: Numerical Simulation. 2011.
105. **Adrian Popp.** Ordovician Proetid Trilobites in Baltoscandia and Germany. 2011.
106. **Ove Pärn.** Sea Ice Deformation Events in the Gulf of Finland and This Impact on Shipping. 2011.
107. **Germo Väli.** Numerical Experiments on Matter Transport in the Baltic Sea. 2011.
108. **Andrus Seiman.** Point-of-Care Analyser Based on Capillary Electrophoresis. 2011.
109. **Olga Katargina.** Tick-Borne Pathogens Circulating in Estonia (Tick-Borne Encephalitis Virus, *Anaplasma phagocytophilum*, *Babesia* Species): Their Prevalence and Genetic Characterization. 2011.
110. **Ingrid Sumeri.** The Study of Probiotic Bacteria in Human Gastrointestinal Tract Simulator. 2011.
111. **Kairit Zovo.** Functional Characterization of Cellular Copper Proteome. 2011.
112. **Natalja Makarytsheva.** Analysis of Organic Species in Sediments and Soil by High Performance Separation Methods. 2011.
113. **Monika Mortimer.** Evaluation of the Biological Effects of Engineered Nanoparticles on Unicellular Pro- and Eukaryotic Organisms. 2011.
114. **Kersti Tepp.** Molecular System Bioenergetics of Cardiac Cells: Quantitative Analysis of Structure-Function Relationship. 2011.
115. **Anna-Liisa Peikolainen.** Organic Aerogels Based on 5-Methylresorcinol. 2011.
116. **Leeli Amon.** Palaeoecological Reconstruction of Late-Glacial Vegetation Dynamics in Eastern Baltic Area: A View Based on Plant Macrofossil Analysis. 2011.
117. **Tanel Peets.** Dispersion Analysis of Wave Motion in Microstructured Solids. 2011.
118. **Liina Kaupmees.** Selenization of Molybdenum as Contact Material in Solar Cells. 2011.
119. **Allan Olsper.** Properties of VPg and Coat Protein of Sobemoviruses. 2011.
120. **Kadri Koppel.** Food Category Appraisal Using Sensory Methods. 2011.
121. **Jelena Gorbatšova.** Development of Methods for CE Analysis of Plant Phenolics and Vitamins. 2011.

122. **Karin Viipsi.** Impact of EDTA and Humic Substances on the Removal of Cd and Zn from Aqueous Solutions by Apatite. 2012.
123. **David Schryer.** Metabolic Flux Analysis of Compartmentalized Systems Using Dynamic Isotopologue Modeling. 2012.
124. **Ardo Illaste.** Analysis of Molecular Movements in Cardiac Myocytes. 2012.
125. **Indrek Reile.** 3-Alkylcyclopentane-1,2-Diones in Asymmetric Oxidation and Alkylation Reactions. 2012.
126. **Tatjana Tamberg.** Some Classes of Finite 2-Groups and Their Endomorphism Semigroups. 2012.
127. **Taavi Liblik.** Variability of Thermohaline Structure in the Gulf of Finland in Summer. 2012.
128. **Priidik Lagemaa.** Operational Forecasting in Estonian Marine Waters. 2012.
129. **Andrei Errapart.** Photoelastic Tomography in Linear and Non-linear Approximation. 2012.
130. **Külliki Krabbi.** Biochemical Diagnosis of Classical Galactosemia and Mucopolysaccharidoses in Estonia. 2012.
131. **Kristel Kaseleht.** Identification of Aroma Compounds in Food using SPME-GC/MS and GC-Olfactometry. 2012.
132. **Kristel Kodar.** Immunoglobulin G Glycosylation Profiling in Patients with Gastric Cancer. 2012.
133. **Kai Rosin.** Solar Radiation and Wind as Agents of the Formation of the Radiation Regime in Water Bodies. 2012.
134. **Ann Tiiman.** Interactions of Alzheimer's Amyloid-Beta Peptides with Zn(II) and Cu(II) Ions. 2012.
135. **Olga Gavrilova.** Application and Elaboration of Accounting Approaches for Sustainable Development. 2012.
136. **Olesja Bondarenko.** Development of Bacterial Biosensors and Human Stem Cell-Based *In Vitro* Assays for the Toxicological Profiling of Synthetic Nanoparticles. 2012.
137. **Katri Muska.** Study of Composition and Thermal Treatments of Quaternary Compounds for Monograin Layer Solar Cells. 2012.
138. **Ranno Nahku.** Validation of Critical Factors for the Quantitative Characterization of Bacterial Physiology in Accelerostat Cultures. 2012.
139. **Petri-Jaan Lahtvee.** Quantitative Omics-level Analysis of Growth Rate Dependent Energy Metabolism in *Lactococcus lactis*. 2012.
140. **Kerti Orumets.** Molecular Mechanisms Controlling Intracellular Glutathione Levels in Baker's Yeast *Saccharomyces cerevisiae* and its Random Mutagenized Glutathione Over-Accumulating Isolate. 2012.
141. **Loreida Timberg.** Spice-Cured Sprats Ripening, Sensory Parameters Development, and Quality Indicators. 2012.
142. **Anna Mihhalevski.** Rye Sourdough Fermentation and Bread Stability. 2012.
143. **Liisa Arike.** Quantitative Proteomics of *Escherichia coli*: From Relative to Absolute Scale. 2012.
144. **Kairi Otto.** Deposition of In₂S₃ Thin Films by Chemical Spray Pyrolysis. 2012.
145. **Mari Sepp.** Functions of the Basic Helix-Loop-Helix Transcription Factor TCF4 in Health and Disease. 2012.

146. **Anna Suhhova.** Detection of the Effect of Weak Stressors on Human Resting Electroencephalographic Signal. 2012.
147. **Aram Kazarjan.** Development and Production of Extruded Food and Feed Products Containing Probiotic Microorganisms. 2012.
148. **Rivo Uiboupin.** Application of Remote Sensing Methods for the Investigation of Spatio-Temporal Variability of Sea Surface Temperature and Chlorophyll Fields in the Gulf of Finland. 2013.
149. **Tiina Kriščiunaite.** A Study of Milk Coagulability. 2013.
150. **Tuuli Levandi.** Comparative Study of Cereal Varieties by Analytical Separation Methods and Chemometrics. 2013.
151. **Natalja Kabanova.** Development of a Microcalorimetric Method for the Study of Fermentation Processes. 2013.
152. **Himani Khanduri.** Magnetic Properties of Functional Oxides. 2013.
153. **Julia Smirnova.** Investigation of Properties and Reaction Mechanisms of Redox-Active Proteins by ESI MS. 2013.
154. **Mervi Sepp.** Estimation of Diffusion Restrictions in Cardiomyocytes Using Kinetic Measurements. 2013.
155. **Kersti Jääger.** Differentiation and Heterogeneity of Mesenchymal Stem Cells. 2013.
156. **Victor Alari.** Multi-Scale Wind Wave Modeling in the Baltic Sea. 2013.
157. **Taavi Päll.** Studies of CD44 Hyaluronan Binding Domain as Novel Angiogenesis Inhibitor. 2013.
158. **Allan Niidu.** Synthesis of Cyclopentane and Tetrahydrofuran Derivatives. 2013.
159. **Julia Geller.** Detection and Genetic Characterization of *Borrelia* Species Circulating in Tick Population in Estonia. 2013.
160. **Irina Stulova.** The Effects of Milk Composition and Treatment on the Growth of Lactic Acid Bacteria. 2013.
161. **Jana Holmar.** Optical Method for Uric Acid Removal Assessment During Dialysis. 2013.
162. **Kerti Ausmees.** Synthesis of Heterobicyclo[3.2.0]heptane Derivatives *via* Multicomponent Cascade Reaction. 2013.
163. **Minna Varikmaa.** Structural and Functional Studies of Mitochondrial Respiration Regulation in Muscle Cells. 2013.
164. **Indrek Koppel.** Transcriptional Mechanisms of BDNF Gene Regulation. 2014.
165. **Kristjan Pilt.** Optical Pulse Wave Signal Analysis for Determination of Early Arterial Ageing in Diabetic Patients. 2014.
166. **Andres Anier.** Estimation of the Complexity of the Electroencephalogram for Brain Monitoring in Intensive Care. 2014.
167. **Toivo Kallaste.** Pyroclastic Sanidine in the Lower Palaeozoic Bentonites – A Tool for Regional Geological Correlations. 2014.
168. **Erki Kärber.** Properties of ZnO-nanorod/In₂S₃/CuInS₂ Solar Cell and the Constituent Layers Deposited by Chemical Spray Method. 2014.
169. **Julia Lehner.** Formation of Cu₂ZnSnS₄ and Cu₂ZnSnSe₄ by Chalcogenisation of Electrochemically Deposited Precursor Layers. 2014.
170. **Peep Pitk.** Protein- and Lipid-rich Solid Slaughterhouse Waste Anaerobic Co-digestion: Resource Analysis and Process Optimization. 2014.

171. **Kaspar Valgepea**. Absolute Quantitative Multi-omics Characterization of Specific Growth Rate-dependent Metabolism of *Escherichia coli*. 2014.
172. **Artur Noole**. Asymmetric Organocatalytic Synthesis of 3,3'-Disubstituted Oxindoles. 2014.
173. **Robert Tsanev**. Identification and Structure-Functional Characterisation of the Gene Transcriptional Repressor Domain of Human Gli Proteins. 2014.
174. **Dmitri Kartofelev**. Nonlinear Sound Generation Mechanisms in Musical Acoustic. 2014.
175. **Sigrid Hade**. GIS Applications in the Studies of the Palaeozoic Graptolite Argillite and Landscape Change. 2014.
176. **Agne Velthut-Meikas**. Ovarian Follicle as the Environment of Oocyte Maturation: The Role of Granulosa Cells and Follicular Fluid at Pre-Ovulatory Development. 2014.
177. **Kristel Hälvin**. Determination of B-group Vitamins in Food Using an LC-MS Stable Isotope Dilution Assay. 2014.
178. **Mailis Päri**. Characterization of the Oligoadenylate Synthetase Subgroup from Phylum Porifera. 2014.
179. **Jekaterina Kazantseva**. Alternative Splicing of *TAF4*: A Dynamic Switch between Distinct Cell Functions. 2014.
180. **Jaanus Suurväli**. Regulator of G Protein Signalling 16 (RGS16): Functions in Immunity and Genomic Location in an Ancient MHC-Related Evolutionarily Conserved Synteny Group. 2014.
181. **Ene Viiard**. Diversity and Stability of Lactic Acid Bacteria During Rye Sourdough Propagation. 2014.
182. **Kristella Hansen**. Prostaglandin Synthesis in Marine Arthropods and Red Algae. 2014.
183. **Helike Lõhelaid**. Allene Oxide Synthase-lipoxygenase Pathway in Coral Stress Response. 2015.
184. **Normunds Stivrīnš**. Postglacial Environmental Conditions, Vegetation Succession and Human Impact in Latvia. 2015.
185. **Mary-Liis Kütt**. Identification and Characterization of Bioactive Peptides with Antimicrobial and Immunoregulating Properties Derived from Bovine Colostrum and Milk. 2015.
186. **Kazbulat Šogenov**. Petrophysical Models of the CO₂ Plume at Prospective Storage Sites in the Baltic Basin. 2015.
187. **Taavi Raadik**. Application of Modulation Spectroscopy Methods in Photovoltaic Materials Research. 2015.
188. **Reio Põder**. Study of Oxygen Vacancy Dynamics in Sc-doped Ceria with NMR Techniques. 2015.
189. **Sven Siir**. Internal Geochemical Stratification of Bentonites (Altered Volcanic Ash Beds) and its Interpretation. 2015.
190. **Kaur Jaanson**. Novel Transgenic Models Based on Bacterial Artificial Chromosomes for Studying BDNF Gene Regulation. 2015.
191. **Niina Karro**. Analysis of ADP Compartmentation in Cardiomyocytes and Its Role in Protection Against Mitochondrial Permeability Transition Pore Opening. 2015.

192. **Piret Laht.** B-plexins Regulate the Maturation of Neurons Through Microtubule Dynamics. 2015.
193. **Sergei Žari.** Organocatalytic Asymmetric Addition to Unsaturated 1,4-Dicarbonyl Compounds. 2015.
194. **Natalja Buhhalko.** Processes Influencing the Spatio-temporal Dynamics of Nutrients and Phytoplankton in Summer in the Gulf of Finland, Baltic Sea. 2015.
195. **Natalia Maticiu.** Mechanism of Changes in the Properties of Chemically Deposited CdS Thin Films Induced by Thermal Annealing. 2015.
196. **Mario Öeren.** Computational Study of Cyclohexylhemicucurbiturils. 2015.
197. **Mari Kalda.** Mechanoenergetics of a Single Cardiomyocyte. 2015.
198. **Ieva Grudzinska.** Diatom Stratigraphy and Relative Sea Level Changes of the Eastern Baltic Sea over the Holocene. 2015.
199. **Anna Kazantseva.** Alternative Splicing in Health and Disease. 2015.
200. **Jana Kazarjan.** Investigation of Endogenous Antioxidants and Their Synthetic Analogues by Capillary Electrophoresis. 2016.
201. **Maria Safonova.** SnS Thin Films Deposition by Chemical Solution Method and Characterization. 2016.
202. **Jekaterina Mazina.** Detection of Psycho- and Bioactive Drugs in Different Sample Matrices by Fluorescence Spectroscopy and Capillary Electrophoresis. 2016.
203. **Karin Rosenstein.** Genes Regulated by Estrogen and Progesterone in Human Endometrium. 2016.
204. **Aleksei Tretjakov.** A Macromolecular Imprinting Approach to Design Synthetic Receptors for Label-Free Biosensing Applications. 2016.
205. **Mati Danilson.** Temperature Dependent Electrical Properties of Kesterite Monograin Layer Solar Cells. 2016.
206. **Kaspar Kevvai.** Applications of ¹⁵N-labeled Yeast Hydrolysates in Metabolic Studies of *Lactococcus lactis* and *Saccharomyces Cerevisiae*. 2016.
207. **Kadri Aller.** Development and Applications of Chemically Defined Media for Lactic Acid Bacteria. 2016.
208. **Gert Preegel.** Cyclopentane-1,2-dione and Cyclopent-2-en-1-one in Asymmetric Organocatalytic Reactions. 2016.
209. **Jekaterina Služenikina.** Applications of Marine Scatterometer Winds and Quality Aspects of their Assimilation into Numerical Weather Prediction Model HIRLAM. 2016.
210. **Erkki Kask.** Study of Kesterite Solar Cell Absorbers by Capacitance Spectroscopy Methods. 2016.
211. **Jürgen Arund.** Major Chromophores and Fluorophores in the Spent Dialysate as Cornerstones for Optical Monitoring of Kidney Replacement Therapy. 2016.
212. **Andrei Šamarin.** Hybrid PET/MR Imaging of Bone Metabolism and Morphology. 2016.
213. **Kairi Kasemets.** Inverse Problems for Parabolic Integro-Differential Equations with Instant and Integral Conditions. 2016.
214. **Edith Soosaar.** An Evolution of Freshwater Bulge in Laboratory Scale Experiments and Natural Conditions. 2016.
215. **Peeter Laas.** Spatiotemporal Niche-Partitioning of Bacterioplankton Community across Environmental Gradients in the Baltic Sea. 2016.

216. **Margus Voolma**. Geochemistry of Organic-Rich Metalliferous Oil Shale/Black Shale of Jordan and Estonia. 2016.
217. **Karin Ojamäe**. The Ecology and Photobiology of Mixotrophic Alveolates in the Baltic Sea. 2016.
218. **Anne Pink**. The Role of CD44 in the Control of Endothelial Cell Proliferation and Angiogenesis. 2016.
219. **Kristiina Kreek**. Metal-Doped Aerogels Based on Resorcinol Derivatives. 2016.
220. **Kaia Kukk**. Expression of Human Prostaglandin H Synthases in the Yeast *Pichia pastoris*. 2016.
221. **Martin Laasmaa**. Revealing Aspects of Cardiac Function from Fluorescence and Electrophysiological Recordings. 2016.
222. **Eeva-Gerda Kobrin**. Development of Point of Care Applications for Capillary Electrophoresis. 2016.
223. **Villu Kikas**. Physical Processes Controlling the Surface Layer Dynamics in the Stratified Gulf of Finland: An Application of Ferrybox Technology. 2016.
224. **Maris Skudra**. Features of Thermohaline Structure and Circulation in the Gulf of Riga. 2017.
225. **Sirje Sildever**. Influence of Physical-Chemical Factors on Community and Populations of the Baltic Sea Spring Bloom Microalgae. 2017.
226. **Nicolae Spalatu**. Development of CdTe Absorber Layer for Thin-Film Solar Cells. 2017.
227. **Kristi Luberg**. Human Tropomyosin-Related Kinase A and B: from Transcript Diversity to Novel Inhibitors. 2017.
228. **Andrus Kaldma**. Metabolic Remodeling of Human Colorectal Cancer: Alterations in Energy Fluxes. 2017.
229. **Irina Osadchuk**. Structures and Catalytic Properties of Titanium and Iridium Based Complexes. 2017.
230. **Roman Boroznjak**. A Computational Approach for Rational Monomer Selection in Molecularly Imprinted Polymer Synthesis. 2017.
231. **Sten Erm**. Use of Mother-Daughter Multi-Bioreactor Systems for Studies of Steady State Microbial Growth Space. 2017.